

Design of an axially controlled spindle unit for high precision diamond turning

Citation for published version (APA):

Renkens, M. J. M. (1997). *Design of an axially controlled spindle unit for high precision diamond turning*. [Phd Thesis 1 (Research TU/e / Graduation TU/e), Mechanical Engineering]. Technische Universiteit Eindhoven. <https://doi.org/10.6100/IR501339>

DOI:

[10.6100/IR501339](https://doi.org/10.6100/IR501339)

Document status and date:

Published: 01/01/1997

Document Version:

Publisher's PDF, also known as Version of Record (includes final page, issue and volume numbers)

Please check the document version of this publication:

- A submitted manuscript is the version of the article upon submission and before peer-review. There can be important differences between the submitted version and the official published version of record. People interested in the research are advised to contact the author for the final version of the publication, or visit the DOI to the publisher's website.
- The final author version and the galley proof are versions of the publication after peer review.
- The final published version features the final layout of the paper including the volume, issue and page numbers.

[Link to publication](#)

General rights

Copyright and moral rights for the publications made accessible in the public portal are retained by the authors and/or other copyright owners and it is a condition of accessing publications that users recognise and abide by the legal requirements associated with these rights.

- Users may download and print one copy of any publication from the public portal for the purpose of private study or research.
- You may not further distribute the material or use it for any profit-making activity or commercial gain
- You may freely distribute the URL identifying the publication in the public portal.

If the publication is distributed under the terms of Article 25fa of the Dutch Copyright Act, indicated by the "Taverne" license above, please follow below link for the End User Agreement:

www.tue.nl/taverne

Take down policy

If you believe that this document breaches copyright please contact us at:

openaccess@tue.nl

providing details and we will investigate your claim.

**Design of an
Axially Controlled Spindle Unit
for
High Precision Diamond Turning**

Marcel Renkens



Design of an Axially Controlled Spindle Unit
for
High Precision Diamond Turning

Marcel Renkens

CIP-GEGEVENS KONINKLIJKE BIBLIOTHEEK, DEN HAAG.

Renkens, Marcel

Design of an Axially Controlled Spindle Unit for High Precision
Diamond Turning / M.J.M. Renkens.

ISBN 90-74445-35-7

© M. Renkens 1997.
All rights reserved

The work described in this thesis was carried out at the Philips Research
Laboratories, Eindhoven.

**Design of an Axially Controlled Spindle Unit
for
High Precision Diamond Turning**

PROEFONTWERP

ter verkrijging van de graad van doctor aan de
Technische Universiteit Eindhoven, op gezag van
de Rector Magnificus, prof.dr. M. Rem, voor een
commissie aangewezen door het College van
Dekanen in het openbaar te verdedigen op
woensdag 1 oktober 1997 om 16.00 uur

door

Michaël Josepha Mathijs Renkens

geboren te Puth

Dit proefontwerp is goedgekeurd door de promotoren:

prof.dr.ir. P.H.J. Schellekens

en

prof.dr.ir. A.J.A. Vandenput

Summary

This thesis describes the design and realisation of a new type of spindle unit for a high precision lathe. The design is focused on a reduction of the axial error motions and an increase of the axial stiffness with respect to the current spindles. Besides, the spindle unit must be able to produce nonrotationally symmetric products with optical surface quality (e.g. astigmatic lenses, beamshapers etc.). The design of the spindle unit is based on a mechatronic approach. Accordingly, it is possible to realise a spindle unit with an improved accuracy and functionality, whereas the number of precision components is minimal.

A hollow cylindrical spindle is used, which is supported by aerostatic radial bearings. A voice coil actuator controls the axial position of the spindle. The radial bearings are also used to guide the axial motions of the spindle. Since the spindle can make axial motions (within one revolution) it is possible to create nonrotationally symmetric products in a relatively simple way. To avoid undesired vibrations of the machine structure, as a result of the dynamic reaction forces, a counter mass has been applied. The coils of the spindle actuator are attached to this counter mass, whereas the permanent-magnetic circuit of the actuator is attached to the spindle. The counter mass is translated by a second voice coil actuator, which operates as the long stroke actuator (total axial motion range of the spindle is about 20 mm). By applying this concept, the spindle unit can take over the function of the axial slide of the lathe. This will lead to an increase of the stiffness of the structural loop between the tool and the product, an increased accuracy and a simplification of the machine concept with respect to the current precision lathes.

The axial position of the rotating spindle is measured by an interference grating system with a resolution of 5 nm. The required cylindrical phase grating was specially developed for this application. Two manufacturing techniques of the grating have been investigated: plasma etching and diamond turning. Both techniques appeared to be feasible. The grating on the prototype has been made by diamond turning because of the relative simplicity of this method.

The axial position control of the spindle is realised by a digital controller (based on a personal computer). This offers a high level of flexibility and gives the possibility

to correct for the reproducible errors in the measured axial position and velocity by software error compensation. The voice coil actuator of the spindle is combined with current control, in this way an ideal force actuator is realised (this means, a force can be generated between two objects without introducing any stiffness). This leads to a high level of linearity of the controlled system.

A prototype, based on the described concept, has been built and tested. The maximum axial error motions are equal to $\pm 0.01 \mu\text{m}$ (maximum fundamental error motion is equal to $\pm 0.003 \mu\text{m}$). The measured axial stiffness is about $1000 \text{ N}/\mu\text{m}$. The bandwidth of the controlled system is equal to 700 Hz . Test-products manufactured on the spindle showed optical surface quality ($R_a \leq 0.01 \mu\text{m}$). At higher axial velocity of the spindle the surface roughness increases as a result of discretisation effects, caused by the digital controller.

A patent application of the design and the corresponding method of making nonrotationally symmetric products has been made.

Contents

Summary	i
Contents	iii
1. Introduction	1
1.1 Spindles for precision diamond turning	1
1.2 Limitation of current precision spindles.....	3
1.3 Design objectives and contents of this thesis	8
2. Active axial spindle bearing based on a voice coil actuator	11
2.1 Minimizing the axial error motion	11
2.2 The actuator.....	15
2.3 The focus error sensor	18
2.4 Control system.....	20
2.5 Mechanical construction	22
2.6 Performance of the prototype.....	23
3. Design considerations for a spindle with axial motion control	27
3.1 Introduction	27
3.2 Limitations of the first prototype with respect to axial motion control.....	29
3.3 The position measuring system	31
3.3.1 Laser interferometer.....	33
3.3.2 Linear scales.....	36
3.4 The actuator configuration	42
3.4.3 Reducing the mass of the magnetic circuit.....	43
3.4.4 Improving the energetic efficiency.....	45
3.4.5 Reducing the reaction forces on the frame	48
3.5 The total concept of the spindle unit	52
4. Interference grating system for measuring the axial position of a rotating body	55
4.1 Introduction	55

4.2	Limits of accuracy	56
4.2.1	Pattern errors	57
4.2.2	Interpolation errors.....	59
4.3	Grating manufacturing methods.....	64
4.3.3	Diamond turning	64
4.3.4	Plasma etching	69
5.	Mechanical construction	77
5.1	The spindle	78
5.2	The aerostatic bearings.....	80
5.3	The countermass.....	83
5.4	The rotation measurement system.....	84
5.5	The countermass position sensor.....	87
5.6	The fixture of the bearing house.....	87
5.7	The position measurement system	91
5.8	The total construction.....	92
6.	Control system	95
6.1	Introduction	95
6.2	Control architecture.....	98
6.2.1	The spindle control	100
6.2.2	The computer system	103
6.2.3	The countermass controller.....	111
6.3	Practical limitations on the system performance.....	112
7.	Experimental evaluation	121
7.1	The prototype	121
7.2	Axial error motions	124
7.3	Dynamic behaviour	128
7.4	The interference grating system	132
7.5	The experimental lathe	140
7.6	Diamond turning tests	141
7.7	Discussion	147

8. Conclusions and recommendations	151
8.1 Conclusions	151
8.2 Recommendations	155
Bibliography	157
Appendix A: Frequency transfer of a sample and zero-order hold system	161
Appendix B: Specifications voice coil systems	165
Appendix C: Technical data of the etching experiments	167
Samenvatting	169
Dankwoord	171
Curriculum Vitae	173

1. Introduction

The most important characteristic of Precision Engineering is to increase the accuracy of equipment and products. The demand for increased accuracy is for a major part fed by the advanced miniaturisation of present day products. Assembling smaller products generally requires smaller manufacturing tolerances. Tolerances less than one micrometre are no longer exceptional. Another trend introduced by miniaturisation is increased complexity of the shape of the products. This is partially caused by integration of multiple functions in one product. Besides this, as in all other fields of production technology, Precision Engineering also has to deal with the general trend of reducing the costs of the products by reducing the production time. To realise an increase of the accuracy while avoiding an exceptional rise of the production costs, a multidisciplinary approach will be inevitable in many cases.

To continue the above mentioned trends, Precision Engineering focuses on the improvement of equipment and technology. Within the field of Precision Engineering many different production techniques are applied. One of these is precision diamond turning, using high precision lathes.

1.1 Spindles for precision diamond turning

During the last decades diamond turning has become a common technique to produce precision products such as lenses, lens moulds, mirrors, video scanners, air bearings etc. These products are machined on high precision lathes. Figure 1.1 shows a schematic representation of a precision lathe as used at the Philips Research Laboratories. On a granite base two slides with hydrostatic bearings are placed per-

pendicular to each other. In these bearings the moving part is separated from the stationary part by a thin film (about $30\ \mu\text{m}$) of high-pressure oil that flows continuously out of the bearing. The rotating spindle, which holds the product, is attached to the z-slide. On the x-slide one or more diamond tools are mounted. Both slides are driven by friction wheel drives. The positions of the slides are measured by a laser interferometer system or by linear scales and are numerically controlled. The shape accuracy which can be reached on these lathes is better than a few tenth's of a micrometre (depending on the dimensions and the shape of the products). The turned surfaces show an optical quality ($R_a < 10\ \text{nm}$).

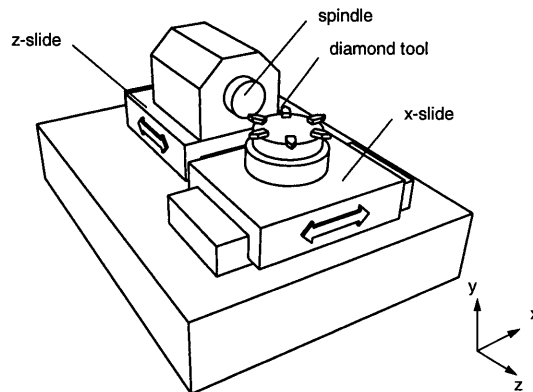


FIGURE 1.1 Schematic representation of a precision lathe

One of the main components of these lathes is the spindle. In most of the precision spindles, aerostatic bearings are applied for the radial as well as the axial bearing. This bearing type is similar to hydrostatic bearings with the oil replaced by pressurised air. The typical thickness of the air film is 5 to $15\ \mu\text{m}$. The main characteristic of these bearings is their very low friction. During the last decades, within the Philips Research Laboratories a number of these precision spindles have been developed for precision grinding and diamond turning applications. Figure 1.2 shows a typical example of such a spindle. Generally, these spindles are driven by a rope.

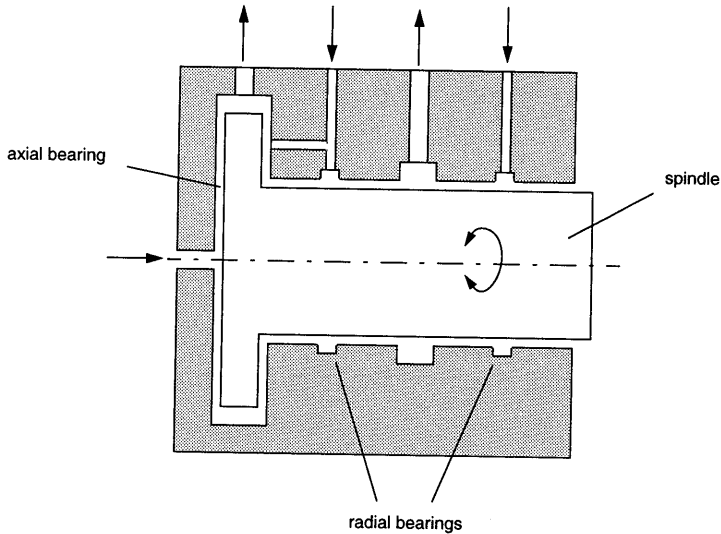


FIGURE 1.2 Cross section of a precision spindle with aerostatic bearings in radial and axial direction.

These spindles are among the best in the world. They are applied in research as well as in high volume applications, for the fabrication of products with sub-micron tolerances in dimension and form features and with surface roughness in the nanometre range. These high specifications of the products ask for very accurate spindles with very small error motions.

1.2 Limitation of current precision spindles

The currently used spindles are accurate enough to produce most of the actual products. But, considering the continuing miniaturisation of precision products, the limitations of the current spindles will soon be reached. As already mentioned, miniaturisation often leads to smaller tolerances of the products. For example in the field of optical data recording, there is a trend to increase the information density (bits per unit area). This can be realised by the application of light sources with shorter wavelengths (up to the UV-region) which asks for lenses with a shape accu-

racy better than $0.1 \mu\text{m}$. Especially for products which are made by face-turning (i.e. the feed of the tool is mainly in the direction perpendicular to the axis of rotation of the spindle) these small form tolerances are difficult to realise. Using current spindles with a rigid coupling between the axial and the radial bearing surfaces, the accuracy of the turned surfaces is mainly limited by the axial error motion of the spindle. This motion is caused by alignment errors of the axial bearing surfaces of the spindle and the bearing house with respect to the axis of rotation of the spindle (see figure 1.3). As a consequence, the spindle moves sinusoidally in axial direction once per revolution [1]. A surface turned on such a spindle will present a shape deviation, as shown in figure 1.3 (exaggerated). The amplitudes of these motions are measured at several precision spindles and vary from $0.02 \mu\text{m}$ [2] to $0.2 \mu\text{m}$ (personal observation). Another consequence of the axial error motion is the excitation of the machine frame by this motion, which can lead to undesired resonances in the machine structure. At the current lathes the spindle speed is limited by this effect.

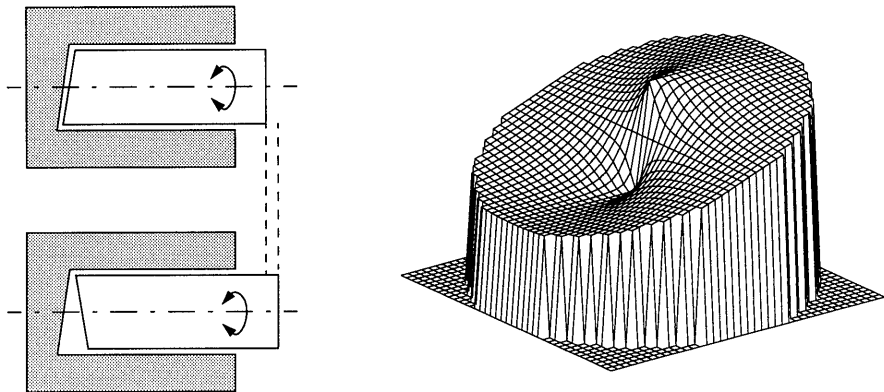


FIGURE 1.3 Alignment errors of the bearing surfaces cause axial error motions of the spindle (left), leading to a shape deviation of a face turned surface (right).

The other mentioned aspect of miniaturisation is the increased complexity of the shape of the products. A special group of products are the precision products with nonrotationally symmetric surfaces. Examples of these products are optical components such as beamshapers, wavefront correctors, off-axis optics, optical encoders,

astigmatic lenses or mechanical components such as spiral groove bearings. Figure 1.4 shows a nonrotationally symmetric surface of a beamshaper. This is a lens, used to transform the elliptical energy distribution originating from a laser-diode into a more circular distribution.

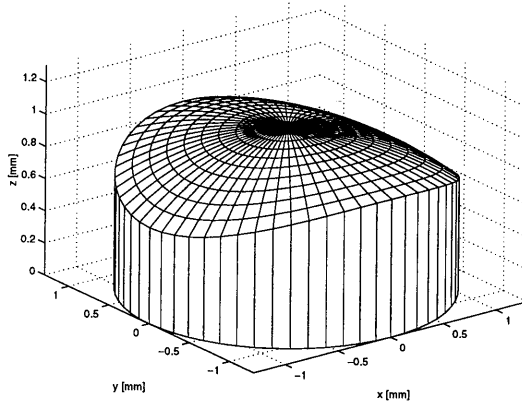


FIGURE 1.4 Nonrotationally symmetric surface of a beamshaper lens

Precision diamond turning can be applied for the manufacturing of nonrotationally symmetric surfaces with high geometric and surface accuracies. For this purpose, a relative motion between the diamond tool and the product has to be performed during one revolution of the spindle. This requires a translation of the product or the diamond tool with an extremely high resolution and accuracy, at a bandwidth significantly higher than the rotational frequency of the spindle. To manufacture a surface as presented in figure 1.4, the axial motion profile between the tool and the product during one revolution must be varied as a function of the radial position of the tool. This is illustrated in figure 1.5. This application makes high demands on the dynamics of the spindle.

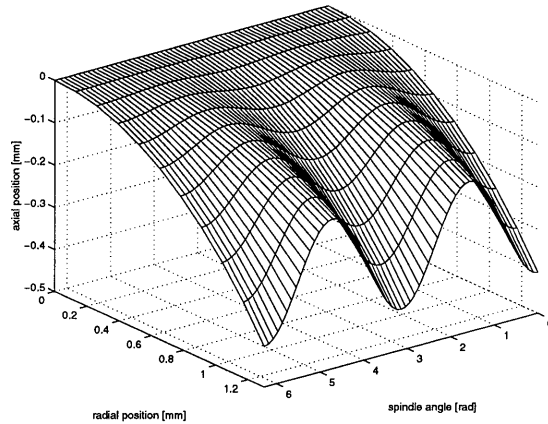


FIGURE 1.5 Axial position of the tool with respect to the product as a function of the spindle angle and the radial position of the tool, based on the beamshaper surface of figure 1.4

Within the Philips Research Laboratories two different techniques have been developed to produce nonrotationally symmetric surfaces by means of diamond turning. In the first technique the diamond tool is actuated, using a so called 'fast tool servo' (see also chapter 2). The bandwidth of the fast tool servo is about 1000 Hz. This technique is applied for the production of spiral groove bearings. However this technique is not suitable for the fabrication of nonrotationally symmetric surfaces for optical applications, since the surface roughness of the turned products is relatively high.

In the second technique, the rotating spindle (together with the product) is translated in axial direction within the radial aerostatic bearings. The spindle is driven in axial direction by a friction wheel drive. The drive is coupled to the rotating spindle by an aerostatic thrust bearing (see also chapter 2). This relatively weak coupling strongly limits the maximum bandwidth of the system to about 80 Hz. This technique is applied for the production of nonrotationally symmetric optics, especially for the production of astigmatic lenses. This type of lenses consists of a normal spherical lens shape and a cylindrical correction superimposed to it. To make these lens shapes the spindle has to perform axial displacements within one revolution with a

maximum amplitude of a few hundred micrometres and a minimum amplitude of about 10 nm (similar to figure 1.5).

A main disadvantage of the system which is driven by a friction wheel drive, is the non-linearity of the system for controlled motions in the sub-micron range. Figure 1.6 shows the closed loop frequency response (gain and phase) of a friction wheel drive, for different displacement amplitudes. For an ideal linear system the gain would be 1 and the phase shift would be 0 degrees, within the bandwidth of the system, for all setpoint amplitudes. Figure 1.6 shows clearly a decrease of the gain of system and an increase of the phase shift for decreasing setpoint amplitudes. This non-linearity of the controlled system is mainly caused by the static friction in the friction wheel drive. When cutting a nonrotationally symmetric surface as presented in figure 1.4 this will lead to shape deviations of the surface, as a result of the additional phase shift and amplitude reduction of the axial motion profiles with small amplitudes (close to the centre of the lens).

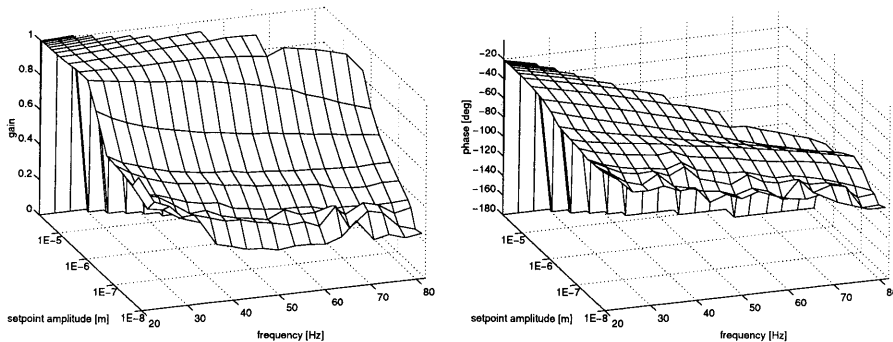


FIGURE 1.6 The closed loop frequency response (gain and phase) of the system, driven by a friction wheel drive, measured at various amplitudes of the setpoint signal

To minimize the adverse effects of these non-linearities, a feedforward correction technique has been applied. Therefore the input signal of the position controlled system is corrected for the non-linearities shown in figure 1.6. This correction on the input signal is calculated off-line.

1.3 Design objectives and contents of this thesis

Within the mechanical department of the Philips Research Laboratories it has been recognised that the above mentioned limitations of the current spindles have to be shifted to fulfil the future requirements on precision products, specially in research application. To realise this, a design project has been formulated. The major objective of this project is the development a new precision spindle, which is distinguished from the current spindles by a reduction of the axial error motions, by an increased axial stiffness and by offering the possibility to create nonrotationally symmetric surfaces. The performance with respect to other aspects should at least be as good as the current spindles.

The design project is a co-operation between Philips Research Laboratories and the Eindhoven University of Technology. The project has been carried out within the Mechanical Engineering Department of the Philips Research Laboratories Eindhoven, within the group 'Complex Systems'. The project is supported by the section Precision Engineering from the Department of Mechanical Engineering of the Eindhoven University of Technology.

The total project has been split into two parts. The first part of the project was focused on reduction of the axial error motions and the increase of the axial stiffness of a precision spindle, by applying an active axial spindle bearing. For this part of the project the following design objectives were formulated.

Design of an active axial spindle bearing with:

- a maximum axial error motion of ± 10 nm
- axial noise (non repeatable error motions) smaller than ± 5 nm
- a minimum axial static stiffness of $100 \text{ N}/\mu\text{m}$
- a surface roughness of the finished surfaces in copper smaller than 10 nm (Ra)
- a minimum number of precision components

A brief description of the prototype of a spindle which meets these requirements will be given in chapter 2, an elaborate description to this prototype can be found in [3].

Besides the fact that the axial position control of the spindle fulfils the specified bearing function, the chosen concept can also be used as a starting-point for a new type of precision lathe. By this lathe nonrotationally symmetric surfaces can be generated by controlled axial motions of the spindle during a revolution of the spindle. Furthermore, a spindle which can perform axial motions, offers the opportunity to eliminate the z-slide of the lathe, since the relative axial motion between tool and product can now be realised by controlled axial motion of the spindle. This will lead to an increased stiffness of the machine's structural loop while the production costs of the machine will decrease. In general this concept will result in a simplified and more accurate precision lathe.

For these reasons the second part of the project has been focused on the development of an axial motion control of the spindle. The spindle has to be able to perform small axial translations (maximum amplitude: 500 μm) during one revolution to create nonrotationally symmetric surfaces. The specifications of the spindle are focused on the production of nonrotationally symmetric optical surfaces (e.g. astigmatic lenses). These surfaces will have a rather 'smooth' shape, which implies relative low spatial frequencies. For example the surface of an astigmatic lens requires a motion of the spindle which is almost equal to a sinusoidal motion with a frequency equal to the double rotational frequency of the spindle (see also chapter 6). Besides the axial motions within one revolution, the spindle should be able to perform a 'slow' axial movement of several millimetres to realise the rotationally symmetric base shape of the products. In general the axial dimensions of the intended products are limited to a few millimetres. Besides the requirements which were mentioned for the first part of the design project, the next goals have been formulated:

- axially controlled motions of the spindle over a minimum stroke of 5 mm
- axially controlled motions of the spindle with a resolution of 5 nm
- axially controlled motions of the spindle within one revolution, synchronised with the rotation of the spindle, with a maximum amplitude of 250 μm (peak-valley: 500 μm) for harmonic displacements at 30 Hz.
- a maximum spindle speed of 3000 rpm
- thermal stability: axial drift within 5 minutes smaller than 0.1 μm at a spindle speed of 3000 rpm or at a harmonic modulation at 30 Hz at an amplitude of 100 μm .

- maximum mass of the product (fixture included) of 500 g.

To come to a concept of a spindle with an axial motion control, emanating from the concept with an active axial bearing, many design considerations have to be taken. The most important of these will be discussed in chapter 3. The total design of a prototype which meets the above mentioned requirements can be split into three sub-systems: The position measuring system, the mechanical construction and the control system. The design and realisation considerations of these sub-systems, which will lead to the final prototype of the spindle, are separately presented in chapter 4, 5 and 6. In chapter 7 the experiments, which are carried out to evaluate the performance of the prototype, and their results will be discussed. Finally, in chapter 8 the conclusions of the design project are presented together with recommendations for future developments.

2. Active axial spindle bearing based on a voice coil actuator

The first part of the design project was focused on the development of an improved axial bearing for precision spindles. The major objectives of this part of the project can be summarised as follows: the axial error motions had to be reduced to about 10 nm whereas the axial stiffness of the spindle had to be increased to more than 100 N/ μm . In this chapter a brief description will be given of the development of a new type of axial spindle bearing which can fulfil these requirements. An elaborate description of the specification, the alternatives, the design considerations and the resulting prototype have been published separately [3].

2.1 Minimizing the axial error motion

The characteristic axial error motion of the currently used spindles is mainly caused by alignment errors of the bearing surfaces of the spindle and the bearing housing. In chapter 1 it has been illustrated that these axial error motions lead to form deviations of the turned surface. The alignment errors of the axial bearing planes can be reduced by applying more accurate manufacturing techniques, but the practical and economic limits seem to be reached here. Some alternatives will be discussed next.

Point bearing

A mechanical option to minimize axial error motions, is to apply a point bearing which coincides with the axis of rotation of the spindle (see figure 2.1). The remaining error motion (Δz) is mainly determined by the alignment error (α) of the bearing plane with respect to the spindle axis and the eccentricity (e) of the point bearing with respect to the axis of rotation. For small values of the alignment error ($\alpha \ll 1^\circ$), the remaining axial error motion Δz can be expressed as:

$$\Delta z = 2 \cdot e \cdot \alpha \quad (2.1)$$

Since the eccentricity e , and the alignment error α will be small, the axial error motion is reduced to a second order deviation. However, a practical problem of the application of a point bearing is the very low axial stiffness.

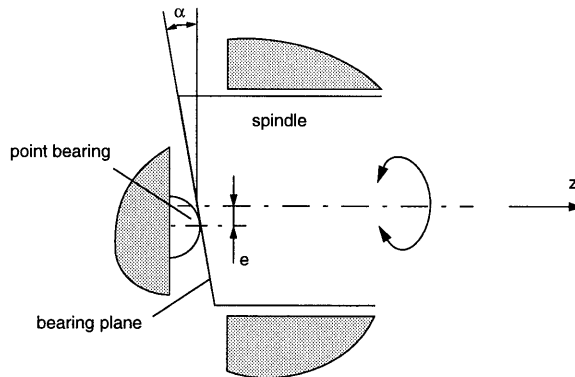


FIGURE 2.1 Schematic representation of an axial point bearing

Self-adjusting thrust bearing

Higher stiffness, combined with small error motions, can be achieved by the use of an aerostatic thrust bearing which is coupled to the fixed world by a ball joint. The ball joint offers the thrust bearing the opportunity to adjust for alignment errors of the axial bearing plane of the rotating spindle. If the centre of rotation of the ball joint coincides with the intersection point of the rotation axis and the bearing surfaces, no axial error motion will occur theoretically. Within the Philips Research

Laboratories a similar bearing configuration has been applied successfully [4]. In a test setup the axial error motion has been reduced to about 10 nm. An attendant benefit of the mechanical disconnection of the radial and the axial bearing, is the possibility to move the rotating spindle in axial direction within the radial air bearings. Therefore the ball joint has to be attached to an actuator. In this case the radial bearing can adopt the function of the axial slide of a lathe. This results in a simplified and improved concept of a precision lathe: since the z-slide can be eliminated the number of geometric errors in the machine will reduce (e.g. the alignment error of the z-slide relative to the rotation axis of the spindle will be eliminated), whereas the stiffness of the structural loop will increase.

Despite an increased stiffness of this concept with respect to a point bearing, the axial stiffness is still relatively low. This is mainly caused by the relatively low stiffness of the ball joint. In combination with the axial thrust bearing the total axial stiffness is approximately 25 N/ μm .

Active axial position control

A very different concept arises if it is possible to measure the relative position between the cutting tool and the product during the cutting process and at the same time adjust this position, using a position measuring system, an actuator and a control system. In principal there are two ways to realise this: adjustment of the tool position or adjustment of the product position.

Adjustment of the tool position is a known technique. In literature several types of so-called fast tool servos have been described. Most of these fast tool servos are based on piezoelectric actuators. They are applied for the manufacturing of nonrotationally symmetric surfaces like spiral groove bearings or wave front correctors [5,6,7,8]. Besides this, fast tool servos are also used to correct for radial error motions of a spindle and to improve the product accuracy in this way [9,10]. In a similar way, a fast tool servo could be applied to compensate for axial error motions. Therefore the relative axial position between the cutting tool and the product needs to be known at every moment during the cutting process. Because of the difficulty of a direct measurement of this relative position, the relative positions of the product and the tool with respect to a fixed frame need to be measured using linear displacement sensors. The accuracy of this configuration, with respect to the axial error

motions, depends mainly on the accuracy of the used sensors and their ability to measure the axial position of a rotating object.

In a controlled system with position feedback, an infinite static stiffness can be achieved at the point where the displacement is measured (see also Chapter 6). This means, if it is possible to measure directly the relative position between the product and the tool an infinite static stiffness between these components can be reached. However in most of the practical applications it is not possible to measure directly the translations of these two components. In that case the maximum total static stiffness depends on the mechanical stiffness between the points where the displacements should be measured (at the tool tip and at the product) and the point where they are measured actually. The dynamical stiffness is mainly determined by the bandwidth of the controlled system. In practice, the bandwidth of a controlled system is mostly limited by the dynamical behaviour (resonances) of the mechanical system.

A major advantage of a fast tool servo is the relatively low moving mass. This means, the bandwidth of the system can be relatively high. An important disadvantage of the use of a fast tool servo to correct for axial error motions is the fact that additional bearings are needed to guide the motions of the tool servo. These additional bearings will introduce a loss of stiffness of the structural loop between the tool and the product.

The second way to correct for axial error motions by adjusting the position between tool and product is by adjustment of the product position. There are three alternatives to realise this:

- actuating the complete axial slide
- actuating the spindle within the radial bearings
- actuating the product with respect to the spindle

An advantage of the first alternative, where the complete axial slide is actuated, is the fact that no additional actuators and guides are necessary. However a very important disadvantage of this method is the high moving mass. Dynamic actuation of such a high mass asks for very high actuation forces and as a result, also leads to

very high reaction forces on the machine frame, which will cause undesired vibrations.

The second alternative is based on the fact that, using an aerostatic radial spindle bearing, the spindle can be translated in axial direction within the radial bearings. In this case the radial bearings serve as an axial guiding for the spindle. If the translations in axial direction, necessary to produce the products, are small with respect to the axial dimensions of the radial bearing (e.g. face turning operations) the total axial displacement between product and tool can be realised in this way. As stated before, this will lead to a simplified and improved machine-concept. The total number of bearings will decrease since the axial slide of the lathe can be eliminated. This will cause an increase of the stiffness of the structural loop between the tool and the product. Besides, the cost of the lathe can decrease. This concept has a considerably smaller moving mass than the concept were the complete slide is actuated but it has a larger moving mass than the concept with a fast-tool-servo. To realise this concept an actuator is needed which drives a rotating spindle in axial direction and a sensor which measures the axial position of a rotating spindle.

In the third alternative, the product is translated in axial direction with respect to the spindle. Therefore an actuator and an additional guide need to be implemented in the rotating spindle. An advantage of this alternative is the low moving mass. An important disadvantage of this concept is the necessity of sliding contacts to transmit the measurement and control signals to the rotating spindle. This will introduce unwanted friction and noise to the system.

Considering the mechanical simplicity and the expected good properties of the concept, the concept of a translating spindle within the radial bearing will be applied. In this concept the axial position of the spindle is controlled by an actuator. An attendant advantage of this concept is the possibility to generate nonrotationally symmetric face-turned surfaces on a relative simple way, by performing controlled axial motions of the spindle during each revolution of the spindle.

2.2 The actuator

The actuator which will be applied must have the ability to displace the rotating spindle in axial direction with respect to the fixed world. Taking in consideration the

requirement of a maximum error motion of 10 nm the resolution of the actuator has to be significantly smaller. In this case a resolution smaller than 1 nm is desired. This makes high demands on the actuator with respect to a minimal backlash and friction.

An actuator which could meet the above mentioned requirements is a piezoelectric actuator. These actuators generate a displacement when a voltage is applied across them. This means an additional bearing element (e.g. an aerostatic thrust bearing) must be used to transmit this displacement to the rotating spindle. The relative low stiffness of such an element in the force loop of the controlled system, will strongly limit the maximum bandwidth of the controlled system. Therefore, an actuator that generates a force which acts directly on the spindle is preferred. This can be realised by use of electromagnetic forces. An actuator which is based on this principle is a *voice coil actuator*. This actuator consists of a coil and a permanent-magnetic circuit (see figure 2.2). In this configuration, a current applied to the coil in the air gap instantly produces a force on the coil. So, the system behaves like 'pre-loaded'. Because of the rotationally symmetric shape of a voice coil actuator, it can easily be used to drive a rotating spindle in axial direction.

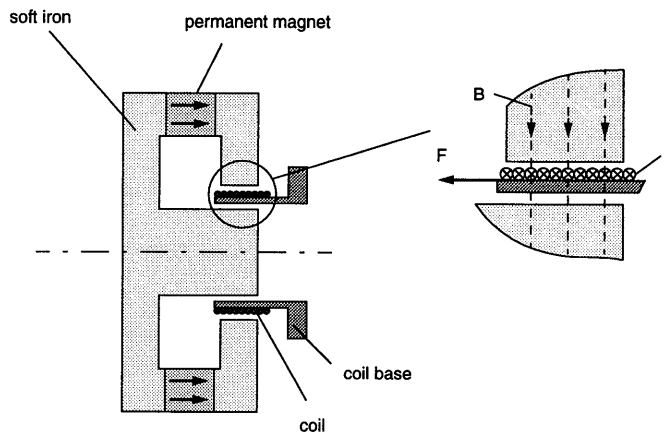


FIGURE 2.2 Schematic representation of a voice coil actuator

The force (F) which acts on the coil as a result of the a current (I) in the windings can be calculated with the *Lorentz formula*:

$$F = (I \times B) \cdot l \quad (2.2)$$

In this formula B is the magnetic flux density in the air gap of the permanent-magnetic circuit. l is the total length of the turns within the air gap of the magnetic circuit. A reaction force, with equal amplitude but opposite directed, will act on the magnetic circuit. For small displacements of the coil with respect to the magnetic circuit, the length l can be considered as a constant (see also chapter 3). As long as the magnetic flux density in the air gap B is constant, the generated force only depends on the current I through the coil. A fundamental advantage of a voice coil actuator is the direct transmission of a force without any mechanical contact, so there will be no mechanical hysteresis in the actuator.

An important advantage of a voice coil actuator is the possibility to transfer forces very 'rigidly' to the moving part, while the static part is mounted very 'weakly'. Since the force transfer is based on an electromagnetic field and not on a mechanical contact, only the stiffness of the transfer of the driving force to the moving part determines the stiffness and the bandwidth of the controlled system. For instance, if the magnetic circuit is mounted rigidly to the moving part and the coil is mounted weakly to the 'earth', the force which acts on the both parts will not be affected by the elastic deflection of the coil as long as the current in the coil and the number of windings within the air gap remains constant. This property can be used to reduce the dynamic reaction forces on the machines frame, by mounting the coil on a counter-mass which is 'weakly' coupled to the frame (see also chapter 3).

When applying a voice coil actuator either the magnetic circuit or the coil must be attached to the moving spindle. In general a minimal mass of the moving part is desired. Since the coil has generally a lower mass than the magnetic circuit, attaching the coil to the moving part would be preferred. However, in that case sliding contacts would be needed to energise the coil. These sliding contacts would introduce undesired friction to the spindle motions, which would cause non-linearities of the system and thus decrease the system performance. Therefore the magnetic circuit is attached to the spindle and the coil is mounted on the frame. Furthermore, using this configuration the heat production at the spindle will be considerably lower than using the configuration with the coil attached to the moving spindle.

For several reasons the moving mass has to be minimised. Therefore *rare earth* magnets are applied in the magnetic circuit. These magnets have a very high magnetic energy per volume. They are used in applications where high magnetic strength and small sizes are needed. The main criteria used for the design of the voice coil actuator are a minimum mass and minimum heat dissipation [3].

2.3 The focus error sensor

The accuracy of the axial position measurement has to be better than the specified axial position accuracy of the controlled spindle. The position of the rotating spindle is measured by an analog optical sensor, a so called focus error sensor. This type of sensor is based on the same optical principles as used in CD-players to maintain the optimum distance between the disc and the focusing lens [11]. Figure 2.3 gives a schematic representation of the applied focus error sensor and shows the output signal of the sensor as a function of the mirror position with respect to the focus point of the sensor (for a more elaborate description see [3]). A displacement of the target surface, in the direction of the optical axis of the system, causes a shift of the image spots on the photo-detectors. This shift leads to a change in the output signals of the detectors. Several types of this sensor are available with different sensitivity, measuring range, focal length etc. depending on the used lenses.

Typical advantages of a focus error sensor with respect to this application are:

- A resolution below 1 nm can be reached
- Within the measuring range a linear relation between the displacement and the output signal (see figure 2.3.b)
- Measurement without any mechanical contact
- Insensitive for magnetic fields
- High bandwidth (100 kHz)
- Known technology within Philips

Typical disadvantages of this sensor with respect to this application are:

- Due to the small spot size (a few micrometre), the sensor is sensitive for dust on the mirror surface or other local effects (e.g. scratches)

- The measurement range is limited to about 5 μm (if a resolution of 1 nm must be achieved)

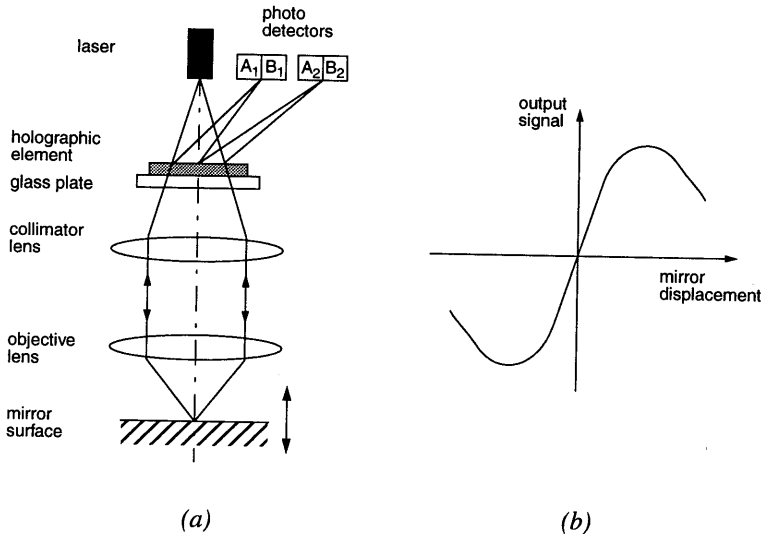


FIGURE 2.3 a. Scheme of the optics of the applied focus error sensor
b. Output signal of the sensor versus the displacement of the mirror

If a focus error sensor is used to measure the axial displacements of the spindle, the appearing measurement errors depend on the eccentricity e of the optical axis of the sensor with respect to the rotation axis of the spindle and by the misalignment α of the normal of the mirror plane with respect to rotation axis of the spindle. This measurement error can also be calculated by equation 2.1. In the prototype a mirror is mounted with a maximum alignment error α of about $5 \cdot 10^{-5}$ rad. The maximum eccentricity e of the optical sensor is 0.02 mm. This implies maximum theoretical error motion of 2 nm.

However, the focus error sensor is also sensitive for rotations of the mirror about an axis perpendicular to the measurement direction of the system. This sensitivity is higher when the numerical aperture of the objective lens is smaller [12]. Experiments have shown that for alignment errors larger than 10^{-4} rad the measurement

errors were considerably higher than could be expected from equation 2.1. For these experiments a point bearing which coincides with the axis of rotation of the spindle has been applied (as presented in figure 2.1). By an optimum alignment of the point bearing, the axial error motion could be minimised to about 10 nm. The spindle was now rotated while the axial motions of the spindle were measured by a focus error sensor. If the mirror was tilted over approximately 1 mrad, the measured axial displacements of the spindle appeared more than 500 nm. This was more than a factor 10 larger than could be expected from equation 2.1. Therefore the alignment of the mirror needs special attention.

2.4 Control system

As described in paragraph 2.1, a concept is chosen of a spindle with aerostatic bearings in radial direction. In axial direction the spindle can translate almost frictionless, guided by the radial air bearings. The axial bearing function is realised by a voice coil actuator, a position sensor and a control system. Figure 2.4 shows the block diagram of the controlled system [3]. The actuator combined with the control system have to keep the spindle at a fixed position, despite disturbance forces which act on the spindle. These disturbance forces will mainly be caused by the cutting process. The disturbance forces will have static as well as dynamic components.

Disturbance forces which act on a free (uncontrolled) mass will lead to displacements of that mass and so introduce position errors. Considering a sinusoidal disturbance force, the resulting position error will be inversely proportional to the square of its frequency. This means a free mass behaves like a low-pass filter for disturbance forces. The power spectrum of the cutting forces introduced by finish-turning shows a static component and dynamic components. The dynamic components with frequencies above 50 Hz are too small to introduce position errors of a free moving spindle with a mass equal to (or larger than) 2 kg, larger than 1 nm. Position errors caused by static forces and dynamic forces with 'low' frequencies have to be suppressed by the controller. Using an integrator in the position controller, the errors caused by static forces will be reduced to zero. This means, theoretically the static stiffness of the system will be infinite [13]. The suppression of the position errors caused by dynamic disturbance forces mainly depends on the bandwidth of the con-

trolled system. Therefore the design of the system was focused on a maximum bandwidth.

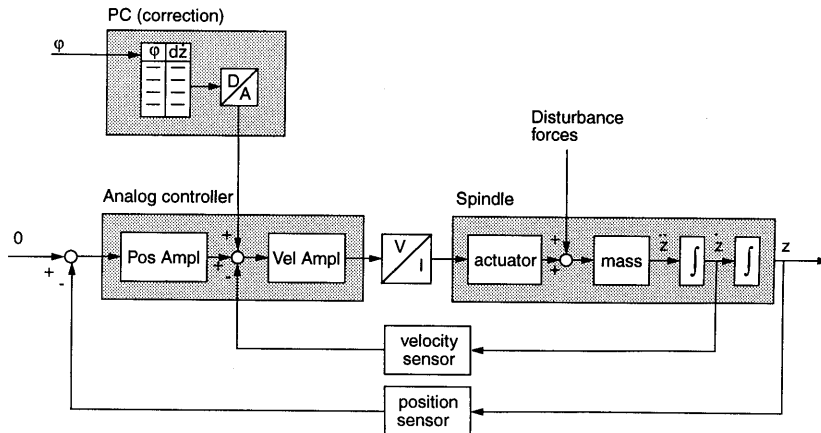


FIGURE 2.4 Block diagram of the controlled system

To obtain a high bandwidth, velocity feedback was applied along with position feedback, which results in the cascade connection as presented in figure 2.4. The velocity information is obtained from an additional voice coil system. In a voice coil a counter-electromagnetic force (emf) is generated, which is proportional to the relative velocity between the coil and the magnetic circuit (see also paragraph 6.2.1). This counter-emf is used as an analog velocity signal. This velocity signal is much more reliable than the signal which can be obtained by differentiation of the position signal. The differentiated position signal would be strongly disturbed by 'high-frequency' noise in the position signal.

However, the velocity signal obtained by the second voice coil can also be subjected to distortions. For example the current in the actuator coil will generate a magnetic field. If the coil of the velocity sensor is subjected to this magnetic field, changing currents in the coil will introduce cross-talk on the velocity. The coil of the velocity sensor has to be shielded from this type of distortions. Furthermore, an eccentricity of the magnetic circuit of the velocity sensor combined with a misalignment of the coil of this sensor, will introduce an error in the velocity signal. This error is a sinu-

soidal signal per revolution of the spindle with an amplitude proportional to the angular speed of the spindle. In the controlled system, this error signal will lead to a harmonic axial error motion of the spindle. Since it is a systematic error, it is possible to correct for this error. Therefore a sinusoidal correction signal is generated by a computer as a function of the spindle angle and the angular speed (see also chapter 5).

To obtain a high static stiffness of the system, an amplifier with dynamical properties (PI) is applied in the velocity loop.

2.5 Mechanical construction

Figure 2.5 shows a schematic representation of the prototype of the spindle with the active axial bearing, as it was developed in the first part of this research program [3].

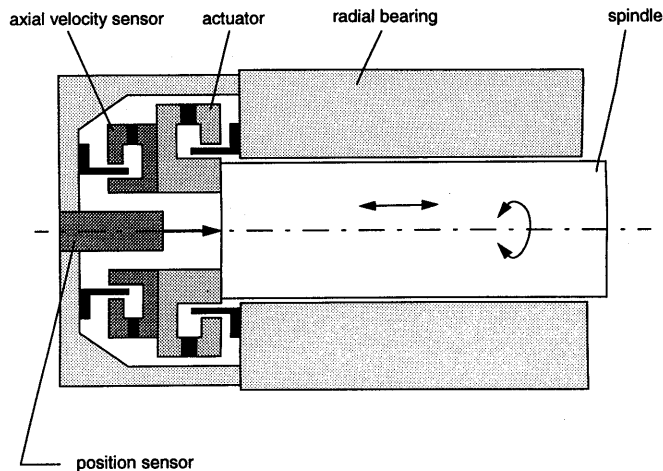


FIGURE 2.5 Schematic representation of a spindle with an axial bearing based on a voice coil actuator

As mentioned before the spindle can translate in axial direction within the radial aerostatic bearings. The applied bearings contain small inlet holes and conical air gaps. This bearing type has been chosen because of a relative high radial stiffness. The radial bearing is fixed to the z-slide of the lathe by a bearing support. The posi-

tion sensor and the coil of the velocity sensor are attached to this bearing support. Both are aligned with respect to the axis of rotation of the spindle. The permanent-magnetic circuits of the actuator and the velocity sensor are mounted on the spindle. The rotation angle of the spindle is measured by an optical measuring system which was specially made for this application. This measuring system will be described in paragraph 5.4.

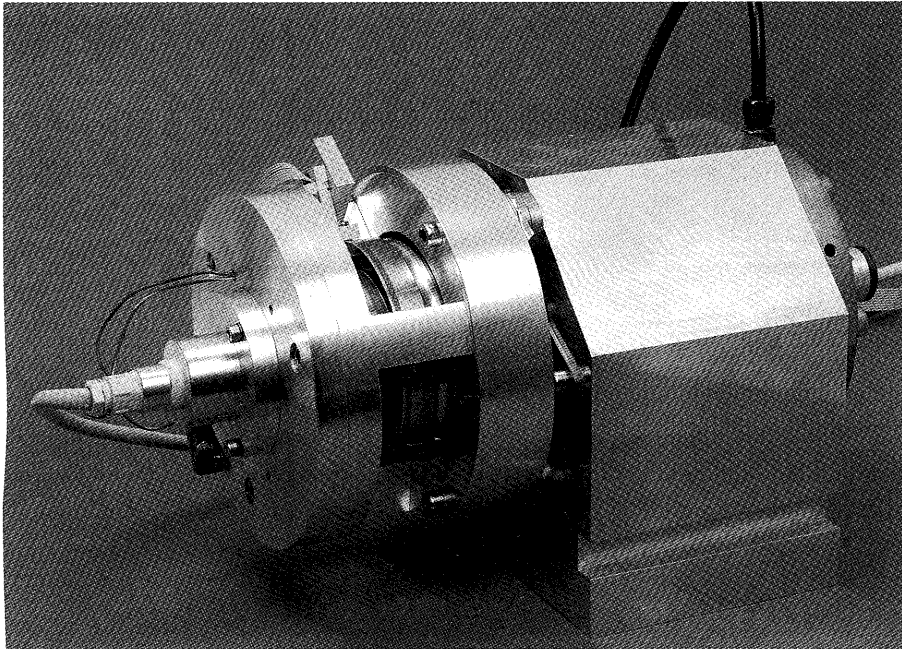


FIGURE 2.6 Photograph of the first prototype

2.6 Performance of the prototype

To evaluate the performance of the prototype with respect to the axial error motions, the error motions of the spindle are measured by a second focus error sensor at the front of the spindle. For this test measurement a mirror is mounted at the front side of the spindle, having an alignment error smaller than 10^{-4} rad with respect to the rotation axis. The maximum eccentricity of the sensor with respect to the axis of rotation is about 0.02 mm. Using equation 2.1 this yields a maximum measurement

error of about 4 nm. Figure 2.7 shows the measured axial displacement of the spindle as a function of the spindle angle. The measured axial error motions of the spindle are about $\pm 0.01 \mu\text{m}$.

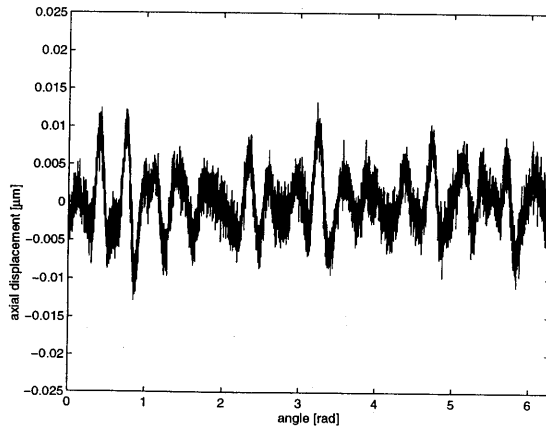


FIGURE 2.7 Measured axial error motion at 1200 rpm

As mentioned before the theoretical static stiffness of the controller is infinite (due to the integrating action of the controller) for disturbance forces smaller than 50 N. For forces higher than 50 N the static stiffness is almost zero, since the current in the coil (and so the force also) is electronically limited. In the chosen concept, the controlled infinite static stiffness is only operative at the back side of the spindle, where the reaction force acts and the displacement is measured. The static stiffness at the front side of the spindle is determined by the mechanical stiffness of the spindle. The measured axial stiffness of the spindle is about $1000 \text{ N}/\mu\text{m}$. This means that the axial static stiffness of this system is more than a factor 10 higher than that of the current precision spindles.

Figure 2.8 shows the bode plot of the closed loop transfer function of the system. The bandwidth of the system (0 dB crossing of the open loop) is about 200 Hz. From experiments it appeared that a further increase is mainly limited by mechanical resonances in the frame of the lathe. These resonances were excited by the reaction forces of the voice coil actuator.

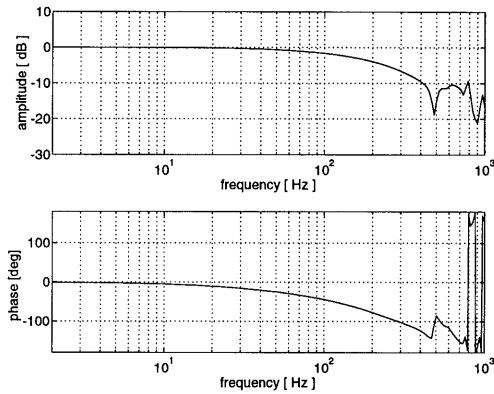


FIGURE 2.8 Bode plot of the closed loop of the controlled system

To evaluate the attainable surface quality of turned surfaces, cutting experiments have been carried out on copper and brass. The finished surfaces have an optical quality, Ra-values of 10 nm have been reached.

3. Design considerations for a spindle with axial motion control

In the previous chapter a concept has been presented of a spindle with an active axial bearing. With respect to current spindles the axial error motions are reduced whereas the axial stiffness has been increased. Since the axial position of this spindle is controlled by an actuator, this concept can be extended to an active axial motion control of the spindle. The realisation of an axial motion control offers the opportunities to develop a new and improved concept of an ultra precision lathe, which can also be used for the production of nonrotationally symmetric products. In this chapter the design considerations will be discussed which were made to realise a spindle with axial motion control, emanating from the spindle concept as described in chapter 2.

3.1 Introduction

In the case of an axial motion control, the spindle will be translated in axial direction (during rotation), guided by the radial aerostatic bearings. The development of such an axial motion control of the spindle serves a double purpose:

First, the axial motion control of the spindle can adopt the function which is currently performed by the z-slide of a lathe. Realising the z-motion in this way has

certain advantages: the direction of the z-translation will automatically coincide with the axis of rotation of the spindle, whereas in the old concept alignment errors will always be present due to the limited alignment accuracy of the spindle with respect to the z-slide. An other advantage of the elimination of the z-slide, is the increase of the radial stiffness between the product and the frame, because generally a slide is a relatively weak element in the total structural loop of a lathe. Further, the costs of a lathe will decrease by elimination of one of the slides. However, in this new concept the range of the axial motion is limited more than in the conventional concept of a lathe with a z-slide, because the radial stiffness at the nose of the spindle will decrease strongly when the protruding length of the spindle increases. This is illustrated in figure 3.1, where the dimensionless radial stiffness at the nose of the spindle is plotted versus the dimensionless protruding length. Both radial bearings are considered as linear springs with equal stiffness c .

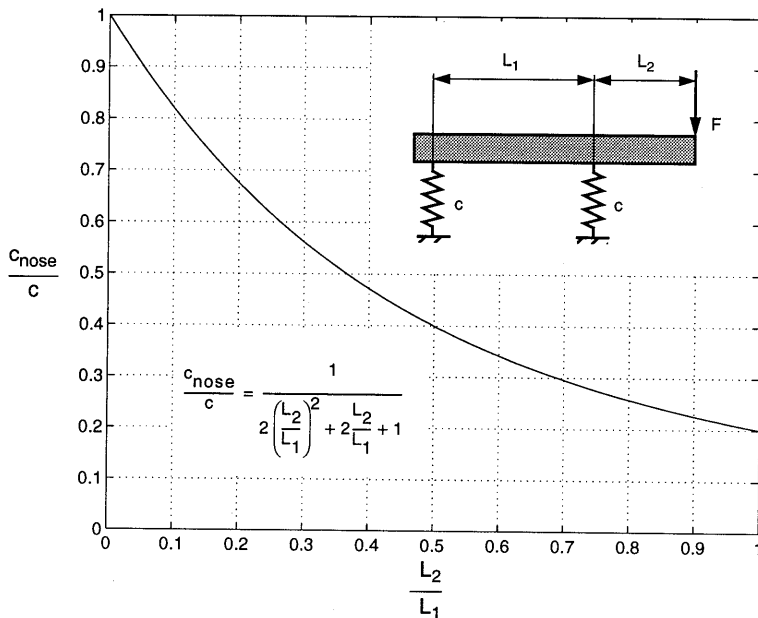


FIGURE 3.1 Dimensionless stiffness at the nose of the spindle versus the dimensionless protruding length

Because the spindle will mainly be used for the production of optical components with small dimensions in axial direction, the maximum protruding length will be relatively small. For the majority of the products the axial displacement between the product and the tool during the cutting process is smaller than 5 mm. However, in practical application it will be desirable to have a larger displacement range, to obtain more flexibility and convenience in the setting of the diamond tools on the x-slide. For this reason the desired displacement range of the system is specified at 20 mm. The accuracy and the resolution of these axial motions of the spindle must be equal to or better than those of the current z-slide of the precision lathes. This means an accuracy of about 0.1 μm and a resolution of 0.01 μm or even smaller. The velocity of these motions will be low ($< 0.1 \text{ mm/s}$), therefore these axial motions will be called 'quasi static' motions.

The second purpose of an axial motion control of the spindle is to create the opportunity to make products which are nonrotationally symmetric, such as astigmatic lenses, beamshapers, off-axis optics etc. To manufacture these products, the spindle has to perform rapid axial motions which must be synchronised with the rotation of the spindle. The required range of these fast motions is limited to a few hundred micrometres. These relatively fast motions will be called 'dynamic' motions. For most of the intended products the nonrotationally symmetric shape is superimposed on a rotationally symmetric basic shape (e.g. a spherical surface). This means the 'dynamic' motions must be superimposed on the 'quasi static' motions.

If the proposed spindle concept could be realised, it would be a starting point for a new generation of precision lathes. These lathes would reach a higher accuracy, using a minimum number of precision components. The main specifications of the new concept have already been presented in chapter 1.

3.2 Limitations of the first prototype with respect to axial motion control

The prototype described in chapter 2 shows very good properties with respect to axial stiffness and the axial error motions. Therefore, in the new concept with motion control, the basic principles of the concept will be maintained for as far as possible. However, there are some limitations of the first prototype with respect to an extension to axial motion control. These limitations will be discussed next.

In the first prototype a focus error sensor is used to measure the axial position of the spindle. This analog position sensor will be unsuitable for measuring the position of a spindle with an axial motion control, since the measuring range of this sensor is limited to about 10 μm . In general, the measurement range of an electronic analog position sensor is limited by the signal to noise ratio of the sensor and the applied electronics. A maximum ratio of 10^4 to 10^5 can be reached, depending on the applied electronics and the required bandwidth. Since a resolution of a few nanometres is necessary (to achieve the required surface accuracy), the maximum measurement range when applying an analog sensor will be limited to about 100 μm (in an optimum situation). In the new concept a measuring range of at least 5 mm is required, whereas a measuring range of at least 20 mm is desired (see paragraph 3.1).

An other limitation of the first prototype with respect to axial motion control, is the limited stroke of the applied voice coil actuator (maximum 2 mm). For larger displacements of the magnetic circuit, the force factor of this actuator will no longer be constant, since the number of turns within the air gap decreases. This will cause non-linearities in the system. Mechanically the stroke of the actuator is limited to 5 mm. Increasing the maximum stroke of the actuator by simply scaling up the current concept of the actuator has several disadvantages. The energetic efficiency will be relatively low, since the resistance and the self inductance will increase proportionally to the length of the coil. Besides, the moving mass will increase by scaling up the current concept of the actuator.

The bandwidth of the position loop of the described prototype is restricted to 200 Hz by the mechanical resonances of the machine frame, which is excited by the reaction forces of the voice coil actuator. A higher bandwidth is desired to obtain minimal axial position errors of the spindle during nonrotationally symmetric cutting. Besides, actuating the spindle at high frequencies leads to a considerable increase of the reaction forces on the frame. For rotationally symmetric cutting the actuator has only to compensate for the axial cutting forces which are limited to a few Newton. However, during nonrotationally symmetric cutting the actuator has to generate also the acceleration forces on the spindle, which can be considerably larger. Figure 3.2 shows the amplitude of the acceleration forces on a spindle (mass: 2 kg) for sinusoidal motions as function of their frequency and amplitude. These large dynamic (reaction) forces can lead to undesired vibrations of the frame. To prevent this and to

obtain a higher bandwidth of the system either the dynamical behaviour of the frame has to be improved or the reaction forces of the voice coil actuator have to be isolated from the frame.

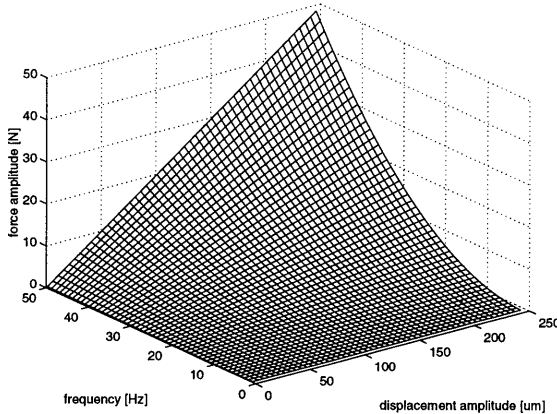


FIGURE 3.2 Amplitude of the driving forces on the spindle ($M = 2$ kg) versus the frequency and the amplitude of the dynamic (sinusoidal) motions

From the previous it can be concluded that the main limitations of the first concept, with respect to an axial motion control, are mainly related to the position measuring system and the actuator configuration. In the next paragraphs some alternatives will be discussed

3.3 The position measuring system

An important problem in realising a spindle with an axial motion control is the absence of an appropriate position measuring system. No commercially available system is known, which measures the axial position of a rotating body and meets the required high specifications with respect to accuracy, resolution and measuring range. For this reason, a dedicated position measuring system has to be developed. Since the development of a completely new position measuring system will take too much time, the system has to be based on a commercially available system by preference.

The required specifications of the position measuring system will be considered first:

- The system has to be capable of measuring the *axial position of a rotating body*.
- The *resolution* of the system has to be 5 nm or smaller. The form accuracy as well as the surface accuracy of a turned product are partly limited by the resolution of the position measuring system. In general the position accuracy of a controlled system can never be better than the resolution of the position measuring system.
- The required *measuring range* of the system is 5 mm. However, as discussed in paragraph 3.1, the desired measuring range is a least 20 mm.
- The requirements with respect to the *accuracy* of the system can be split into two parts: The first part is related to the axial error motion of the spindle. Since the maximum error motion of the spindle is specified at 10 nm, the measuring system has to be able to measure the axial position of the spindle, within one revolution, with an uncertainty of at most 10 nm. The second part of the accuracy requirements refers to the errors over the total measuring range of the system. To reach shape accuracies of 0.1 μm , the linearity errors of the measuring system over the total measuring range need to be equal to or smaller than 0.1 μm .

The accuracy of the system can possibly be optimized by using software error compensation techniques. These techniques can be applied to minimise the axial error motions as well as to improve the linearity of the system over the total measuring range. It has to be realised that software error compensation is only suitable for the correction of systematic errors of the measurement system.

- The measurement system must be able to measure motions with a *maximum velocity* of 0.1 m/s. This requirement is determined by the velocity which will be reached by performing harmonic motions with an amplitude of 500 μm , at a frequency of 30 Hz (see chapter 1).

As already discussed in the previous paragraph, an analog measuring system can not fulfil both the requirements considering the resolution and measuring range. This means, an incremental displacement system has to be applied.

Within precision engineering there are only two types of linear displacement measuring systems with a resolution in the nanometre range and a measuring range of several millimetres: laser interferometer systems and linear scales. Both are applied in measuring machines as well as production machines like precision lathes. In the next paragraphs the possibilities, the advantages and the disadvantages of both systems will be discussed.

3.3.1 Laser interferometer

During the last decades laser interferometry has been widely applied within the field of precision engineering. The high accuracy of this system is based on the high frequency stability of the laser source ($10^{-8} < \Delta f/f < 10^{-7}$) and the inherent accuracy of interferometry, since the wavelength of the emitted light is used as measuring unit. Because of this the frequency stabilized He-Ne-laser is also used as the scientific base for the new metre-definition since 1983. Laser interferometry offers the opportunity of linear displacement measurement over a long range (up to 50 m) with a high resolution (down to 1 nm), without making mechanical contact.

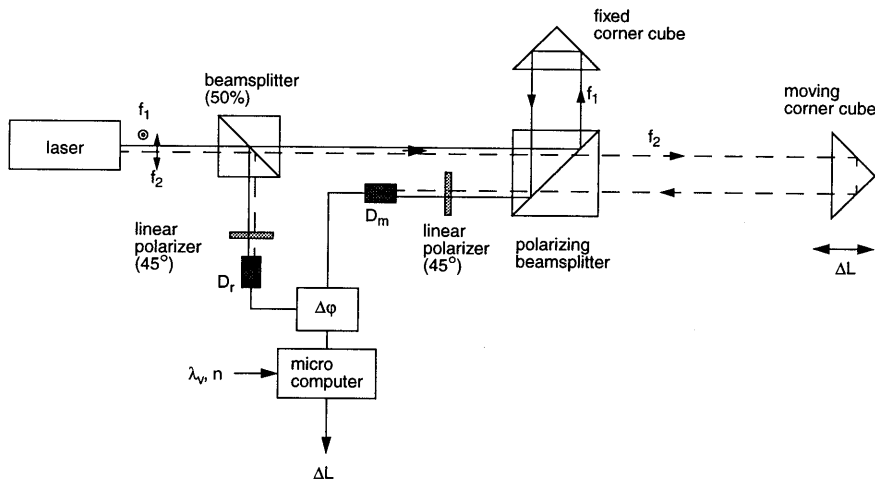


FIGURE 3.3 Schematic representation of a heterodyne laser interferometer system

Figure 3.3 gives a schematic representation of a commonly used laser interferometer system (heterodyne principle). In this setup two orthogonally polarized beams with different frequencies (f_1 and f_2) are emitted by the laser source. In the polarizing beamsplitter the beam which is polarized perpendicular to the drawing plane is deflected, whereas the beam which is polarized parallel to the drawing plane is transmitted. In this way both 'arms' of the interferometer are created. After reflection in corner cubes, both beams come together in the polarizing beam splitter. After

passing a linear polarizer (at an angle of 45° with respect to both polarization axes), both beams will interfere. The intensity of the interfering beams is measured by the optical detector D_m . This detector will measure a harmonic signal with the beat frequency $\Delta f (= f_1 - f_2)$. Detector D_r will measure the reference signal with the same beat frequency Δf . If the corner cubes are not moving the phase difference between the reference and the measuring signal will remain constant. A displacement of one of the corner cubes will introduce a shift in this phase difference ($\Delta\phi$). In this configuration a displacement of the moving corner cube over a distance which equals a half wavelength of the laser light will introduce a phase shift of 2π radians. If the wavelength of the laser light is known, the displacement can be calculated from the measured phase shift by a micro-computer. The wavelength of the emitted light is determined by the frequencies (f_1 and f_2) of the light source, the velocity of the light in vacuum c_o and the refractive index of environmental air n . This means, the phase shift $\Delta\phi$ due to a displacement ΔL of the mirror, can be calculated by the following expression:

$$\Delta\phi = 4\pi \frac{\Delta L n f_m}{c_o} \quad (3.1)$$

Here f_m is the mean frequency of f_1 and f_2 . The refractive index of the air is influenced by the temperature, pressure and the constituents of the air. In practice the relative accuracy of a laser interferometer is mainly limited by the uncertainties in the determination of the refractive index of the air.

Generally a Helium-Neon laser is applied in commercial interferometer systems. This laser source emits light with a wavelength of 633 nm. This implies a resolution (without interpolation) of 316.5 nm for the configuration in figure 3.3. Laser interferometer systems are available in different configurations. For very accurate applications configurations with plane mirrors are applied instead of corner cubes. These configurations contribute to a higher resolution and stability of the optical system [14, 15]. An example of such a configuration is shown in figure 3.4. In this configuration two quarter wave plates are used to obtain the desired beam pattern. If the laser light passes a quarter wave plate two times, the polarisation direction of the light is rotated 90° .

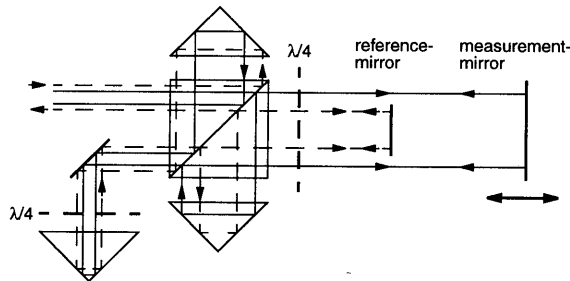


FIGURE 3.4 Plane mirror interferometer (Hewlett Packard)

After interpolation of the interference signal a resolution of 1 nm (or even smaller) can be achieved. However, it has to be realised that the accuracy of the interpolation is limited by non-linearities between the measured phase shift $\Delta\phi$ and the actual displacement of the corner cube. These non-linearity errors are mostly caused by the fact that the applied optics are not perfect. In practice this effect will lead to interpolation errors with a typical magnitude of 5-10 nm [16].

Plane mirror configurations could also be used to measure the axial position of a rotating spindle. For this purpose a plane mirror needs to be attached to the spindle, in the same way as is done at the prototype of chapter 2. The accuracy of this setup is dependent on the alignment accuracy of the mirror and the eccentricity of the laser beams with respect to the axis of rotation of the spindle. The resulting error can again be calculated from equation 2.1. As shown in chapter 2, the measurement errors which results from these effect can be reduced to a few nanometres.

A major disadvantage of laser interferometer systems is their high sensitivity for fluctuations in the refractive index of the environmental air. This leads to fluctuations in the optical path length of the interferometer and thus to deviations of the measured displacements. The fluctuations in the refractive index are caused by for instance temperature variations, turbulences of the air and changes in the constituents of the air. Global and relatively 'slow' fluctuations can be corrected by use of a refractometer or a compensator system. These systems determine (changes in) the refractive index of the air. However in a lathe the refractive index can be strongly

influenced by local and relatively 'fast' effects, which are very difficult to compensate for. The main local changes in the refractive index are caused by turbulences in the air, introduced by moving parts or air bearings. Other local effects on the refractive index are the use of coolant or local heat sources. To obtain a maximum accuracy the laser beams have to be screened for this local fluctuations of the refractive index as much as possible. If an interferometer system is used for the measurement on a rotating mirror the beam can not be screened completely and thus the measurement will always be disturbed by turbulences of the air caused by the rotation.

Additional disadvantages of a laser interferometer system are the high costs and relative high complexity of this system.

3.3.2 Linear scales

A possible alternative for laser interferometers are the so-called interferential scales. These scales are incremental displacement measuring systems. Figure 3.5 shows a scheme of such a measurement system. This system consists of an optical grating scale, an opto-electronic reading head and electronics for counting and data-acquisition. Interferential scales can reach a resolution down to 1 nm, while their measuring range can be more than 500 mm.

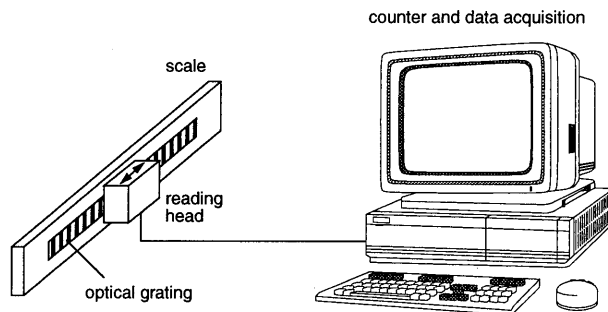


FIGURE 3.5 Scheme of an interferential grating system

These systems are supplied by several manufacturers, with each their own features. But in general they operate on a similar way and have similar characteristics. In the

following the *Heidenhain* system will be described, since within the Philips Research Laboratories good experience has been gained with this type of scales during the last years. These systems have been implemented on a number of measuring and production machines.

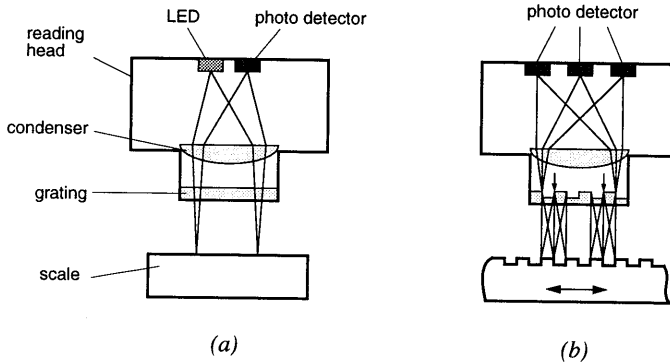


FIGURE 3.6 Cross sections of the reading head and the scale (schematic); section a is perpendicular to section b.

An elaborate description of the physical principles of the Heidenhain system can be found in [17], a brief description will be presented below. Figure 3.6 shows the construction of the reading head. This head contains a light source (LED), a condenser, a transparent phase grating and three photo detectors. Figure 3.6.b shows the diffracted beams, this view is perpendicular to the view of figure 3.6.a. The scale consists of a reflective phase grating, with a grating period g , equal to the period of the grating in the head. Since the LED is placed in the focal plane of the condenser, the transparent phase grating is lightened by a parallel beam. This beam is diffracted in several directions by the grating. At the reflective phase grating of the scale the light is diffracted again. Due to the special shape of this phase grating, the intensity of the zero order diffraction on this grating is almost zero. This is caused by the fact that the rectangular shaped grooves of the grating have a depth which equals a quarter of the wavelength of the light ($\lambda/4=220$ nm) and a width which equals half the grating period (g). Subsequently the reflected beams pass the phase grating of the reading head and are diffracted again. Finally, the light of the lowest three diffraction orders (-1, +1 and 0) is focused on the three photo detectors by the condenser.

A further explanation will be given using figure 3.7, where the beam paths are 'unfolded'. This means G1 is the same grating as G3, both represent the phase grating in the reading head. In this figure G2 represents the grating on the scale.

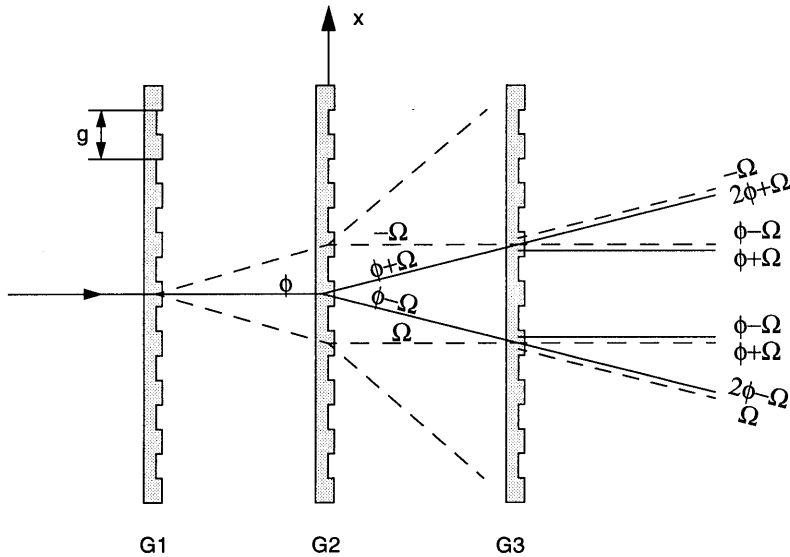


FIGURE 3.7 Unfolded representation of the optical paths

On grating G1 the zero order diffraction is shifted in phase by an amount ϕ with respect to the +1 and -1 order diffraction. These three diffraction orders are diffracted again on the grating G2. By moving grating G2 in x-direction with respect to the grating G1 (=G3), the +1 order diffraction of this grating is shifted by an amount Ω , whereas the -1 order is shifted by an amount $-\Omega$. This phase shift Ω is determined by the translation in x-direction of the scale (grating G2):

$$\Omega = 2\pi \frac{x}{g} \quad (3.2)$$

Where g represents the grating period.

The zero order diffraction is eliminated on this grating. By transmitting the grating G3 the beams are diffracted and phase shifted in the same way as at G1. After grating G3 the beams of equal direction will interfere. It can be proved that using a non-monochromatic incoherent light source only the -1, 0 and +1 orders of diffraction will contribute to interference [17].

As shown in figure 3.7, in the +1 direction a beam with a phase shift of $2\phi + \Omega$ will interfere with a beam with a phase shift $-\Omega$. In complex notation the amplitude U_1 of the resulting beam can be described as:

$$U_1 = e^{j(2\phi + \Omega)} + e^{-j\Omega} = e^{j\phi} (e^{-j(\phi + \Omega)} + e^{j(\phi + \Omega)}) \quad (3.3)$$

The resulting intensity J_1 can be calculated by:

$$J_1 = U_1 \cdot U_1^* = 2(1 + \cos 2(\phi + \Omega)) \quad (3.4)$$

In the 0 direction the beams with a phase shift $\phi + \Omega$ will interfere with a beam with a phase shift $\phi - \Omega$. The resulting amplitude U_0 can be described as:

$$U_0 = e^{j(\phi + \Omega)} + e^{j(\phi - \Omega)} = e^{j\phi} (e^{j\Omega} + e^{-j\Omega}) \quad (3.5)$$

The intensity J_0 can be described as:

$$J_0 = 4 \cos^2 \Omega = 2(1 + \cos 2\Omega) \quad (3.6)$$

For the -1 direction the intensity can be calculated in a similar way:

$$J_{-1} = 2(1 + \cos 2(\Omega - \phi)) \quad (3.7)$$

Substitution of equation 3.2 in the expressions of the intensities J yields:

$$J_{-1} = 2 \left(1 + \cos \left(2\pi \frac{2x}{g} - 2\phi \right) \right) \quad (3.8)$$

$$J_0 = 2 \left(1 + \cos \left(2\pi \frac{2x}{g} \right) \right) \quad (3.9)$$

$$J_1 = 2 \left(1 + \cos \left(2\pi \frac{2x}{g} + 2\phi \right) \right) \quad (3.10)$$

Each of the three photo detectors in the focal plane of the collimator produces an electrical signal which is proportional to the intensity of one of the three diffraction orders. Thus, a displacement of the scale in x-direction results in three signals, which are periodically with half the grating period and have a phase shift of 2ϕ with respect to each other. Due to the special shape of the grating in the head (G1, G3), the phase shift 2ϕ equals 120° . The three harmonic signals which are mutually shifted in phase by an amount of 120° , are electronically converted to two harmonic signals which are shifted 90° from each other. These are commonly used output signals for many of the current measuring systems.

The output signals of the reading head can be interpolated in a relatively simple way. Interpolators with an interpolation factor up to 500 can be applied. *Heidenhain* delivers a number of different interferential grating systems with different grating periods (from $0.512 \mu\text{m}$ to $8 \mu\text{m}$, see also table 4.1). The systems with the smallest grating period can achieve a resolution of 1 nm after interpolation. However, it must be realised that interpolation errors will occur as a result of alignment errors (of the reading head with respect to the scale) or incorrect tuning of the electronics. This problem will be further discussed in paragraph 4.2.2.

Due to symmetry and the relatively short optical path, this system has a relatively low sensitivity for environmental effects such as turbulences in the air or changes in the temperature, pressure and constituents of the air. The sensitivity of the system for changes in temperature is mainly determined by the thermal properties of the material of the scale. The highest thermal stability can be achieved by applying Zerodur (coefficient of expansion $< 10^{-6}$). An other advantage of linear scales with respect to laser interferometer systems is the relatively low price of these systems. Linear scales are about a factor 10 cheaper than laser interferometer systems. However, in general the maximum linearity accuracy which can be achieved using linear scales, will be lower than the linearity accuracy which can be achieved using a laser interferometer system. To improve the linearity accuracy of an interferential scale, the systematic linearity deviations can be made subject of calibration procedures, mapped and then corrected by software error compensation. In this way an accuracy of 5 - 20 nm can be reached [19].

In principle a linear scale is not suitable for measuring the axial position of a rotating body, unless it would be possible to realise a grating structure on a cylindrical

surface (as shown in figure 3.8). The grating period and the shape of the grooves on the cylinder must be equal to those of the grating on the scale. In that case a commercially available reading head could be applied without essential changes, because the optical paths in the plane of diffraction (figure 3.6.b) are not disturbed by the curvature of the cylindrical surface. Distortions in the optical paths in the plane perpendicular to the axis of rotation of the cylinder (figure 3.6.a) can cause an attenuation of the measurement signals, because the reflected light is no longer focused at one point at the photo detectors but at a line on the detectors plane. If necessary, this effect can be corrected by use of a cylinder lens.

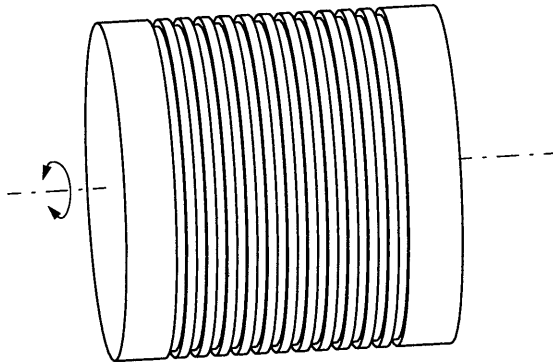


FIGURE 3.8 Grating structure on a cylindrical body

The accuracy of this system is mainly depending on the 'straightness' of the groove pattern (i.e. axial run out of the groove pattern as a function of the spindle angle), the deviations in the grating period and the alignment accuracy of the cylinder with respect to the axis of rotation of the spindle.

If it would be possible to realise a phase grating on a cylindrical surface, it would lead to a measurement system for the specified application with clear advantages over a laser interferometer system. Therefore, the feasibility of the realisation of a cylindrical phase grating will be investigated. This will be described in chapter 4.

3.4 The actuator configuration

In the spindle concept, as described in the previous chapter, a voice coil actuator (as shown in figure 3.9.a) is used for control of the axial position of the spindle. However, the use of such a voice coil actuator for the axial motion control of the spindle (over a stroke of at least 20 mm) will have certain disadvantages. To obtain an optimal tuned system at every axial position of the spindle, the force factor of the actuator (the ratio between the force and the current) must be constant over the total motion range. Therefore the number of turns within the air gap has to be constant over the total range. This can be realised in two different ways: In the first alternative a long coil is used in combination with a short air gap (see figure 3.9.b). In this configuration the length of the coil has to be at least equal to the sum of the stroke and the length of the air gap. In the second alternative a short coil is combined with a long air gap (see figure 3.9.c). In this configuration the length of the air gap has to be at least equal to the sum of the stroke and the length of the coil.

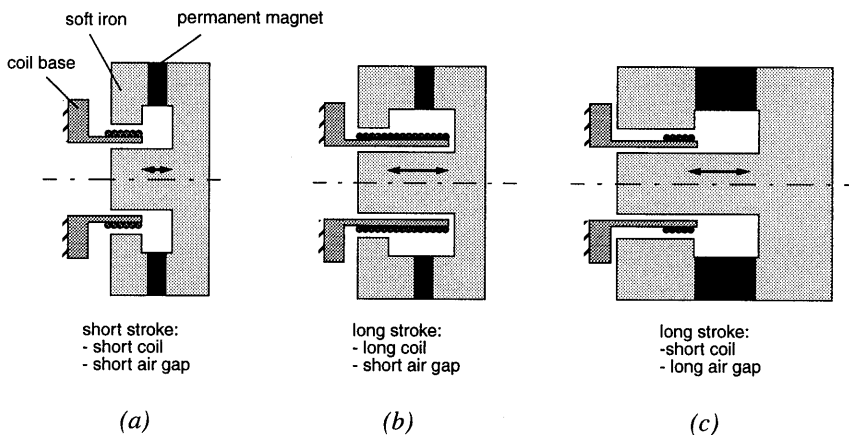


FIGURE 3.9 The influence of an increase of the stroke of a voice coil actuator on the dimensions of the coil and magnetic circuit

The first alternative, will have a low energetic efficiency, since only a small part of the coil will contribute to the force generation, whereas the total coil contributes to the heat dissipation. An other disadvantage of a configuration with a long coil, is the relatively large self inductance of the coil, which will worsen the electro-dynamic

properties of the actuator. With respect to the original configuration, the axial length of the magnetic circuit has to be enlarged to give the coil the possibility to move completely into the circuit. This will lead to an increase of the mass of the magnetic circuit. Since the circuit is attached to the moving spindle, a large increase of the mass is unacceptable.

The second alternative, with a short coil and long air gap, requires an even bigger increase of the material in the magnetic circuit (permanent magnet as well as soft iron). The volume of the soft iron has to be increased to create a longer air gap and the volume of the permanent magnet has to be increased to establish an equal strength of the magnetic field in this large air gap volume. This leads to a considerable increase of the mass of the circuit. From the previous it can be concluded that for large displacements both solutions have certain disadvantages. In the next sub-paragraphs some possibilities will be discussed to come to a better solution.

3.4.3 Reducing the mass of the magnetic circuit

The mass of a permanent-magnetic circuit can be minimised by using a modern high performance rare-earth magnet [3]. The most powerful permanent magnets at the moment are made of neodymium-iron-boron (NdFeB). The mass of a magnetic circuit can be further reduced by applying a soft magnetic material, which gets saturated only at a high level of the magnetic flux density. This means a minimum volume of soft magnetic material can be used to contain a maximum amount of magnetic flux. A soft magnetic material which fulfils this requirement is cobalt-iron (CoFe). An attendant advantage of this material is the high specific resistance, which helps to minimise eddy currents in the magnetic circuit. Eddy currents in the magnetic circuit will be induced by changes in the magnetic field, caused by fluctuating currents in the coil.

The moving mass on the spindle can be reduced by modifying the configuration of the circuit. This can be done by splitting up the magnetic circuit, as presented in figure 3.10. In this configuration only a part of the magnetic circuit is attached to the moving spindle, the other part of the circuit and the coils are fixed to the earth. Due to the splitting of the circuit, both parts are subjected to magnetic reluctance forces. In an ideal situation the resulting radial and axial reluctance forces on both parts will be zero. However in a practical situation there will always act a resulting radial

reluctance force on both parts, due to eccentricity of both parts and the out-of-roundness of both parts.

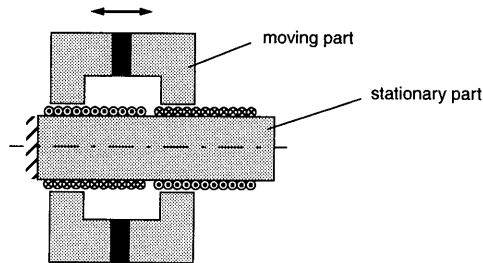


FIGURE 3.10 Reducing the mass of the circuit by splitting it up into two parts

An eccentricity of the stationary part with respect to the axis of rotation of the spindle leads to a stationary force on the spindle (comparable with a gravitation force). This force will not introduce radial error motions of the spindle. An eccentricity of the rotating (and translating) part of the magnetic circuit with respect to the axis of rotation, will lead to a constant rotating force on the spindle. This force will excite the machine frame with a frequency equal to the rotation frequency of the spindle. Nevertheless, this force will not introduce radial error motions of the spindle, provided that the radial stiffness of the spindle bearings is equal in all directions. This precondition is fulfilled if the radial displacements of the spindle are small with respect to the height of the air gap. In that case, eccentricity of both parts of the circuit with respect to the axis of rotation will not lead to radial error motions of the spindle. However, out-of-roundness of one or both parts of the magnetic circuit combined with eccentricity will lead to a fluctuating radial force, which always causes radial error motions of the spindle. The magnitude of these error motions depends on the amplitude of the fluctuations and the radial stiffness of the spindle bearings. A fluctuating radial force can also introduce vibration in the total construction. Therefore, the out-of-roundness of both parts must be minimised.

Besides the radial forces, also axial reluctance forces can act on both parts. When the outer part of the magnetic circuit moves to (or further then) the end of the static part the magnetic resistance of the circuit will change and causes a change of the

magnetic energy in the circuit. As a result an axial force will act on both parts. This force will pull both parts together. However, if the length of the static part of the magnetic circuit is considerably longer than the sum of the length of the moving part and the axial motion range, these axial reluctance forces will be negligible. An axial reluctance force can also be caused by remanent magnetism in the static part. This means the soft magnetic material has been locally permanently magnetised. This effect can be minimised by the applying cobalt-iron as soft magnetic material, since the remanent magnetism in this material will be very low.

3.4.4 Improving the energetic efficiency

To obtain a high thermal stability of a construction, the internal heat production should be as constant as possible. The heat production in the actuator will be proportional to the square of the force which has to be generated by the actuator. The force which the actuator has to generate, depends on the cutting process. This force will have the largest magnitude during rough-turning and nonrotationally symmetric turning (for the acceleration and deceleration of the spindle mass) and will be relative low (< 1 N) during the finishing of rotationally symmetric products. This means the actuator can not be considered as a constant heat source. Therefore, minimisation of the fluctuations in the heat production has to be realised by a maximum thermal efficiency of the actuator. A voice coil actuator has a maximum thermal efficiency if the heat dissipation (P_{disp}) per unit force (F) has a minimum. For a simple voice coil actuator with a coil length equal to the depth of the air gap (comparable to figure 3.9.a), the following expression can be derived [3]:

$$\frac{F}{\sqrt{P_{disp}}} = B_g \frac{\sqrt{V_{cu}}}{\sqrt{\rho}} \quad (3.11)$$

With V_{cu} as the volume of the coil material in the air gap, ρ as the specific resistance of the coil material and B_g as the magnetic flux density in the air gap. The maximum volume of the coil material within the air gap volume is limited by the volume of the coil base, the required clearance between the coil and the magnetic circuit and the space factor of the coil. Normally the space factor of a coil is about 75%, a higher level of about 85% can be reached by using special winding techniques. Considering the specific resistance of regular winding materials, copper ($\rho = 1.7 \cdot 10^{-8} \Omega\text{m}$) and silver ($\rho = 1.6 \cdot 10^{-8} \Omega\text{m}$) have the lowest specific resistance.

The magnetic flux density in the air gap is limited by the saturation level of the soft magnetic material. For most of the commonly used soft magnetic materials the saturation level is about 1.5 to 2 Tesla. Cobalt iron has a saturation level of about 2.5 Tesla. A maximum flux density in the air gap of the magnetic circuit means also a maximum magnetic energy W_g in the air gap since:

$$W_g = \frac{B_g^2}{2\mu_0} V_g \quad (3.12)$$

With V_g the volume of the air gap and μ_0 the permeability of the vacuum. If the permeability of the soft magnetic material is supposed to be infinite (which is a justified assumption for as long the magnetic flux density in the soft magnetic material stays below the saturation level), the magnetic energy in the air gap will be equal to the magnetic energy in the permanent magnet. The magnetic energy in the permanent magnet W_m can be calculated by the following expression:

$$W_m = \frac{1}{2}(B_m H_m) V_m \quad (3.13)$$

With B_m the flux density of the magnet, H_m the magnetic field strength of the magnet and V_m the volume of the permanent magnet. Equation 3.13 shows that a maximum magnetic energy per volume (W_m/V_m) is reached if the product $B_m H_m$ has a maximum. The maximum value of this product (BH_{max}) is a typical property of magnetic materials. The highest value of BH_{max} can be reached by using neodymium iron boron (NdFeB) as magnetic material. Whether the high value $B_m H_m$ is actually reached in a magnetic circuit depends on the dimensions of the permanent magnet with respect to the dimensions of the air gap [3].

Considering the previous the permanent-magnetic circuit will be made of cobalt iron (soft magnetic material) and NdFeB (permanent-magnetic material). The circuit will be dimensioned to obtain a flux density in the air gap which is close to the saturation level of the cobalt iron, whereas the magnetic flux density B_m and field strength H_m of the permanent magnet are close to the optimum value BH_{max} of the applied material.

Despite an optimally dimensioned magnetic circuit, the energetic efficiency of the total voice coil actuator will still be low if a coil is used which is considerably longer

than the depth of the air gap. In that case only a small part of the coil contributes to the generation of the force whereas the total coil contributes to the heat dissipation. There are two alternatives to overcome this problem.

The first alternative is commutation: This means instead of one long coil several short coils are applied, which can be switched on and off separately. Only the coils which are in or very close to the air gap need to be energised. Therefore the position of the magnetic circuit with respect to coils must be known. This technique is commonly used in linear as well as rotating motors. Since the actuator is used as a direct drive of a precision spindle, the commutation of the coils should not introduce disturbances in the force on the spindle. Every position disturbance (even in the sub-micron range) of the spindle can be recognised in the turned optical surface. This means, the coils which are switched must be outside of the permanent-magnetic field of the circuit. Also the currents in the coils which are actually generating the force (i.e. the coils in the air gap) may not be affected by the switching of the other coils. To realise this a relative complex commutation strategy has to be developed.

The second alternative to overcome the problems of a long coil and to avoid commutation, is the use of a hybrid system which consists of a 'short stroke' actuator and 'long stroke' actuator. In this case a short coil will travel with the magnetic circuit (of the short stroke actuator). As a consequence a long stroke actuator is necessary to move the coil. Figure 3.11 shows a schematic representation of this configuration. Because the dynamic motions of the spindle are relative small (maximum a few hundred micrometre), the coil only needs to follow the 'quasi static' motions of the circuit. In principle, the length of the coil of the short stroke actuator can be limited to the depth of the air gap plus the magnitude of the 'dynamic' motions. A disadvantage of this concept is the need for a tracking system, consisting of an actuator, a control system and a position sensor which measures the position of the coil with respect the magnetic circuit. However the performance of this tracking system with regard to resolution, position error and bandwidth can be low.

The system as presented in figure 3.11 will be applied in the new spindle, since this alternative combines a low moving mass and a high energetic efficiency. Besides, the part of the magnetic circuit which holds the coils can function as part of the counter-mass to reduce the dynamic reaction forces to machine frame. This will be discussed in the next paragraph.

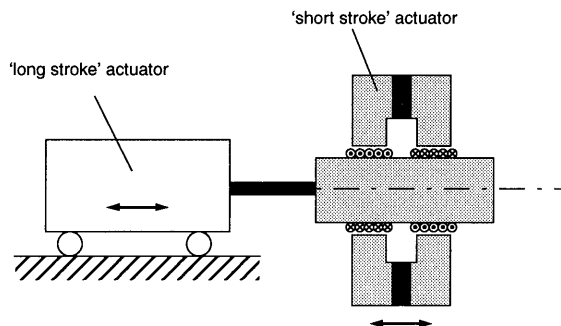


FIGURE 3.11 Schematic view of a coil that travels with the actuator

3.4.5 Reducing the reaction forces on the frame

The Lorentz force, which is generated by the current in the coil, will act on the permanent-magnetic circuit on the spindle as well as on the coil. The force on the coil has an equal magnitude but will be opposite directed with respect to the force on the magnetic circuit. This means, if the coil is attached to the machine frame, the frame will directly be excited by the reaction forces on the coil. This aspect will become increasingly important if the spindle is actuated at high frequencies, which is necessary to produce non-rotationally symmetric surfaces. The reaction forces will be relatively high, because the magnitude of the reaction forces is proportional to the square of the actuation frequency.

Figure 3.12.a shows a controlled ideal system, driven by a 'direct drive' like a voice coil actuator. Depending on the measured displacement z of the load a servo force F is generated, which acts on the load and on a frame with an infinite mass and stiffness. However in a practical situation the stiffness and the mass of the machine frame is limited, which is schematically presented in figure 3.12.b by the spring and the damper between the frame and the 'earth'. This implies that the frame will deflect and vibrate as a result of the reaction forces. Vibrations and deflections of the frame will limit the performance of a controlled system in terms of bandwidth, overshoot and settling time [18]. Particularly the reaction forces with a frequency that equals one of the eigenfrequencies of the frame will cause problems.

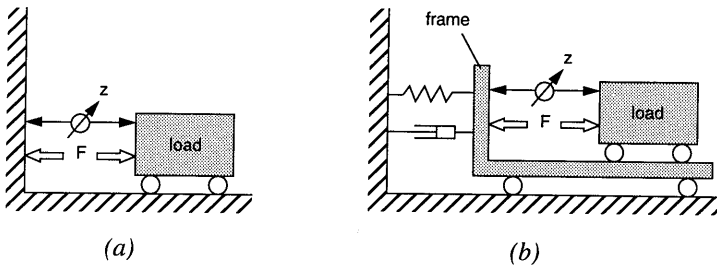


FIGURE 3.12 Schematic representation of a direct drive
 a. ideal system
 b. realistic system on a frame with limited stiffness

Generally the negative effects of the reaction forces on the performance of the machine are reduced by improving the mechanical properties of the frame. Commonly used approaches are: increasing the stiffness of the frame, increasing the (active) damping or increasing the mass of the frame. However, a more fundamental approach is to reduce the actual excitation forces on the frame. One way to realise this, is by using a counter mass. This is schematically presented in figure 3.13.

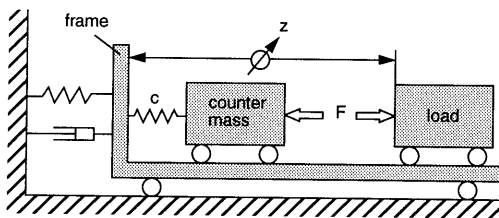


FIGURE 3.13 Direct drive combined with a counter mass

In this system the force which drives the load acts no longer directly on the frame but on the counter mass with mass M which is coupled to the frame by a spring with a stiffness c . The reaction forces on the frame are now determined by the displacement of the counter mass and the stiffness of the coupling of the counter mass to the frame. The principle of a counter mass can easily be applied to a voice coil drive system, because the force which acts on the coil and on the magnetic circuit is inde-

pendent of a relative motion between both parts, provided that the current in the coil and the number of turns in the air gap is constant during this motion.

Figure 3.14 shows the ratio between the reaction forces on the frame and the driving forces on the load as a function of the frequency. For the system of figure 3.13 (curve b in figure 3.14) the reaction forces on the frame are equal to the driving forces on the load for low frequencies ($f \ll f_o$). For high frequencies ($f \gg f_o$) the reaction forces on the frame are reduced tremendously by using a counter-mass. For frequencies around the eigenfrequency f_o of the counter-mass the reaction forces are amplified, due to the resonance of the counter-mass. This amplification around the eigenfrequency can be reduced by applying a damper parallel to the spring (curve c). However this damping will lead to less reduction of the reaction forces on the frame for high frequencies. Instead of a reduction of 40 dB per decade (dB = $20 \log$) which is reached without damper, a reduction of 20 dB per decade will be reached by using a damper.

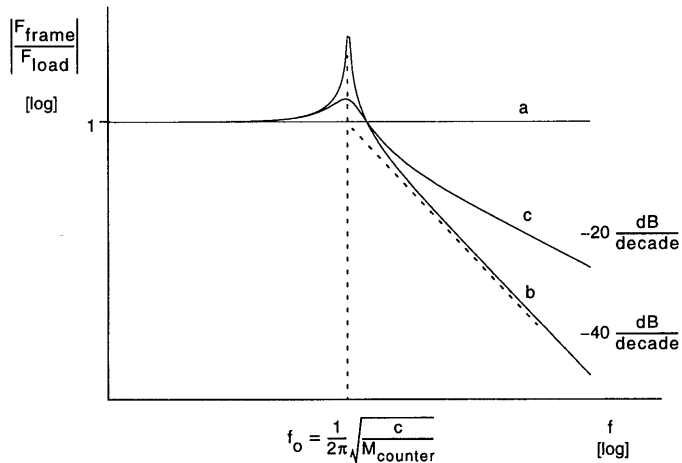


FIGURE 3.14 Ratio of the reaction forces on the frame and the driving forces on the load as a function of the frequency for several systems:
a. direct drive without counter-mass
b. direct drive with counter-mass (without damping)
c. direct drive with damped counter-mass

To realise an adequate reduction of the reaction forces on the frame during nonrotationally symmetric cutting, the eigenfrequency of the counter mass has to be considerably lower than the actuation frequency of the spindle (the 'load' of figure 3.13). At high frequencies the energy of reaction forces is almost completely transformed to kinetic energy of the counter mass. Only the small part of the energy, which is accumulated in the spring, can be transferred to the frame. Now, the amplitude ratio of the motions of the counter mass and the spindle is inversely proportional to the mass ratio of the counter mass and the spindle.

From the previous it can be concluded that for an optimum reduction of the reaction forces on the frame, the eigenfrequency of the counter mass must be as low as possible. This can be realised by a high mass of the counter mass and a low stiffness of the (mechanical) coupling to the frame.

Another way to realise this is by applying a second controlled 'direct drive' (e.g. a voice coil actuator) which drives the counter mass by a force F^* . This yields the same results, because a direct drive which drives a free mass, combined with proportional position feedback has the same characteristics as a mass-spring system. In this configuration the position of the counter mass with respect to the load has to be controlled with a low bandwidth. In the same way as a big mass on a weak spring, this controller will behave as a low-pass filter for the transfer of reaction forces to the frame. Figure 3.15 shows a representation of such a system. The position of the counter mass with respect to the frame (z^*) is measured and used as feedback in the controller (see also chapter 6).

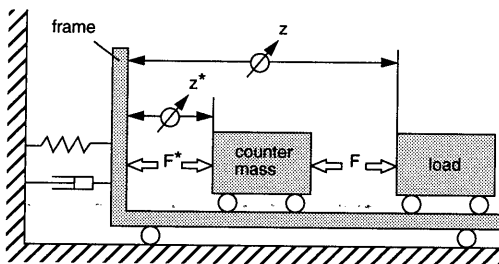


FIGURE 3.15 Counter mass driven by a direct drive with small controller bandwidth.

This system can easily be combined with the system of figure 3.11. In this way an actuator configuration is obtained with a relative high energetic efficiency, combined with an isolation of the 'high-frequency' reaction forces. In that configuration the counter mass has to follow the 'quasi static' motions of the spindle. This implies that the position of the counter mass with respect to the spindle must be kept constant by a controller. The bandwidth of this controller must be low to realise the desired isolation of dynamic reaction forces.

3.5 The total concept of the spindle unit

In the previous paragraphs, concepts have been presented for the position measuring system and the actuator configuration for a spindle with an axial motion control. This has resulted to a new spindle concept, which is schematically presented in figure 3.16.

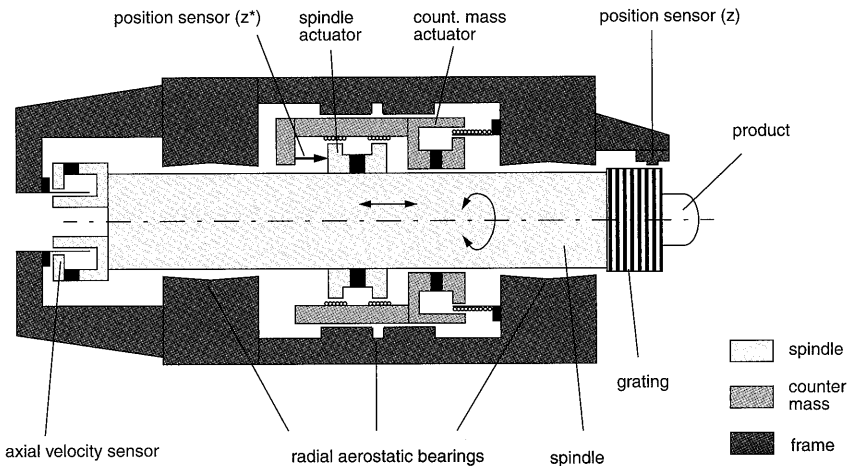


FIGURE 3.16 Total concept of a spindle unit with axial motion control (schematically)

At the front a cylindrical interferential phase grating has been attached to the spindle. The reading head which measures the axial displacement of the grating is attached to the bearing housing. In this way the thermally induced errors are minimised, since the axial displacement of the spindle is measured as close as possible to

the product. On the back side a voice coil system is attached to the spindle. This voice coil system is used as an analog velocity sensor, on the same way as at the first prototype [3]. In the middle of the spindle a permanent-magnetic circuit is attached to the spindle. The driving forces on this magnetic circuit are generated by currents in the coils which are fixed to the counter-mass.

The counter-mass is driven by a voice coil actuator. The magnetic circuit of this actuator is attached to the counter-mass, whereas the coil of the actuator is attached to the bearing house. The energetic efficiency of this actuator is relative low since a long coil has been combined with a short air gap (as discussed in paragraph 3.4). However, the efficiency of this actuator is less relevant since the power dissipation of this actuator will be relatively low, because it only has to generate the static component of the disturbance forces (cutting forces) and the acceleration forces to realise the quasi static motions and not the acceleration forces for the dynamic motions which are considerably larger (as mentioned in paragraph 3.2). The position of the counter-mass with respect to spindle (z^*) is measured by an analog contactless sensor. The signal of this sensor is used in a low-bandwidth position controller, which forces the counter-mass to follow the quasi static motions of the spindle.

The system as presented in figure 3.16 will be elaborately discussed in the next chapters. The main issues regarding the position measuring system will be considered in chapter 4. Chapter 5 presents the main aspect of the mechanical construction. The applied control system will be discussed in chapter 6.

4. Interference grating system for measuring the axial position of a rotating body

In the previous chapter it has been shown that an interference grating system has clear advantages with respect to a laser interferometer system for measuring the axial position of the spindle. However, an interference grating system is only suitable to measure the axial position of a rotating body if the grating structure can be manufactured on a cylindrical surface. In this chapter the main issues regarding the realisation of such a grating will be discussed. Also typical error sources of the position measuring system in the proposed configuration will be discussed.

4.1 Introduction

The cylindrical grating structure will be developed for use in combination with a commercially available reading head. This has been done for two reasons. The first reason is that the required curvature of the grating surface will not disturb the optical paths in the plane of diffraction, provided that the dimensions of the grooves of the grating pattern on the cylinder correspond with those of the grating in the reading head. As already mentioned in chapter 3, it will only lead to changes in the optical paths in the plane perpendicular to the plane of diffraction: the point focus on each of the three detection surfaces will be transformed to a line focus. This effect can cause a loss of signal. If necessary, this can be corrected using a cylindrical lens.

The second reason for applying a commercially available reading head is that the development of a complete measuring system (cylindrical grating, reading head and electronics) would be very time-consuming and expensive, and is therefore beyond the scope of this project.

Within the Philips Research Laboratories, good experience has been gained with interferential scales manufactured by *Heidenhain*. Since the principles and the specifications of the systems of other suppliers are almost identical it has been decided to fit the dimensions of the grating to a *Heidenhain* reading head. The grating structure of these systems consists of rectangular grooves. The depth of these grooves equals a quarter of the wavelength of the light source (LED or solid state laser) and the width of the grooves is equal to half the grating period. The dimensions of the grooves of the grating pattern on the cylinder must be equal to those of the *Heidenhain* systems. Furthermore the grating surface must be reflective and must have an optical surface quality. Table 4.1 gives an overview of the available systems and their specifications.

System:	LIP 101	LIP 401	LIP 382
Grating period [μm]	8	4	0.512
Depth of the grooves [μm]	0.22	0.22	0.17
Resolution [μm]	0.01	0.005	0.001

TABLE 4.1 Brief overview of the interferential scales program of the *Heidenhain* company

From this overview it can be concluded that two systems meet the requirement with respect to the resolution (≤ 5 nm). The systems *LIP 382* can even reach a resolution of 1 nm. However the width of the grooves of this grating is so small that it will be very hard to manufacture them by the intended methods (see paragraph 4.3). For this reason the development of the phase grating on a cylindrical surface will be focused on the system *LIP 401*.

4.2 Limits of accuracy

The accuracy of an interference grating system is mainly limited by the geometrical accuracy of the grating pattern. The error structure of the grating pattern on the cyl-

inder is even more complex than the error structure of a linear scale, since the grating errors are not only a function of the measurement coordinate of the scale, but also a function of the circumferential position on the cylinder. In general the errors of an interferential grating system can be split in pattern errors and interpolation errors. In the next sub-paragraphs the origin and the effects of both types of errors will be discussed in general. In paragraph 4.3 these items will be discussed with respect to the manufacturing of a cylindrical the grating structure.

4.2.1 Pattern errors

In a practical situation the grating structure on the scale will always show deviations. These deviations can be split in three groups, which will be discussed next.

Pitch errors

Deviations in the pitch of the grating will introduce linearity errors of the measuring system. In general these errors are due to the inherent imperfections of the grating manufacturing process. Neglecting the instability of the scale material (e.g. due to creep), these errors will remain constant over a long period. In general the variations of the pitch errors over the total length of the scale are rather smooth. For this reason these errors can be corrected relatively easily by software error compensation. After calibration on discrete points the linearity errors can be stored in the controller and can be used for on-line compensation. For normal linear scales (not cylindrical) the maximum linearity errors can be brought down to approximately 30 nm for scales up to about 200 mm [19] (without software error compensation). The magnitude of the pitch errors of the cylindrical grating depends on the applied manufacturing method.

Thermally induced errors

In a practical situation the total system will be subjected to fluctuating thermal loads. This will cause variations of the temperature distribution in the grating. Depending on these variations and the coefficient of expansion of the grating material, thermal deformations of the grating will occur. A uniform change in the temperature deviation with respect to the reference state will lead to constant scale error. If this change in temperature can be measured and the coefficient of expansion is known, this error can easily be corrected by on-line compensation. However a much more complicated situation arises if the changes in the temperature distribution of

the grating are non-uniform. This will result to a non-uniform deformation of the grating. In the worst case this will result in variations in the pitch errors as well as in the straightness errors. This situation will be very complex to correct for. There are two alternatives to minimise the non-uniform temperature deformations. The first alternative is the use of a grating material with a very low coefficient of expansion (E.g. Invar: $\alpha \approx 1 \cdot 10^{-6} \text{ K}^{-1}$ or Zerodur: $\alpha \approx 5 \cdot 10^{-8} \text{ K}^{-1}$). The second alternative is the use of a material with high thermal conductivity (e.g. aluminium) to ensure a rapid stabilization of the temperature after a change in the thermal load.

Straightness errors

In contrast to a normal system with a linear scale, a system with a cylindrical grating pattern will also be subjected to straightness errors of the grating pattern. These errors can be considered as an axial run out of the groove pattern (as shown in figure 4.1). They will lead to measurement errors on the axial position as a function of the rotation angle of the cylinder. In a controlled system (without software error compensation) these straightness errors will cause axial error motions of the spindle. The magnitude of the straightness errors depends on the applied manufacturing method of the grating. The possibility to correct for these errors depends on the cycle time of the position controller, the angular speed of the cylinder and the spatial frequencies (in circumferential direction) of the error pattern. The correction of these straightness errors will be even more difficult if they are a function of the axial position on the cylinder

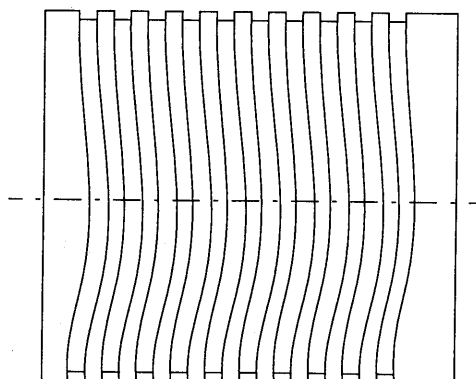


FIGURE 4.1 Straightness errors on the groove pattern

4.2.2 Interpolation errors

These errors are caused by deviations in the interpolation of the measuring signals which are produced by the reading head. As described in chapter 3 the reading head produces two signals S_1 and S_2 which are sinusoidal signals, with both a period equal to half the grating period and which are mutually 90° shifted in phase, the so-called phase quadrature signals. These can be represented by:

$$S_1 = \cos\Omega \quad \text{and} \quad S_2 = \sin\Omega \quad (4.1)$$

with:

$$\Omega = 2\pi \frac{2x}{g} \quad (4.2)$$

Here x represents the relative displacement between the reading head and the scale and g represents the grating period. These two analog signals from the reading head are interpolated to two digital signals with a N times higher frequency, which are also 90° shifted in phase (see figure 4.2). These signals are used by the counter of the digital controller. The value of the counter corresponds to the displacement x , with measuring unit $g/8N$. Note that the resolution of this digital displacement value is 4 times higher than the period of the digital signals, since every flank of both signals corresponds to a count.

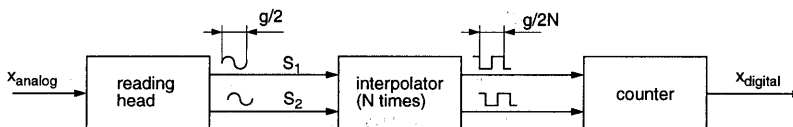


FIGURE 4.2 Conversion of the analog measuring signals to a digital position signal

The function of the interpolator is to define the instantaneous phase angle of the phase quadrature signals in discrete steps (Ω_{int}). Theoretically the function of the interpolator can be represented as:

$$\Omega_{\text{int}} = \text{atan}\left(\frac{S_2}{S_1}\right) \quad (4.3)$$

The working of the interpolator is based on distortion-free harmonic signals. However in a practical situation the phase quadrature signals of the reading head can be subjected to distortions. These are induced by deviations of the diffraction pattern of the system, caused by alignment errors of the reading head with respect to the scale or by groove shape errors of the gratings (e.g. deviations in the depth or the width of the grooves). The distortions will cause interpolation errors, which results in linearity errors with a periodicity of half a grating period.

Typical distortions on the phase quadrature signals (S_1 and S_2) are:

- The harmonic signals S_1 and S_2 have a *dc-offset*.
- The *phase shift* between the harmonic signals S_1 and S_2 is unequal to 90° .
- The signals S_1 and S_2 have *unequal amplitudes*.
- *Second harmonics* are superimposed on the signals S_1 and S_2 .

These distortions on one of the phase quadrature signals can be represented mathematically as:

$$S_1^* = D_1 + (1 + D_2) \cos(\Omega + D_3) + D_4 \cos(2\Omega) \quad (4.4)$$

In this equation D_1 , D_2 and D_3 represent respectively the distortions in the dc-offset, the amplitude and the phase shift from signal S_1 with respect to signal S_2 . The distortion on the signal S_1 by a second harmonic is represented by D_4 . In practice both signals (S_1 and S_2) can be subjected to the mentioned distortions.

Distortions caused by misalignment of the reading head with respect to the scale can be eliminated for the major part by optimizing the mechanical alignment of the reading head with respect to the scale. However, deviations in the groove shapes are caused by the manufacturing process of the grating and can not be eliminated afterwards.

For small values of the distortions ($D_i \ll 1$) the resulting relative interpolation error (interpolation error divided by the signal period) caused by one of these distortions can be calculated by substituting equation 4.4 in 4.3 and subsequently determining the partial derivatives for the various distortions:

$$\frac{\Delta\Omega_{int}}{2\pi} = \frac{1}{2\pi} \frac{\partial\Omega_{int}}{\partial D_i} D_i \quad (i = 1, 2, 3, 4) \quad (4.5)$$

Figure 4.3 shows the partial derivatives ($\partial\Omega/\partial D_i$) over one signal period (Note: the signal period equals half the grating period).

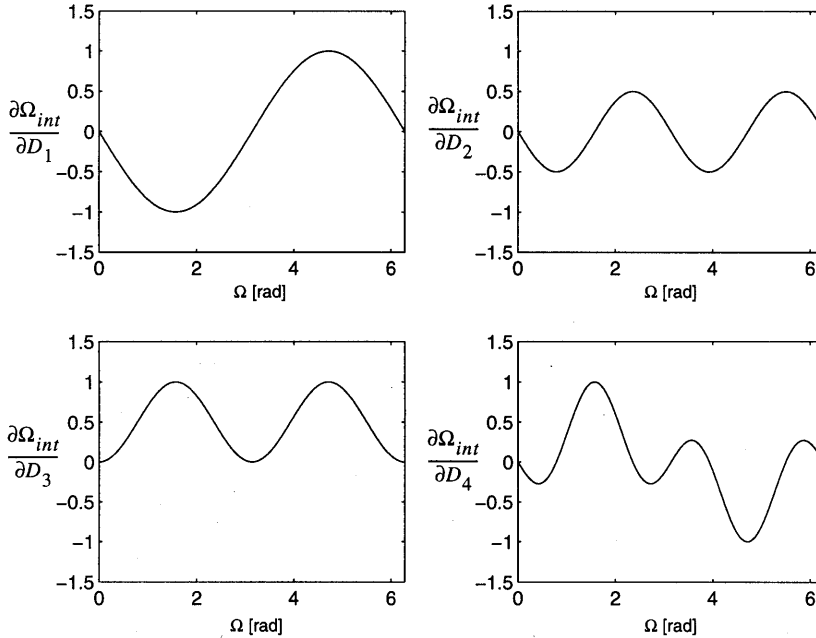


FIGURE 4.3 Partial derivatives of the phase angle calculated by the interpolator to the various distortions D_1 , D_2 , D_3 and D_4 .

As can be seen from figure 4.3 the resulting interpolation errors will be fundamentals or higher harmonics of the signal period. These errors are hard to correct for by usual software compensation techniques, since the number of calibration points must be very large (at least a few points within every grating period). However the distortion can partly be eliminated by electronic compensation. *Heidenhain* offers the possibility to electronically adjust for the dc-offset, the amplitude ratio and the phase shift of the two analog measuring signals.

To realise an optimal mechanical alignment of the head and an optimal electronic adjustment, the measuring signals S_1 and S_2 (or even better the arising interpolation errors) have to be monitored. The most simple and common way to realise this, is by generating a Lissajous figure of the phase quadrature signals S_1 and S_2 (for instance on an oscilloscope). For distortion free signals the resulting Lissajous figure will be a perfect circle with the centre at the origin of the plot. However due to the distortions the Lissajous figure will deviate from a perfect circle. Figure 4.4 shows the typical Lissajous figures caused by one of mentioned the distortions of equation 4.4.

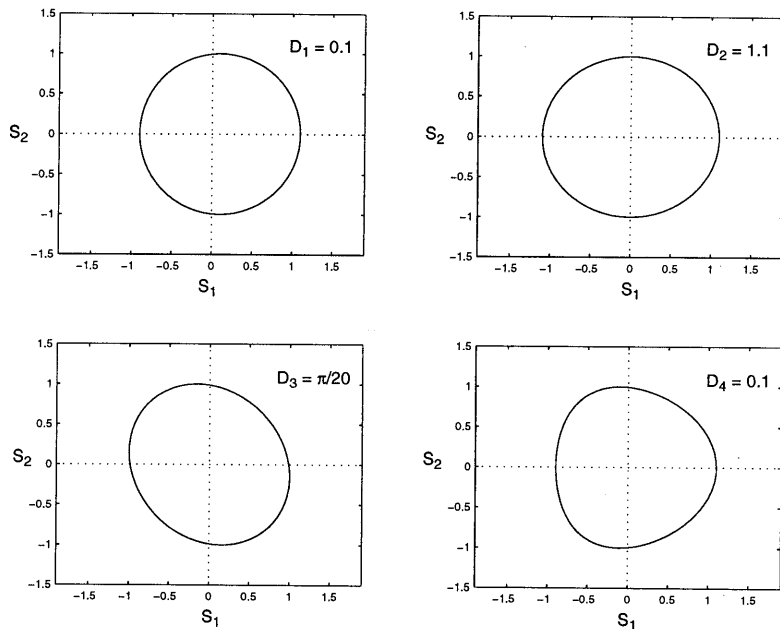


FIGURE 4.4 Lissajous figure of S_1 and S_2 signals with distortions

However a perfect circle of the Lissajous figure does not always guarantee distortion-free measuring signals. Figure 4.5 shows the Lissajous figure which is almost a perfect circle (deviation with respect to best fit circle $< 0.5\%$), whereas the harmonic signals have considerable distortions with respect to dc-offset, amplitude ratio and a second harmonic (on both signals). Figure 4.5 shows also that the resulting relative interpolation errors are about 5%.

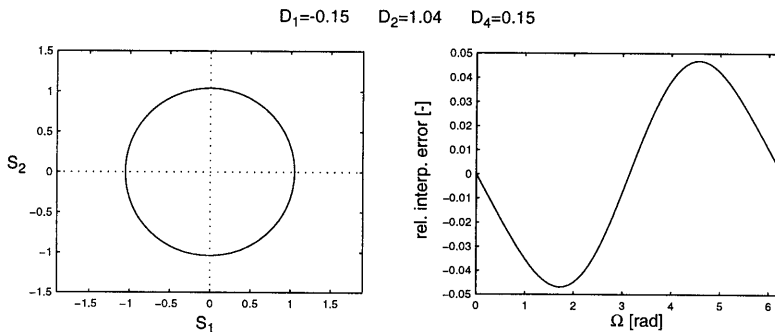


FIGURE 4.5 Almost perfect Lissajous figure despite distortions

The resulting interpolation error can be explained by the fact that the Lissajous figure gives only information on the phase quadrature signals as a function of each other and not as a function of time. In the example of figure 4.5 the angular speed of the vector which describes the Lissajous figure will fluctuate in time whereas the actual speed of the reading head with respect to the scale is constant.

An alternative method uses an analysis of the interpolated position signal as a function of time. This method is based on the fact that distortions on the phase quadrature signals cause deviations on the interpolated signal which are periodical (fundamentals or higher harmonics) with these signals. If a motion can be achieved for which the velocity is constant with time, then the harmonics of the (interpolated) position signal can be decomposed for analysis. For this purpose a spectrum analyser can be used. To obtain an optimum tuning of the electronics, the measured harmonics have to be minimal. Note that if the interpolated position signal is used as feedback for the realisation of the motion with a constant velocity, the frequency of the phase quadrature signals must be preferably higher than the bandwidth of the controlled system. Otherwise the velocity of the controlled system will fluctuate, since it will follow the position signal with the interpolation errors.

The described electronic tuning of the phase quadrature signals is only suitable if the distortions of the signals are constant. In a practical situation the distortions can vary over time or as a function of the position on the scale. In that case the settings of the electronics have to be updated continuously. This is not possible using the

current available electronics. To realise this some adaptive correction techniques are proposed, in which stored model parameters are updated continuously [20, 21]. For as long these techniques are not commercially available, the quality of the groove pattern must be as constant as possible over the total length of the pattern.

4.3 Grating manufacturing methods

To investigate the feasibility of measuring the axial position of a rotating spindle by an interference grating system, a prototype of a grating pattern on a cylinder has to be made. Normally linear scales are made by etching techniques. However the common used techniques for lacquering and illumination of the etching mask, can only be used on flat surfaces and not on a cylindrical surface. Two alternative manufacturing methods will be discussed next: diamond turning and plasma etching.

4.3.3 Diamond turning

Diamond turning is a known technology for the manufacturing of micro-groove structures [22, 23]. However the minimum groove width of the structures described in literature is generally limited to about 10 μm . Within the Philips Research Laboratories, some experience has been gained in manufacturing grating structures by diamond turning, with a grating period of a few micrometres. Most of these grating pattern consists of triangular shaped grooves. Essential problems of the current grating are the rectangular shape of the grooves and the small depth of the grooves. The grooves must be cut by a special diamond tool with a flat tip with a maximum width of 2 μm .

The cylindrical grating structure has to be manufactured on a precision lathe. The obtained structure will be susceptible to the various error sources as described in paragraph 4.2. In particular the straightness errors and the groove shape errors need to be minimal, because these are most difficult to correct by software error compensation. The relevant errors with respect to diamond turning will be discussed next.

Pitch errors

The pitch errors of the grating will be caused by axial position errors of the diamond tool with respect to the workpiece. These are mainly caused by errors of the axial

measurement system of the lathe, by rotation errors of the axial slide (due to an Abbe-offset) and by thermal effects.

If the displacement of the slides is measured by interferential scales of the type *LIP 401*, the pitch of the scale on the slide equals the pitch of the grating which has to be cut. This implies that pitch errors of the grating, caused by constant interpolation errors will be eliminated.

The effect of rotation errors of the axial slide can be minimised by minimising the Abbe-offset. Since the radial motions of the tool during the cutting process are very small (220 nm) the Abbe-offset can be reduced to zero. This can be done by placing the scale of the axial slide on the line which crosses the tip of the diamond tool during the cutting of the grooves.

The pitch errors caused by thermal effects can be minimised by a maximum thermal stability of the total environment. This means the lathe has to be placed in a conditioned room. Besides this, the temperature of the oil in the hydrostatic bearings needs to be conditioned. A maximum thermal stability of the spindle can be obtained by driving the spindle at the same speed as used for turning, during a certain time before the actual cutting process is started.

Straightness errors

Straightness errors of the groove pattern will mainly be caused by axial error motions of the spindle and vibrations of the tool relative to the workpiece. Using the spindle with the active axial bearing (described in chapter 2), the axial error motions can be reduced to about 10 nm. Therefore a spindle based on this concept (mounted on a precision lathe) will be used for the turning experiments. The influence of the tool vibrations during the cutting process will be probably negligible since the same setup has been used already for face turning experiments which yielded optical surfaces with roughness values below 10 nm (Ra).

Note, that if the cylindrical grating has to be placed on an other spindle than it was made on, it will always lead to a measurement error caused by misalignment of the axis of the cylindrical grating with respect to the rotation axis of the spindle. Non-parallelism of both axes will cause a sinusoidal measurement error with a period equal to one revolution of the spindle. It will be very difficult to reduce this error to

the specified value (< 10 nm) by mechanical adjustment. We have alternative methods to reduce this error. The first method is by applying software error compensation. Therefore the controller has to generate a sinusoidal correction signal as a function of the spindle angle. This correction signal will be added to the setpoint of the controller. The second method to correct for this alignment error, is by using two reading heads which are placed diametrical. The actual axial position of the spindle must now be calculated from the average axial position value, measured by both reading heads.

Groove shape errors

The main deviations in the groove shape are related to the depth, the width and the flatness of the grooves. Considering the wear of the small tool tip, it would be preferable to cut the top surface and the grooves with separate tools. However the depth of the grooves is very small (220 nm), so it will be difficult to cut the top surface and the grooves with two different tools. Because in that case the radial (x) position of both tools with respect to each other has to be determined with an accuracy much better than 100 nm. For this reason the grooves as well as the top surface have to be cut with the same diamond tool (see figure 4.6). If the flat end on the tool tip is smaller than half the grating period ($2 \mu\text{m}$), the tool must also be translated in axial direction in the bottom of the grooves to obtain the required width of the grooves. The actual width of the tool can be determined by cutting some test grooves and subsequently measuring the width of these grooves using an atomic force microscope (AFM).

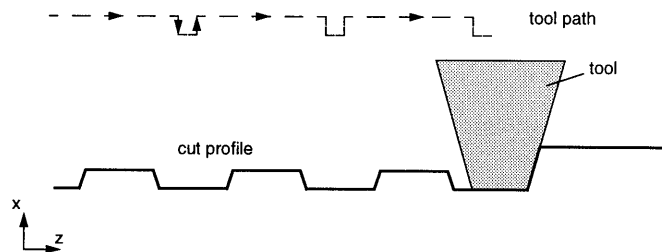


FIGURE 4.6 Profile cutting of the grating pattern

The flatness of the grooves is mainly determined by the profile accuracy of the diamond tool. This profile accuracy depends on the original shape of the tool and the wear of the tool during the cutting process. The wear of the tool depends on the cutting conditions and the material which has to be cut. The first cutting experiments are carried out in electroless nickel. This is a common used material for the diamond turning of optical surfaces (e.g. lens moulds, mirrors etc.). Due to the very fine crystalline structure of this material, a very low surface roughness can be obtained. With respect to other materials (e.g. aluminium, copper), electroless nickel is less sensitive to oxidation or the attack of other chemicals. Besides it has a higher hardness than copper or aluminium, this means it will be less sensitive to damage by mechanical contact. However the tool wear during cutting will be slightly higher.

The first turning experiment has been carried out on a T-base precision lathe (as shown in figure 1.1) with hydrostatic slides driven by friction wheel drives. The position of the slides is measured by interferential scales of the type *Heidenhain LIP 401*. The spindle with the active axial bearing (as described in chapter 2) is placed on the axial slide, to obtain minimal axial error motions of the spindle. These experiments are not focused on an optimal reduction of the errors caused by rotation errors of the axial slide and by thermal effects, since in general these effects cause coarse cycle errors which are easy to correct by software compensation.

The turning experiments have been carried out on a copper shaft (\varnothing 60 mm) covered with a layer of about 100 μm electroless nickel. Figure 4.7 shows an AFM-image and the corresponding measuring results of the grating pattern. In this test grating the width of the grooves is not compensated for the tool width (which is too small).

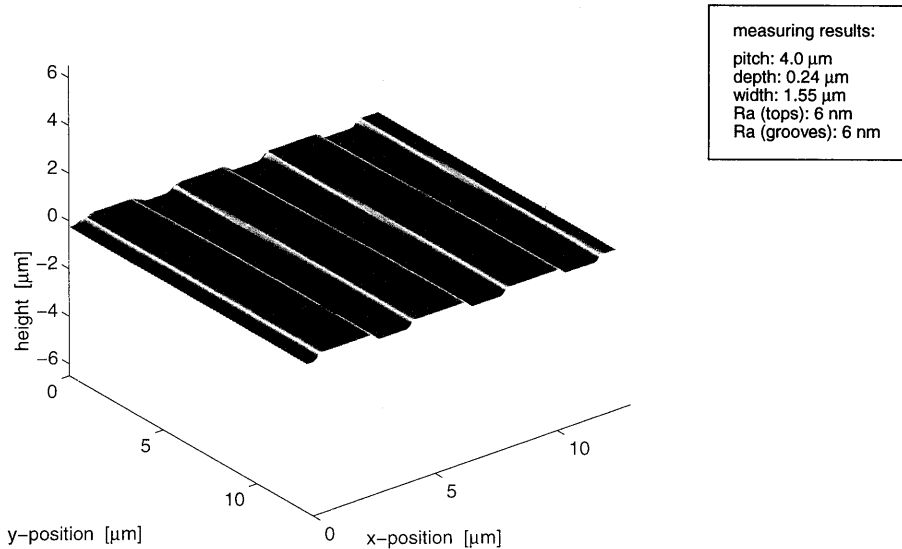


FIGURE 4.7 AFM-plot of grating pattern made by diamond turning

The manufactured grating structure has been tested on the lathe, by translating the axial slide of the lathe and measuring this displacement by a reading head. The signals of this reading head can be compared with those of the reading head on the original scale on the lathe. From these experiments it can be concluded that the quality of the obtained phase quadrature signals (with respect to signal to noise ratio and distortions) of both reading heads is almost equal. The measuring results will be further discussed in chapter 7.

From these test results it can be concluded that diamond turning is a very suitable technique for the manufacturing of a prototype of a grating pattern on a cylinder. An essential benefit of this method is the absence of alignment errors of the cylindrical grating with respect to the rotation axis of the spindle it has been fabricated on. However for batch production this method will be rather expensive due to the long production time and the short working life of the diamond tool.

4.3.4 Plasma etching

An other method for the manufacturing of micro structures is the so-called plasma etching. This etching technique originally has been used in the semiconductor industry. At the moment it is also frequently used within the device technology for the manufacturing of micro-structures. For example, within the Philips Research Laboratories plasma etching has been used for the manufacturing of optical phase gratings consisting of rectangular shaped grooves with a pitch of 0.25-100 μm and a depth of the grooves of 0.1-1.5 μm . In contrast to most other etching techniques, which show almost uniform (isotropic) etching in all directions, plasma etching has the possibility to realise anisotropic (directional) etching [25]. This property is of special interest for the manufacturing of a phase grating structure with rectangular shaped grooves. An other distinctive characteristic of plasma etching, is the possibility to realise a very low surface roughness of the etched surfaces. Even optical surface quality can be achieved, provided that an appropriate material and the correct process conditions are applied. Optical phase gratings are commonly manufactured in quartz, applying a plasma of CHF_3 .

The etching process is carried out in a reactor. Normally this reactor consists of a vacuum chamber with two parallel electrodes inside and a gas-supply system. A high frequency generator, connected to one of the electrodes, maintains a plasma between the electrodes. The supplied gas will be ionised partly and will be split in reactive parts which can react with the workpiece. Due to the special design of the reactor, the ions are accelerated outside the actual plasma in the direction of the non-grounded electrode on which the workpiece is placed. Due to this effect the etching process becomes anisotrope, i.e. directed perpendicular to the plane of the electrode (see figure 4.8). However for the manufacturing of a grating structure on a cylinder, the etching process has to be directed radial to the cylinder. An experiment showed that this can be realised by placing a solid aluminium cylinder on the non-grounded electrode. The plasma now encloses the cylinder, which causes radial etching over a large region (except the edge regions) of the cylinder (see figure 4.8.b).

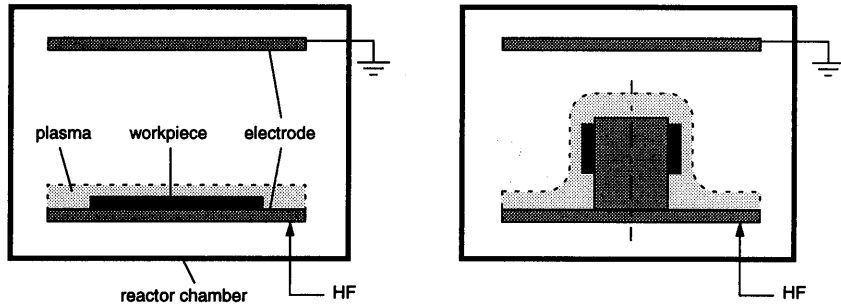


FIGURE 4.8 Plasma etching reactor: normal setup for planar workpieces (left) and modified setup for radial etching (right)

Before a workpiece can be etched, an etching mask has to be applied to the surface of workpiece. The etching velocity of this mask must be preferably lower than that of the workpiece. After the etching process the mask must be removable. Generally, these masks are made by lithographic techniques. However most of these techniques are only suitable for planar surfaces. Next, the successive process steps will be discussed which must be carried out to realise a grating structure on a cylinder of quartz by plasma etching.

Lacquering

A thin layer (maximum a few micrometres thickness) of photoresist has to be applied to the outer surface of the cylinder. For planar workpieces spinning techniques are applied which spread the resist by the centrifugal force. For a cylindrical surface this technique can not be used. An alternative method is by dumping the cylinder into diluted photoresist and subsequently lifting the cylinder out of the solution. The diluent will evaporate whereas the resist remains on the surface. The thickness of the remaining layer can be influenced by the amount of the resist with respect to the diluent and by the lifting velocity.

Illumination

A possible method is illuminating each groove of the pattern with an optical spot while the spindle rotates. The diameter of this spot must be at most $2\ \mu\text{m}$. After the illumination of each groove, the cylinder has to be translated in axial direction with respect to the spot over a distance of one grating period ($4\ \mu\text{m}$). This can be realised by mounting the quartz cylinder on the spindle of a precision lathe (see figure 4.9). The cylinder is now rotated by the spindle and translated in axial direction by the z-slide. An argon ion laser (emitting the UV-wavelengths of 351.1 nm and 363.8 nm) will be used for the illumination. The objective which focuses the laser beam is attached to the x-slide of the lathe. This slide can be used for focusing the spot on the surface of the cylinder. Optimal focusing can be realised by observing the parallelism of the beam which is reflected by the cylinder surface and passes the beam splitter. If the focusing point of the beam coincides with the cylinder surface, the reflected beam will be parallel.

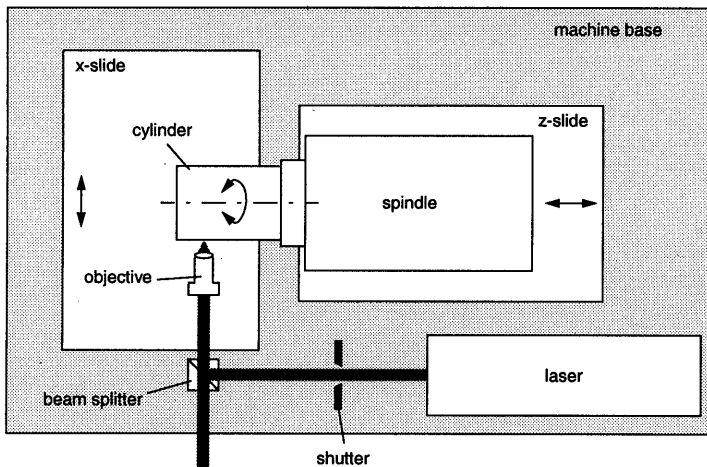


FIGURE 4.9 Schematic representation of the illumination setup

This setup for the illumination process is similar to that of the diamond turning process, with the diamond tool replaced by an optical spot. For the discussion with respect to the pitch errors and the straightness errors of the grating pattern induced by the manufacturing process we can refer to paragraph 4.3.3.

The main groove shape errors originating from this manufacturing method are variation in the groove width. These are caused by variations in the width of the illumination zone, due to an out of focus of the cylindrical surface, as a result of shape deviations of the cylinder and alignment errors of the cylinder with respect to the axis of rotation. Since the laser emits a Gaussian TEM₀₀ beam, the focused beam will also be Gaussian (assuming an aberration-free system). The depth of focus $\pm\Delta x$ can now be derived from the formula which describes the divergence of a Gaussian beam, i.e. the radius w of the beam as a function of the position in the propagation direction x [24]:

$$w(x) = w_0 \sqrt{1 + \left(\frac{\lambda x}{\pi w_0^2}\right)^2} \quad (4.6)$$

where x is the distance propagated from the 'waist' (place where the wavefront is flat: in this case the focus point) of the beam, w_0 is the radius of the Gaussian beam at the waist and λ is the wavelength of the laser light. By setting $w(x) = 1.05w_0$ (to allow for 5% increase) and solving for $x = \Delta x$, it yields:

$$\Delta x \approx \frac{0.32\pi w_0^2}{\lambda} \quad (4.7)$$

With a wavelength of the laser light of 360 nm and a required focus spot diameter of 2 μm the corresponding depth of focus is equal to 2.8 μm . This means that the sum of the out-of-roundness and the alignment errors of the cylinder has to stay within this value, to prevent variations larger than 5% on the groove width. This condition makes high demands upon the shape accuracy of the quartz cylinder. An alternative solution is the use of an auto-focus system. To realise this the out of focus has to be measured and used in a closed loop system to adjust the x -position of the objective continuously.

Development

After the illumination the photosensitive resist has to be developed in a developing bath. The illuminated resist will be removed. The remaining resist will serve as a mask during the plasma etching process.

Plasma etching

The cylinder can now be etched in the etching reactor. The etching time determines the depth of the grooves. From experiments it has appeared that the etching time for a groove depth of 220 nm is about 10 minutes. After the etching process the mask has to be removed from the surface. This can be done in the same etching reactor using an oxygen plasma. This plasma will only remove the remaining resist and not affect the quartz surface.

Applying a reflection coating

Finally a reflection coating (e.g. chrome or silver) has to be applied to the outer surface of the cylinder. Vacuum evaporation is a common technique to apply this type of coatings. To obtain a homogeneous coating the total surface, the cylinder has to be rotated during the evaporation.

To investigate the feasibility of the described manufacturing method, several experiments have been carried out. For these experiments pieces of a quartz tube (dimensions: $\text{Ø}52 \times 46 \times 55$) have been used. Since the out of roundness of these cylinders is much larger (about 50 μm) than the depth of focus of a Gaussian beam with a focus diameter of 2 μm , it is not possible to create the required small grooves on these cylinders. Therefore the laser beam is focused to a larger spot of about 10 μm diameter. This spot has a depth of focus of 70 μm . All the described process steps, except the vacuum evaporation, have been carried out. The distance between the successive grooves is relatively large (about 100 μm) to investigate the influence of variations of the illumination time and illumination intensity. Figure 4.10 and figure 4.11 show SEM (scanning electron microscope) images of the etched grooves on the cylinder.

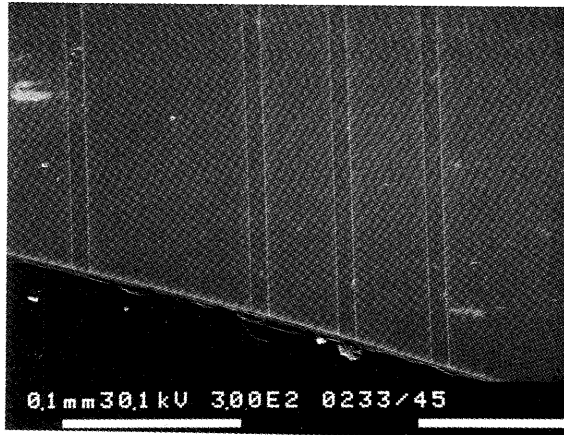


FIGURE 4.10 SEM image of the etched grooves on (a piece of) a quartz cylinder

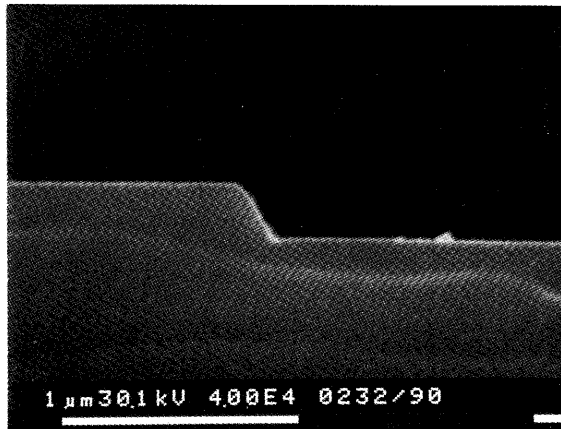


FIGURE 4.11 SEM image of a cross section of one of the grooves

As expected, the grooves have a width of about $10\ \mu\text{m}$. Figure 4.11 shows a typical etching profile with non-vertical walls. This is caused by the fact that the walls of the mask were also non vertical (due to the Gaussian intensity distribution of the

applied spot) and were partly removed during the etching. However this effect will not cause problems, since the depth of the grooves is small with respect to the width of the grooves.

After the etching process the quartz still shows an optical surface quality. Figure 4.12 shows the measured depth of the grooves as a function of the axial position of the cylinder. From these results it can be concluded that the radial etching velocity is nearly uniform over a range of about 35 mm (maximum variations in depth $\approx 10\%$).

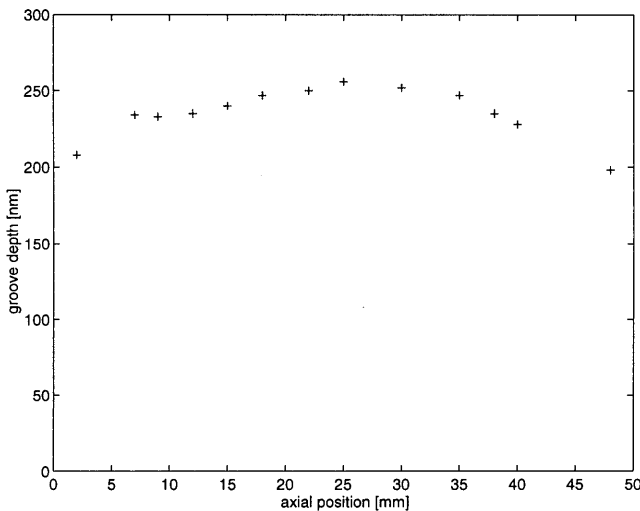


FIGURE 4.12 Measured depth of the etched grooves versus the axial position on the cylinder

Despite the fact that no grating structure is manufactured with the required specifications, we can conclude that plasma etching is also a suitable manufacturing method. However, to obtain a grating structure with the required specifications, the shape deviations (cylindricity) of the quartz cylinder has to stay within a few micrometres. This requirement combined with an optical surface quality of the cylinder will be very hard to realise, since in general the polishing process will affect the shape of the cylinder adversely. The use of an auto-focus system, to overcome

this problem, is also rather complicated. An other disadvantage of this method is the fact that after the illumination step, the cylinder has to be removed from the spindle. Replacing the cylinder to the spindle after the etching process will always introduce alignment errors (as already described in paragraph 4.3.3). Compared to diamond turning, the described process is rather laborious for manufacturing one or a few prototypes. However, for the manufacturing of larger amounts of cylindrical grating structures plasma etching would be an attractive manufacturing method.

Considering the above mentioned arguments, diamond turning will be applied for the manufacturing of a cylindrical grating structure on the first prototype of the spindle. If the concept appears to be successfully and a larger amount of cylindrical grating structures must be manufactured in future, the manufacturing method based on plasma etching can be further developed.

5. Mechanical construction

In this chapter the realisation of the mechanical construction of the prototype as presented in chapter 3 will be discussed. Figure 5.1 shows again a schematic representation of this spindle and the location of the main subsystems. These subsystems will be discussed separately in the next paragraphs. Besides, aspects related to manufacturing and assembling will be considered.

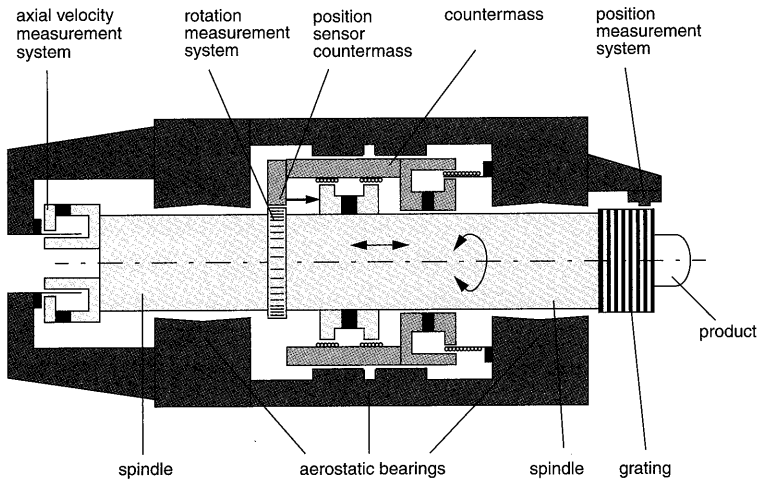


FIGURE 5.1 Schematic representation of the spindle with axial motion control

5.1 The spindle

The concept of the spindle configuration as presented in chapter 3 makes special demands upon the mechanical design of the spindle:

Since the spindle is guided by radial aerostatic bearings, with an air gap of $8\ \mu\text{m}$ (see also paragraph 5.2), the shape and the dimensional accuracy of the spindle must be very high. In general the cylindricity of a precision spindle (using aerostatic bearings) must be better than $1\ \mu\text{m}$. This specification restricts the manufacturing techniques and the materials which can be applied. Diamond turning and precision grinding are manufacturing techniques which can reach this high specification.

During non-rotationally symmetric cutting the spindle has to perform dynamic axial motions. Considering sinusoidal motions, the heat dissipation in the coil will be proportional to the square of the total moving mass. This means the spindle mass has to be minimised to obtain a minimal heat dissipation. The chosen configuration makes special demands on the spindle material. Since the spindle runs through the permanent-magnetic circuit of the actuator (see figure 3.16), the spindle material must have a low magnetic permeability. Otherwise the magnetic flux will not pass the air gaps but will flow through the spindle.

The deflection of the spindle due to external loads has to be minimal, which implies a high equivalent stiffness at the nose of the spindle. This stiffness is determined by the stiffness of the bearings (see also figure 3.1) and the mechanical stiffness of the spindle. The mechanical stiffness of the spindle depends on the shape of the spindle and the applied material. To realise a high radial stiffness combined with a minimal mass indicates the spindle will be hollow. The applied material should have a high specific stiffness (E/ρ , where E is the Young's modulus and ρ is the specific mass of the material). A high specific stiffness will also be beneficial to obtain high natural frequencies of the spindle, since for the natural frequencies ω_n of a mechanical construction we can write [26]:

$$\omega_n \propto \left[\frac{E}{\rho} \right]^{\frac{1}{2}} \quad (5.1)$$

To prevent undesired vibrations during the cutting process, the mechanical resonances of the spindle and the construction may not be excited by disturbance forces related to the cutting process. Disturbance forces in radial direction are mainly caused by imbalance of the spindle or magnetic reluctance forces (as discussed in chapter 3), which have a frequency equal to the rotational frequency of the spindle. This means that the natural frequencies of the resonances of the spindle in radial direction must always be higher than the rotational frequency of the spindle. The natural frequencies of the axial resonances must be higher than the required controlled bandwidth in axial direction.

Table 5.1 gives an overview of the specific stiffness for some construction materials which could be applied.

Material:	$E \text{ [N/m}^2\text{]} \times 10^{10}$	$\rho \text{ [kg/m}^3\text{]} \times 10^3$	$E/\rho \text{ [Nm/kg]} \times 10^7$
Aluminium	7	2.7	2.6
Titanium	9	4.5	2
Al_2O_3	25 - 40	3.9	6.4 - 10.3
SiC	30 - 50	3.2	9.4 - 15.6

TABLE 5.1 Specific stiffness of several materials

The ceramics Al_2O_3 and SiC have a high specific stiffness. Applying these ceramics would yield an optimum solution with respect to the stiffness and the mass of the spindle. However it has to be realised that these materials are difficult to machine compared to aluminium. An other disadvantage of these materials is their open structure, which can lead to inadmissible bearing noise. This effect will arise particularly if aerostatic bearings with inlet orifices are applied [27]. Besides, this project is focused on the development of a prototype, therefore it is important to have the possibility to assemble (and disassemble) the components (e.g. the magnetic circuit of the velocity sensor, the grating and the product fixture) in a relatively easy way. For these reasons it has been decided to apply aluminium as the spindle material of the first prototype. By using aluminium, bolted joints can be used for the attachment of the components to the spindle.

The spindle will be manufactured by diamond turning. To protect the spindle against mechanical damage (e.g. due to failure of the air supply) a relatively hard opal coating (≈ 350 Vickers hardness) will be applied to the spindle after diamond turning. This coating makes the spindle also corrosion resistant. The dimensions of the spindle are: $\varnothing 50 \times 34 \times 285$ mm.

The magnetic circuit of the axial velocity sensor is attached to the back side of the spindle (see figure 5.2). The magnetic circuit of the actuator is glued to the spindle. The specifications of the applied magnetic circuits are presented in appendix B. The grating and the mounting plate are attached to the front plane of the spindle. To prevent misalignment or deformation of the cylindrical grating caused by mounting the product, the grating as well as the mounting plate are both directly bolted to the spindle and have no direct mechanical contact to each other.

The total mass of the spindle and the attached components, as shown in figure 5.2, is 1.9 kg.

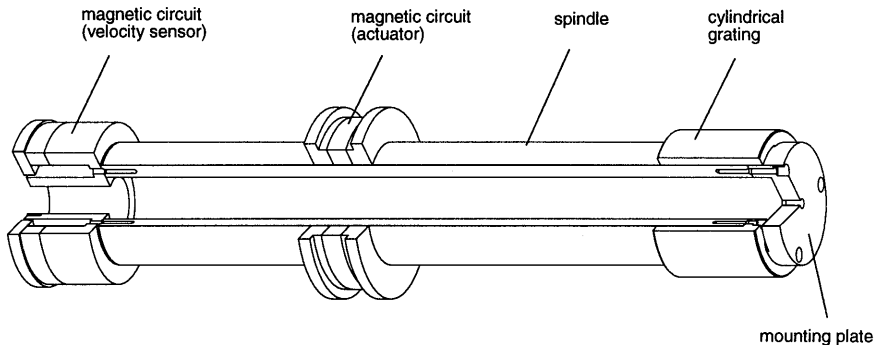


FIGURE 5.2 The spindle, the magnetic circuits and the grating (cutaway representation)

5.2 The aerostatic bearings

Compared to most other bearing types, aerostatic bearings distinguish themselves by a very low friction and very small error motions. During the last decades, within the Philips Research Laboratories much experience has been gained in designing

and manufacturing aerostatic bearings. Models have been developed to predict the static and dynamic behaviour of these bearings. The applied bearings are designed utilizing software packages based on these models [28].

In the described concept aerostatic bearings are applied for the radial bearing of the spindle and the countermass, an additional aerostatic bearing is used for locking the rotation of the countermass (see figure 5.3). For the radial bearing of the spindle two bearings are applied. These bearings utilize conical air gaps (minimal air gap $8\ \mu\text{m}$, maximal air gap $20\ \mu\text{m}$) with small inlet orifices ($\varnothing 0.3\ \text{mm}$, 8 per bearing). This bearing type is chosen for its relatively high radial stiffness. The conicity of the air gap and the dimensions of the inlet orifices are optimized to obtain a maximal radial stiffness. The calculated stiffness of each bearing equals $80\ \text{N}/\mu\text{m}$ (at a supply pressure of 6 bar).

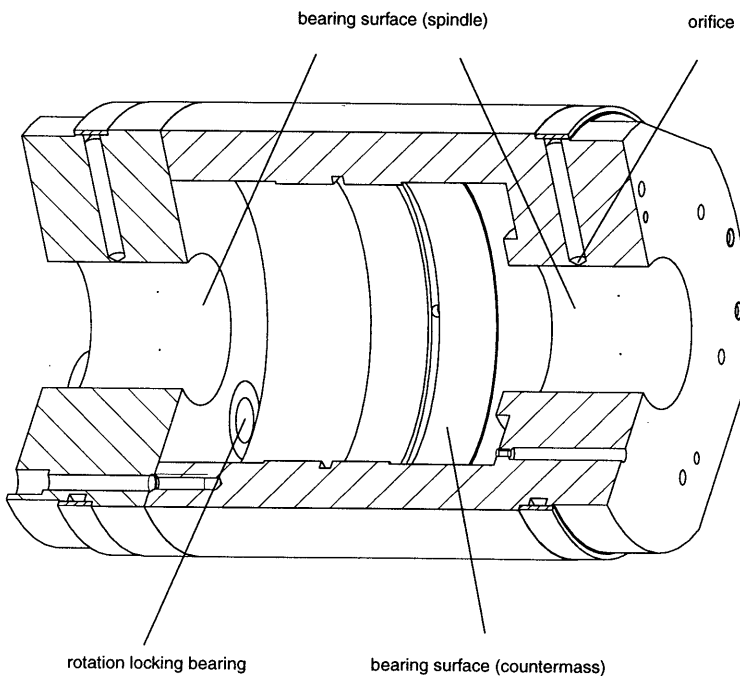


FIGURE 5.3 The bearing house (cutaway representation)

The dynamic behaviour of the spindle (in radial direction) is calculated using a finite element model of the spindle and the bearings [29]. In this model the aerostatic bearings are considered as linear springs, the magnetic circuits are considered as rigid bodies which are attached to the 'flexible' spindle. These calculations yield a lowest natural frequency of 845 Hz. This means the radial resonances of the spindle will never be excited by the rotational frequency ($N_{\max} = 3000 \text{ rpm} = 50 \text{ Hz}$) of the spindle.

During nonrotationally symmetric cutting the counter-mass will perform dynamic motions. To minimise the dynamic disturbance forces on the frame caused by these motions, the friction in the guiding of the counter-mass has to be minimal. For the small dynamic motions (limited to a few hundred micrometre) this could possibly be realised by applying a guiding based on flexible leaf springs. However the counter-mass must also be able to follow the quasi static motions of the spindle over a distance of about 25 mm. Therefore the counter-mass is also guided by a radial aerostatic bearing, which is placed between the bearings of the spindle and is concentric with them (as shown in figure 5.3). To lock the counter-mass for rotations, an additional aerostatic bearing has been applied (the so-called 'rotation locking bearing'), that guides a pin which is attached to the counter-mass (see also figure 5.4).

The bearing house is manufactured by diamond turning and made of bronze. To enable the assembling of the spindle and the bearings, the total bearing house has to be split into two parts. The front part contains one of the spindle bearings and the counter-mass bearing. The back part contains the other spindle bearing and the rotation locking bearing. To enable an accurate alignment between both parts, the outer surfaces and the mating surfaces are manufactured together with the bearing surfaces. The outer surfaces can now be used as a reference for the radial alignment of both parts with respect to each other. The actual alignment of both parts is realised by placing both parts on a precision rotation table and subsequently aligning both parts in radial direction with respect to the rotation axis of the table. Now both bearing parts can be bolted to each other. In this way the radial alignment error can be reduced to less than $2 \mu\text{m}$.

The air supplies for the four bearings are situated at the back side of the bearing house. The pressure of the bearings for the spindle, the counter-mass and the rotation locking can be adjusted separately.

5.3 The countermass

As shown in figure 5.4, the countermass consists of the soft-magnetic yoke, the coils, the magnetic circuit of the countermass actuator, the countermass bush and the rotation locking pin.

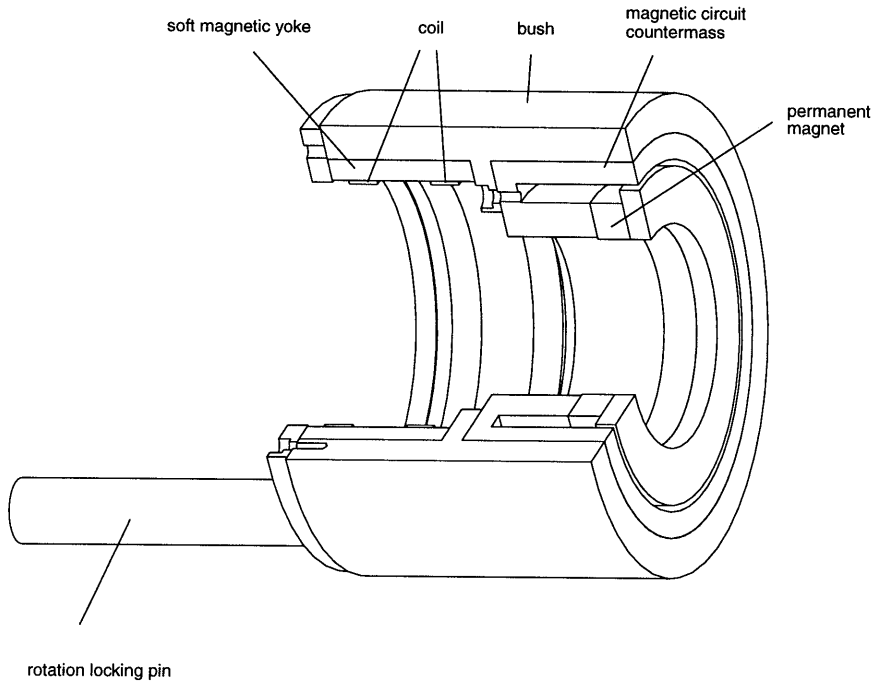


FIGURE 5.4 Countermass (cutaway representation)

The soft-magnetic yoke is a part of the magnetic circuit of the spindle actuator and is made of cobalt-iron. The coils of the spindle actuator are encapsulated by lacquer and glued into the soft magnetic yoke. The magnetic circuit of the countermass actuator is also a part of the countermass. The coil of this actuator will be attached to the bearing house. The bush of the countermass which is guided by the aerostatic bear-

ing is made of aluminium and covered with an opal coating. Since the reading head of the rotary encoder will be attached to the counter-mass (see paragraph 5.4) the counter-mass has to be locked for rotation. For this reason a locking pin is attached to the counter-mass. This pin is guided by the rotation locking bearing (see figure 5.3). To prevent overconstraining of the counter-mass, the pin is coupled by an elastic element which only constrains two degrees of freedom (axial translation and rotation around the spindle axis)

The total mass of the counter-mass is 2.1 kg and thus almost equal to the moving mass of the spindle (1.9 kg). This means that if the counter-mass is considered as a free moving mass, which is valid for frequencies above the bandwidth of the counter-mass controller, the amplitude of the dynamic motions of the counter-mass will be almost equal to that of the spindle (as mentioned in paragraph 3.4.5). Since the dynamic motion of the spindle are limited to a maximum of a few hundred micrometre, the maximum relative motion between the spindle and the counter-mass will be about half a millimetre. This small value of the maximum relative motion is beneficial, because it implies that the coils of the spindle actuator need only to be a little longer than the depth of the air gap of the magnetic circuit, to establish a constant force factor of the actuator during the motion. It means also that the energetic efficiency of the spindle actuator can be high, because almost all turns of the coils will be in the air gaps of the magnetic circuit.

5.4 The rotation measurement system

The rotation of the spindle is measured by an optical system. This system consists of a ring with slits which is attached to the spindle and a reading head which is attached to the counter-mass (as represented in figure 5.5). Note that the actual location of the ring and the reading head is different than in figure 5.1, whereas the principle stays the same.

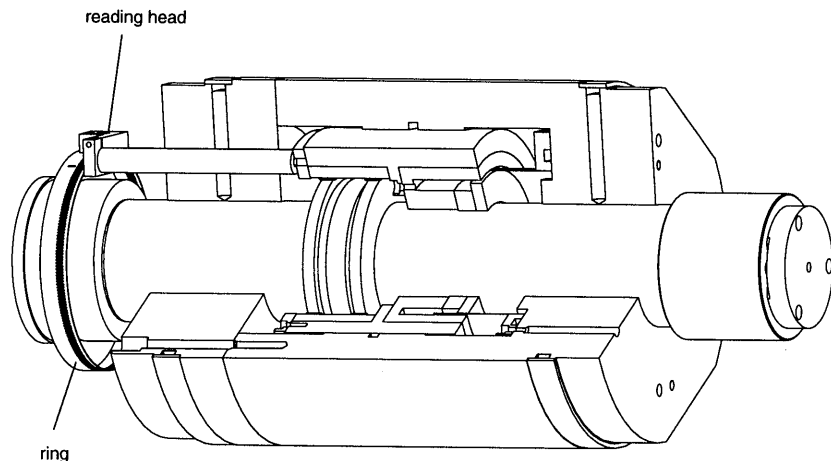


FIGURE 5.5 The reading head mounted to the counter-mass (cutaway representation)

The reading head contains LED's, photo sensitive transistors and a mask (see figure 5.6). Depending on the angular position of the ring, the transistors are illuminated by the light of the LED's, which passes the slits in the ring and the mask. A rotation of the ring will lead to fluctuations in the amount of light on the transistors, which causes a fluctuating output signal of the transistors. These output signals are digitized to obtain a square-wave signal. The mask contains two slit patterns which are a quarter of the pitch (of the slit pattern) shifted with respect to each other. This yields two output signals, which are also a quarter of a wave-period shifted relative to each other. The resulting resolution of the system is equal to a quarter of the pitch of the slits, besides the direction of the rotation can be determined now. Since the ring contains 450 slits the angular resolution of this system is equal to 0.2° . This angular resolution seems to be rather low compared to the required axial resolution. However it has to be realised that due to the smooth shape and the relative small axial dimensions (maximal a few hundred micrometres) of the nonrotationally symmetric shape of the intended products, the axial displacement of the spindle can be described accurately as a function of the rotation angle by a relative small number of

points. Besides, an increase of the resolution of the rotation measurement system will only lead to an improvement of the system performance if the frequency of pulses generated by the rotation measurement system is lower than the cycle frequency of the controller (3.3 kHz). In the prototype this will only occur at angular velocities lower than 110 rpm (see also chapter 6). In most of the applications the rotational velocity of the spindle will be considerably higher. This means that for the moment the resolution of the rotation measurement system will not be a limitation to the system performance.

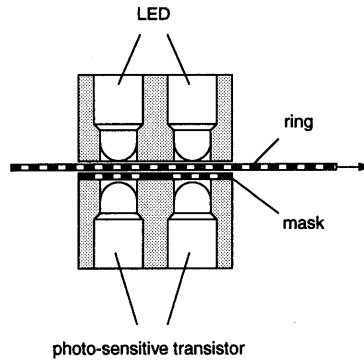


FIGURE 5.6 Schematic representation of the principle of the rotation measuring system

For an absolute measurement of the spindle angle, a reference signal once per revolution is required. This signal is obtained by an additional slit in the ring and an additional LED and transistor in the reading head (see also figure 5.7).

Since the counter mass follows the 'quasi static' motions of the spindle and has been locked for rotation, the reading head of the rotation measurement sensor can be attached to the counter mass (as can be seen in figure 5.5). The maximum relative motion (about half a millimetre) between the counter mass and the spindle will not disturb the rotation measurement.

5.5 The countermass position sensor

Since the countermass has to follow the 'quasi static' motion of the spindle, the relative position of these two component has to be measured. This is realised by a measuring system which is integrated in the rotation measurement system. An additional photo-sensitive transistor in the reading head measures the axial position of the ring with respect to the countermass. Figure 5.7 presents an exploded view of the system and shows the functions of the successive LED-transistor pairs. Depending on the axial position of the ring with respect to the reading head the position measuring transistor will be partly covered by the ring, which reduces the output signal of the transistor. In this way an analog measuring signal is obtained, which can be used for position control of the countermass.

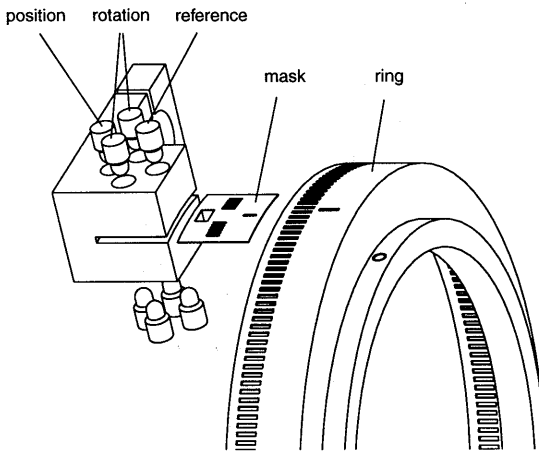


FIGURE 5.7 Exploded view of the measurement system for the spindle rotation and the countermass position

5.6 The fixture of the bearing house

Within this design project the bearing support is considered as a part of the machine frame, therefore the actual design of the bearing support falls outside the scope of this project. The bearing support is supposed to have a constant temperature, which

can be realised by active temperature control. However, the fixture of the bearing house to the bearing support must be considered carefully. This fixture has to ensure a high thermal stability of the position of the rotation axis of the spindle and the front plane of the bearing house. The position of the front plane must be stable because the reading head of the axial position measuring system will be attached to this plane.

The currents in the coils and the friction in the air gaps of the spindle bearings are the major internal heat sources of the spindle. This implies that the internal heat generation will be rotationally symmetric. Since the bearing house shows a high symmetry with respect to the rotation axis, the resulting temperature distribution in the bearing house will be symmetric also. The fixture of the bearing house to the bearing support is realised by 3 mounting blocks at the front side and 3 mounting blocks at the back side. These blocks are positioned at an angle of 120° with respect to each other (see figure 5.8). Since these blocks are relatively weak in radial direction and relatively stiff in tangential direction, they allow a radial expansion of the bearing house without introducing high stress in the bearing house. Due to the symmetry, the axis of rotation will coincide with the thermal centre of this construction. This means that as long as the temperature distribution in the bearing house stays rotationally symmetric the axis of rotation will show no thermal drift.

A high thermal stability of the front plane is obtained by the fact that the mounting blocks used at the front side have a much higher (30 times) axial stiffness than the blocks at back side. The ratio of the axial displacement of the front and the back plane caused by thermal expansion of the bearing house will be inversely proportional to the ratio of the axial mounting stiffness of both planes. The axial distance between the planes is equal to 205 mm. Since the bearing house is made of bronze (coefficient of thermal expansion: $19 \cdot 10^{-6} \text{ K}^{-1}$), the thermal expansion of the bearing house will be equal to $3.9 \text{ } \mu\text{m/K}$, resulting in a thermal drift of $0.13 \text{ } \mu\text{m/K}$ of the front plane and $3.77 \text{ } \mu\text{m/K}$ of the back plane.

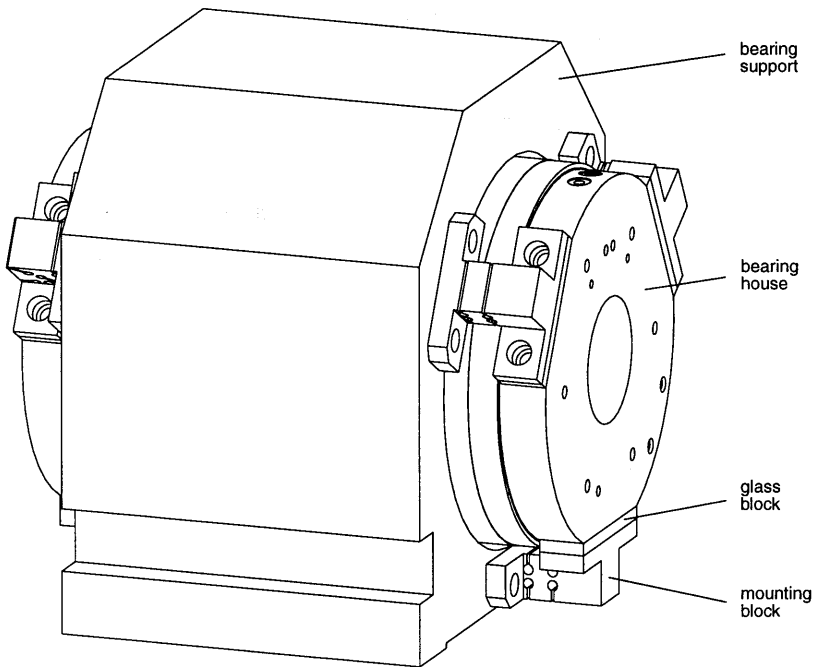


FIGURE 5.8 The bearing house mounted in the bearing support (bolts are not drawn)

To minimize the thermal load of the bearing support by the internal heat sources of the spindle, the bearing house is thermally isolated from the support by isolation blocks made of glass, which are placed between the mounting blocks and the bearing house. In this way the thermal resistance for heat transfer from the bearing house to the bearing support by conduction (calculated value: 7.7 K/W) is about 15 times higher than the thermal resistance of the bearing house for free convection to the environmental air (calculated value: 0.5 K/W). Assuming that the environmental air as well as the bearing support have a constant temperature of 20 °C, 92% of the generated heat will be transferred to the environment and only 8% to the bearing support.

The heat production in the spindle bearings is proportional to the square of the rotational speed of the spindle. The heat generation at 3000 rpm is equal to 1.3 W. (This

value was obtained from the calculations of the software package which has been mentioned already in paragraph 5.2). The heat production in the coils of the actuators is proportional to the resistance of the coils and to the square of the currents in the coils. The current in a coil is proportional to force generated by the actuator. When turning rotationally symmetric products the actuators only have to generate a force equal to the axial cutting force, which will be at most 1 N. This will lead to a maximum heat dissipation of 0.02 W in the spindle actuator and 0.27 W in the counter-mass actuator, as can be calculated from the specifications actuators as presented in appendix B. However during turning nonrotationally symmetric surfaces the spindle actuator has to generate also the acceleration forces of the spindle which can be considerably higher than the cutting forces (as already shown in figure 3.2). The dissipated power (P_{disp}) in the actuator caused by the generation of sinusoidal motions of the spindle with frequency f and amplitude \hat{z} , can be calculated by:

$$\begin{aligned}
 P_{disp} &= \frac{1}{2} I^2 R \\
 &= \frac{1}{2} \left(\frac{F}{k_f} \right)^2 R \\
 &= \frac{1}{2} \left(\frac{M 4 \pi^2 f^2 \hat{z}}{k_f} \right)^2 R \\
 &= \frac{8 \pi^4 M^2 f^4 \hat{z}^2 R}{k_f}
 \end{aligned} \tag{5.2}$$

Where I is the amplitude of the current in the coil, R is the resistance of the coil, F is the amplitude of the generated force, k_f is the force factor of the actuator and M is the mass of the spindle. Figure 5.9 shows the heat dissipation of the spindle actuator as a function of the frequency and the amplitude of the sinusoidal motions. From this figure it can be seen that the dissipated power will strongly increase at high frequencies and large amplitudes.

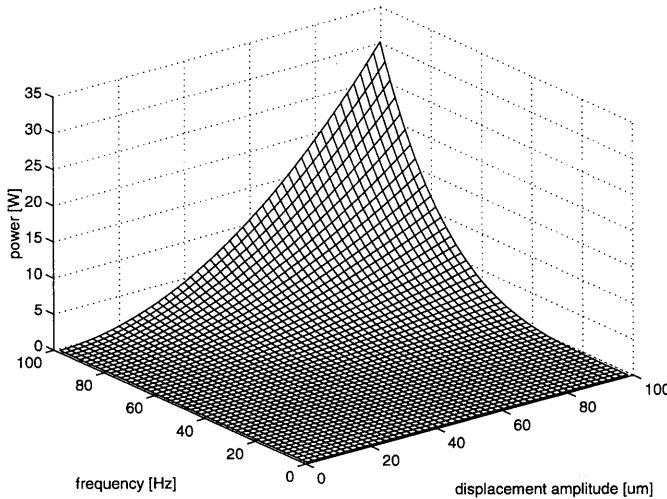


FIGURE 5.9 Dissipated power in the coil of the spindle actuator versus the frequency and the amplitude of sinusoidal motions of the spindle

5.7 The position measurement system

As already mentioned the cylindrical grating is attached to the front plane of the spindle, whereas the reading head is mounted to the front plane of the bearing house (see figure 5.10). In this way the axial displacement of the spindle can be measured very close to the product, which is beneficial to reduce the errors caused by thermal deformations. The thermal errors can be further minimized by making the cylinder of a material with a low coefficient of thermal expansion (e.g. Invar or Zerodur). However for practical and financial reasons the cylindrical grating of the first prototype will be made of copper with a layer of electroless nickel upon it.

The support which is used to mount the reading head to the bearing house offers the opportunity to adjust the head accurately with respect to the cylindrical grating in the most critical directions. The head can translate in x-direction and can be rotated around the vertical y-axis. In this way an optimal alignment of the head with respect to the grating can be achieved.

In a practical situation the cylindrical grating as well as the reading head has to be protected against dust (e.g. chips or lubricant). This can be realised by applying two concentric cylinders: one cylinder is attached to or integrated with the mounting plate on the spindle, the other cylinder is attached to the bearing house. The exhausted air from the air bearings will create a positive pressure difference between the inner cylinder and the environment. The resulting air flow in the gap between both cylinders will prevent that dust will come into the inner cylinder. The actual construction of these components is beyond the scope of this project.

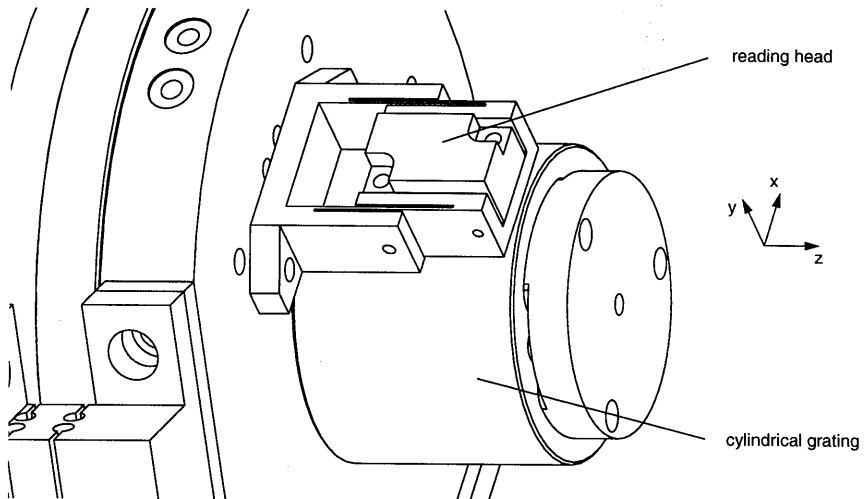


FIGURE 5.10 Detailed view of the reading head

5.8 The total construction

In the previous paragraphs the main components of the total construction have been discussed and shown separately. Figure 5.11 shows the complete prototype of the spindle unit.

At the back side a triangular plate is attached to the bearing support, which holds the coil of the axial velocity sensor. Besides this coil, also a focus error sensor can be attached to this plate concentric with the rotation axis of the spindle. This sensor will be used for the axial position control during the manufacturing of the cylindrical grating. The focus error sensor can also be used to evaluate the performance of

the grating system (see also chapter 6). For these applications a mirror is attached to the magnetic circuit at the back side of the spindle. The rotation of the spindle will be realised by a dc-motor using a rope.

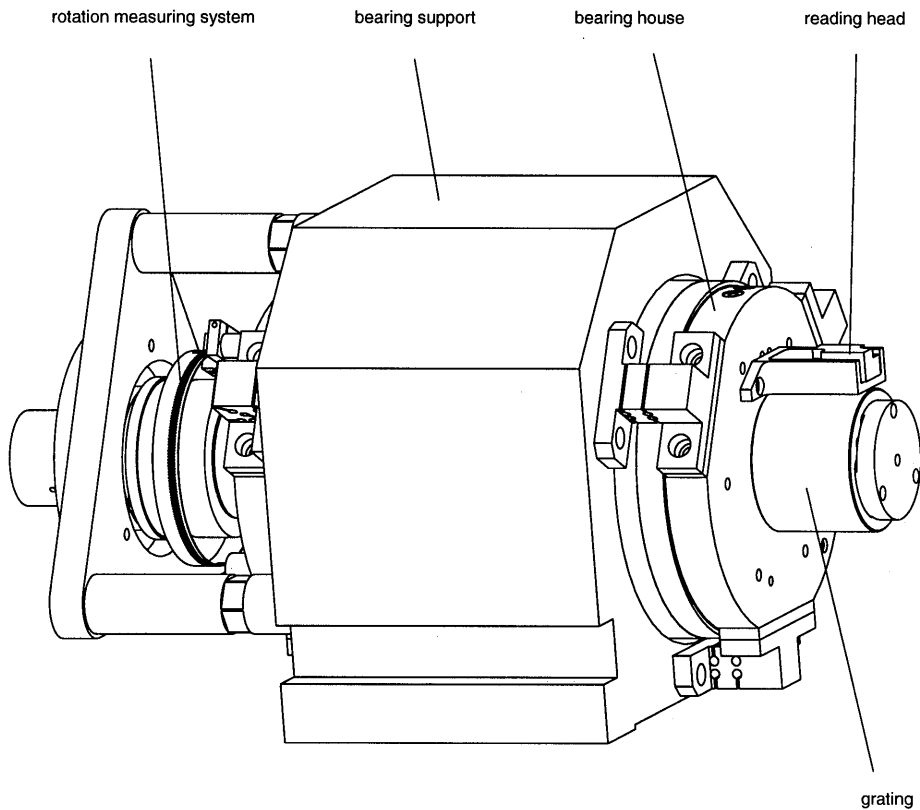


FIGURE 5.11 The total construction

6. Control system

The main function of the control system is the position control of the spindle (i.e. generating the input signal for the spindle actuator on the basis of the actual setpoint signal and measured position of the spindle). Besides, the control system will be used for software error compensation, position control of the counter-mass and data acquisition. In this chapter the main issues concerning the architecture of the control system will be presented. The chosen architecture will be argued and explained. The main sub-systems (the spindle control, the computer and the counter-mass controller) will be discussed separately. Furthermore, the calculation and the implementation of the software error compensation for minimising the axial error motions of the spindle will be considered. Finally, practical limitations on the system performance will be discussed.

6.1 Introduction

As a result of the chosen concept, the dynamic model of the system can be relatively simple. Due to the fact that the friction caused by the aerostatic bearings is very low and the mechanical axial stiffness of the spindle is relatively high (about $500 \text{ N}/\mu\text{m}$), the spindle can be considered as a free moving mass which is driven by a force generating (Lorentz) actuator. Ascertain from rough calculations no axial resonances of the mechanical structure of the spindle are expected below 1000 Hz. Since the driving force of the actuator will go through the centre of gravity of the spindle and the radial eigenfrequencies are high with respect to the rotation frequency (as discussed in paragraph 5.2), the system can be considered as one-dimensional.

As mentioned in chapter 3, a closed-loop system will be used to control the axial position of the spindle. Figure 6.1 shows a simplified representation of the spindle configuration. The forces of the actuator act on the magnetic circuit which is coupled rigidly to the spindle. Besides these driving forces also disturbance forces, which are mainly caused by the cutting process, will act on the spindle. The disturbance forces combined with the driving forces will cause displacements of the spindle. These displacements are measured by the position measuring system and compared with the desired position (setpoint), the difference of both signals is called the position error signal e . This signal is used by the controller to generate the input signal of the actuator.

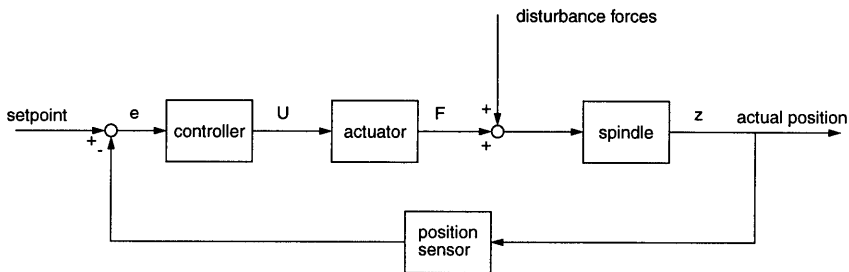


FIGURE 6.1 Simplified representation of the closed-loop position control of the spindle

This means the controller has two major tasks: first, following the setpoint signal as good as possible and secondly minimizing the axial position disturbances, caused by the disturbance forces on the spindle. In other words, the tasks of the controller is to minimize the position error e . The steady-state component of the position error can be reduced to zero (theoretically) by implementing an integrating action in the controller. This means the static stiffness of the controlled system would be infinite. In practice the static stiffness is limited by the noise level or digitizing level of the position measuring system and the maximum force which can be generated by the actuator.

The position error during dynamic motions of the spindle will be small if the bandwidth of the system is high with respect to the actuation frequency. Besides, a high

bandwidth will improve the disturbance reduction (dynamic stiffness) of the system. The design of the system is focused on a bandwidth, which is at least 10 times higher than the maximum actuation frequency (30 Hz). Since the dynamic behaviour of the mechanical system seems to be ideal over a frequency range of at least 1000 Hz, no serious problems are expected to reach a bandwidth of at least 300 Hz. For this reason a classical controller (PI/PID) will be implemented.

A bandwidth which is considerably higher than the specified actuation frequency of 30 Hz will also be necessary for the manufacturing of nonrotationally symmetric optics at an angular velocity of a few hundred rpm with high accuracy. For example, figure 6.2 shows the profile of a beamshaper surface (as presented in figure 1.4) as a function of the spindle angle. Despite the fact that the profile looks like a sinusoidal signal with a periodicity of a 180 degrees (the second harmonic of the rotational frequency), the signal contains also higher harmonics as shown in the spectrum of this signal in figure 6.3. To manufacture this profile with an accuracy better than $0.1 \mu\text{m}$, frequencies up to the sixth harmonic of the rotational frequency should be followed without significant loss of gain or phase shift. This means, to manufacture this shape at a rotational frequency of the spindle of 10 Hz (600 rpm) with a profile accuracy of $0.1 \mu\text{m}$, the bandwidth of the system should be at least 60 Hz.

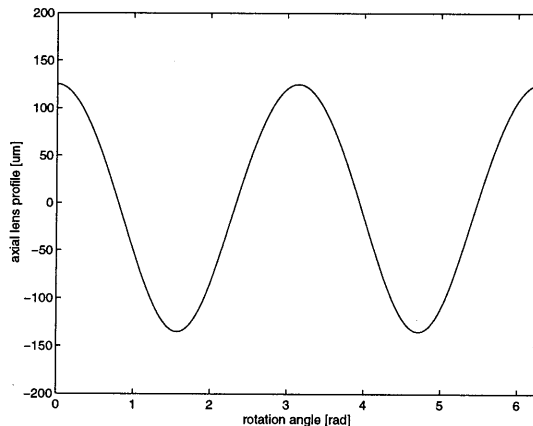


FIGURE 6.2 Axial profile of a beamshaper optic as function of the rotation angle of the spindle

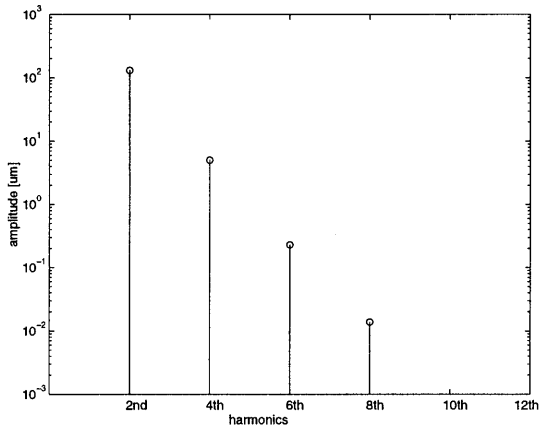


FIGURE 6.3 Spectrum of the profile as presented in figure 6.2

The bandwidth of the closed-loop system can be increased by increasing the gain of the open-loop. However, this can cause stability problems which will be discussed in the next paragraph.

6.2 Control architecture

Figure 6.4 shows an overview of the complete control architecture of the spindle. The control system contains analog as well as digital electronics. The velocity loop of the spindle as well as the counter-mass control are completely analog. The position loop of the spindle, the error compensation and the data-acquisition are digital. In the next sub-paragraphs the main issues with respect to the spindle control, the counter-mass control and the computer system will be discussed.

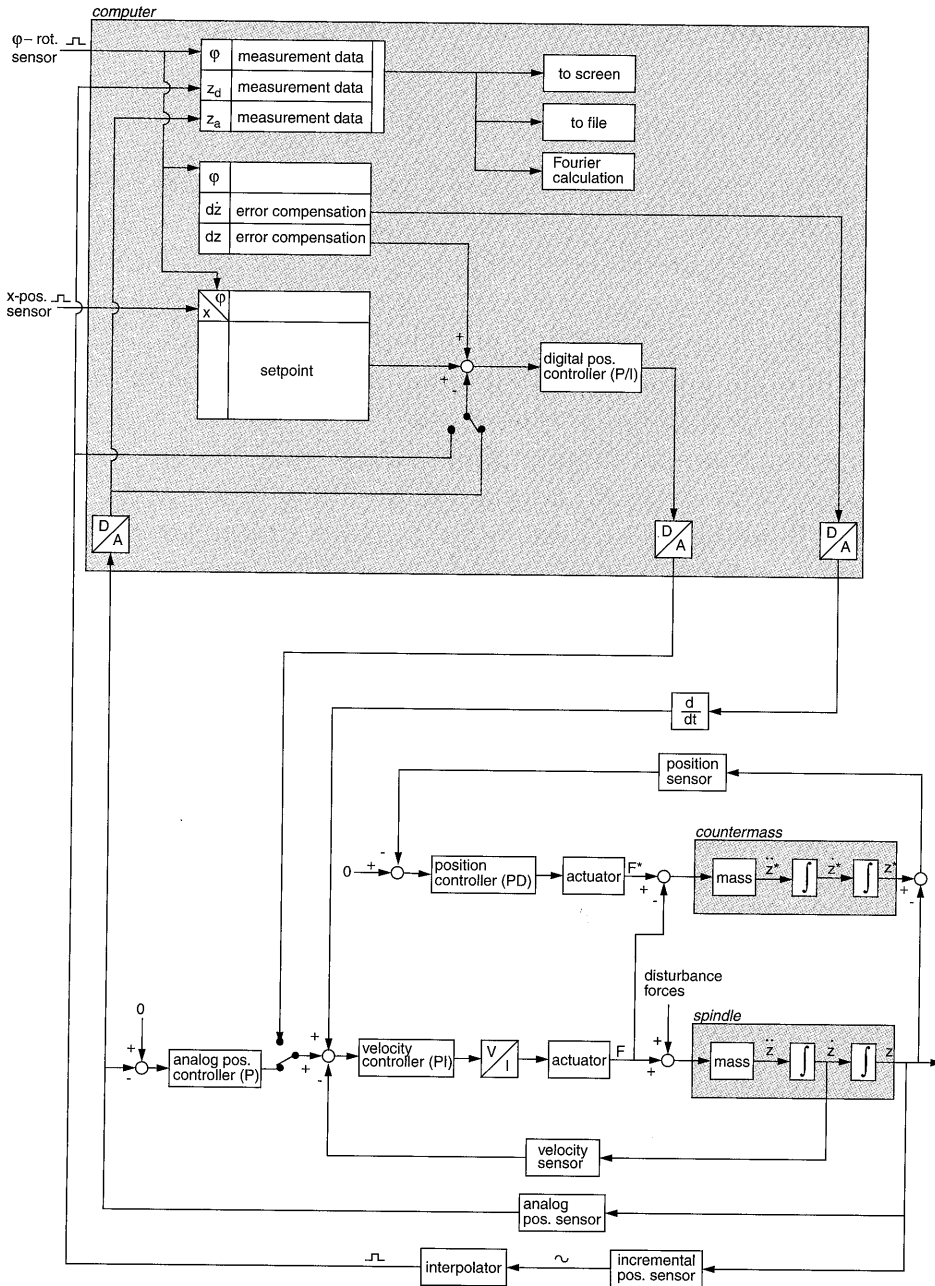


FIGURE 6.4 Overview of the control architecture

6.2.1 The spindle control

In this sub-paragraph the most important issues related to the position control of the spindle will be discussed subsequently.

Velocity feedback

If the spindle is considered as a free moving mass and the controller contains only proportional gain, the system as described in paragraph 6.1 will be unstable theoretically (180 degrees phase lag at the 0 dB crossing of the open loop). Since no damping in the system is assumed, it behaves similar to a simple mass-spring-system, which will show a resonance at the eigenfrequency. Stability of this system can be obtained by adding damping to this system (to create a phase lead at the 0 dB crossing of the open loop). In many controlled systems this is realised by implementing a differentiating action in the controller (PD- / PID-controller). However, the signal to noise ratio will deteriorate by applying a differentiating action, specially at low velocities. Differentiating a position signal to obtain velocity information often leads to noise spikes. This will be detrimental to the system performance unless the resolution of the position sensor is about 10 times higher than the required mechanical resolution [30].

This problem can be overcome by implementing a sensor which measures the axial velocity of the spindle directly and applying position as well as velocity feedback. This will lead to a cascade connection (see figure 6.4). To measure the axial velocity of the spindle a voice coil system can be used. An axial motion between the coil and the magnetic circuit will induce a voltage over the coil, the so-called *counter electromagnetic force* (counter-emf). This voltage is proportional to the relative axial velocity of the coil and the magnetic circuit. It arises from the phenomenon that a Lorentz force acts on the free electrons in a wire that moves in a magnetic field and causes a potential difference over the wire.

Figure 6.5 shows the electrical equivalent circuit diagram of a Lorentz actuator. Here R is the resistance of the coil, L is the self-inductance of the coil and k_f is the force factor of the actuator. From this figure it can be seen also that the voltage measured over an open coil (which implies no currents in the coil) is proportional to the relative axial velocity v between the coil and the magnetic circuit. It is easy to

prove that the ratio of the counter-emf and the velocity is equal to the force factor k_f of the Lorentz actuator.

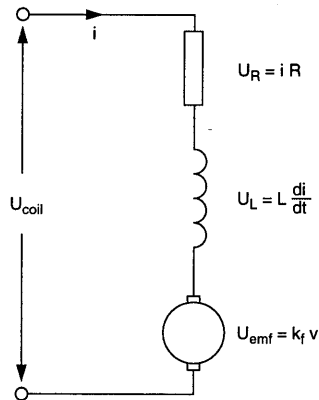


FIGURE 6.5 Electrical equivalent-circuit diagram of a voice coil system (or a Lorentz actuator)

From figure 6.5 it can be seen that the axial velocity of the spindle can also be derived from the counter-emf in the Lorentz-actuator. To determine the counter-emf of the actuator, the current i through and the voltage U_{coil} across the coil of the actuator need to be measured and the resistance R , the self inductance L and the force factor k_f must be known. However, this method of determining the velocity appears to be less accurate, since it is subjected to much more measurement inaccuracies (e.g. the noise on the signal will have a detrimental influence on the determination of di/dt) and it will be subjected to variations of the system parameters (e.g. variations of the resistance of the coil due to thermal effects in the coil).

For this reason the axial velocity information of the spindle will be obtained by measuring the voltage across the open coil of an additional voice coil system. The magnetic circuit of the voice coil is attached to the spindle whereas the coil is attached to the frame (as already presented in chapter 3). It has to be realised that the velocity measurement can be disturbed by an induced voltage in the coil due to

changes in the coupled flux of the coil. Faraday's law of induction says that the voltage induced in a coil is proportional to rate of change of the coupled flux of the coil. This means the coil has to be shielded for external changing magnetic fields, which are caused by the currents in the coil of the actuators. This can be realised by placing conductive material between the coil of the actuator and the coil of the velocity sensor [3]. In the construction, this shielding of the velocity sensor is realised by the bronze of the bearing house.

The coupled flux of the coil will change also if the amount of flux in the air gap of the permanent-magnetic circuit changes. This can occur if soft magnetic material is moved near to the magnetic circuit, as a result a part of the flux of the permanent-magnetic circuit will pass the soft magnetic material instead of the air gap. This means all external effects which can cause changes in the total amount of magnetic flux in the air gap have to be avoided. A possible solution to realise this is the use of a magnetic shielding.

To maintain a maximal signal to noise ratio an analog controller is applied in the velocity loop. To improve the static stiffness of the system (which means minimising the static component of the position error) a PI controller is implemented.

Voltage to current conversion

As can be seen from equation 2.2, the force generated by the Lorentz actuator is proportional to the current in the coil. However the output signal of the controller will be a voltage and not a current. From the electrical equivalent-circuit diagram (figure 6.5) of a Lorentz actuator it can be seen easily that the current in the coil will not be proportional to the applied voltage over the coil (because in general $di/dt \neq 0$ and $v \neq 0$). To realise linearity between the output voltage of the controller and the force generated by the actuator a voltage to current convertor is applied. This is realised by feedback of the voltage across an additional measuring resistance which is connected in series with the coil of the actuator (not explicitly shown in figure 6.4).

Position measurement

The axial position of the spindle can be measured by the interference grating system as described in chapter 4 and by an analog position sensor. The interference grating system is an incremental position measuring system. The reading head of this system produces the phase quadrature signals which have a signal period of $2 \mu\text{m}$.

These harmonic signals are the input signals of the interpolator which generates the so-called TTL signals (two square wave signals) with a hundred times smaller signal period. Using the 90 degrees phase shift between both TTL signals a measuring resolution of $0.005 \mu\text{m}$ will be reached.

The axial position of the spindle can also be measured by an analog sensor. This is a so-called focus error sensor, as described in paragraph 2.3. The sensor is attached to the triangular plate on the back side of the bearing support, concentric with the rotation axis of the spindle. The sensor measures the axial displacement of a mirror which is attached to the spindle. The analog sensor will be applied for the position control of the spindle during the manufacturing of the grating structure, because a spindle with very small axial error motions is required for this application. In chapter 2 it was shown that the axial error motions of the spindle can be reduced to about $0.01 \mu\text{m}$ by applying a similar configuration. The focus error sensor can also be used to evaluate the performance of the incremental position measuring system and to improve the performance of this system by determining the data for software error compensation (see paragraph 6.2.2). In a final (production) version of the spindle unit, the focus error sensor can be removed after the manufacturing of the grating structure and the determination of the software error compensation data.

Position controller

The position controller can be analog as well as digital (implemented in the computer). It will be clear that the analog controller can be applied only in combination with the analog position sensor. The analog controller contains only a gain (no integrating or differentiating action). This gain is tuned to obtain a maximal bandwidth of the system. In the digital position controller, besides the gain also an integrating action can be implemented. The integrating action will reduce the position error to zero during motions with constant velocity.

6.2.2 The computer system

The digital position control of the spindle, the software error compensation and the data-acquisition is realised by a 80486 personal computer. For the interfacing to the spindle, the computer is equipped with an additional analog and digital I/O board (Keithley DAS-1602) and an encoder interface board (Keithley M5312). This configuration is chosen because of the high level of flexibility, which is of special inter-

est during the development of a prototype. An additional reason to choose this configuration, is the fact that within the group, where this project has been carried out, a considerable amount of experience with the applied hardware and software was already available. To realise an actual production machine in future, a more dedicated configuration will be chosen.

The I/O board which is implemented, contains 2 analog output channels and 8 analog input channels (in figure 6.4 only one of these is used). The encoder interface board has 2 digital input channels, which will be used to read the signals of the incremental position measuring system and the rotation measuring system. However, to realise the final version of the spindle unit, a third digital signal (x-position of the tool) has to be read. As a result of the present limitation no nonrotationally symmetric test-products can be manufactured, which require a variation of the axial motion profile as a function of the radial position of the tool (like the beamshaper of figure 1.4 and figure 1.5). Despite this limitation this configuration can be used for a large number of experiments to evaluate the performance of the spindle unit.

The software which carries out the digital control and the data-acquisition is programmed in Turbo Pascal. The program runs with a cycle time of 0.3 ms. Within every cycle of the program the following activities are carried out:

- Reading the input signals of z and φ
- Setpoint generation
- Calculation of the control action
- Error compensation

These activities will be discussed separately below.

Reading the digital input signals of z and φ

The output signal of the analog position sensor is digitized by the AD-convertor on the I/O board. The actual value of the signal is read within every cycle of the control program. The output signals of the incremental position measuring system and the rotation measuring system are counted continuously up to a maximum frequency of 300 kHz. The actual values of these signals also are read within every cycle of the control program.

Setpoint generation

To realise non-rotationally symmetric products, the spindle has to perform axial motions within one revolution of the spindle, as a function of the actual rotation angle (ϕ) and the position (x) of the tool. If the complete axial motion ('dynamic' as well as 'quasi static') between the tool and the product has to be realised by the spindle, the axial spindle motion and the motion of the x-axis need to be synchronised to each other (linear and circular interpolation). In the test-configuration (see also chapter 7) this will be impossible because the x-axis will be controlled separately by a CNC-controller (NUM 760). This test-configuration will be similar to the configuration as presented in figure 1.1. The rotationally symmetric base shape of the products can be realised by the motions of both slides (controlled by a CNC controller). During the tests, the axial motion control of the spindle will only be used to generate the non-rotationally symmetric part of the product's shape. Therefore the axial position of the spindle as a function of the rotation angle is stored in a look-up table. Within every cycle of the control program the setpoint value is generated.

In future, the synchronisation between the x-axis and the spindle motion (to achieve interpolation) can be realised using a DSP-based motion controller, which controls the spindle as well as the x-axis.

Calculation of the control action

Within every cycle of the control program the position error signal is calculated as the difference between the measured axial position and the setpoint signal. This signal will be multiplied by the gain of position controller. If the integrating action is programmed, the position error is integrated over time and added to this signal. The gain of the proportional and integrating actions can be changed on-line from the keyboard. The amplified position error signal is converted to a voltage by the DA-converter on the I/O board and injected in the velocity loop.

Error Compensation

In chapter 2 it has already been mentioned that the measured axial velocity signal can be subjected to disturbances, which cause axial error motions of the spindle. These disturbances are mainly caused by alignment deviations of the magnetic circuit and the coil of the velocity sensor. For instance an eccentricity e of the magnetic

circuit with respect to the rotation axis of the spindle combined with a non-parallelism α between the coil and the rotation axis of the spindle (as shown in figure 6.6) introduces a sinusoidal deviation on the measured velocity δz . The resulting measurement deviation can be described as:

$$\delta z = 2\pi f_s e (1 - \cos \alpha) \sin(2\pi f_s t) \quad (6.1)$$

This means, the deviation has a period equal to one revolution of the spindle and an amplitude proportional to the angular velocity of the spindle. For as long as the frequency of this disturbance signal is below the bandwidth of the closed-loop system, the resulting position error will be proportional to the amplitude of the disturbance signal and thus also proportional to the angular velocity of the spindle.

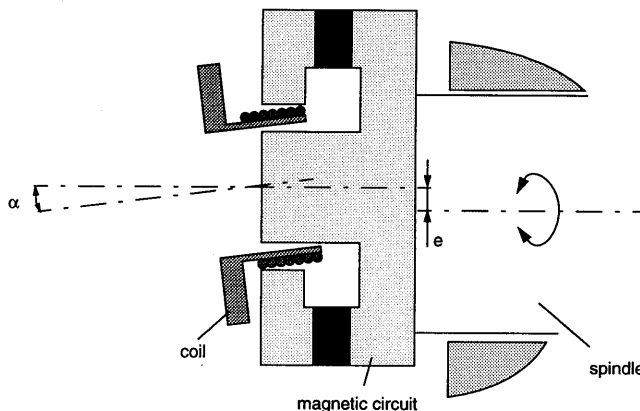


FIGURE 6.6 Alignment errors of the magnetic circuit and the coil of the voice coil system (velocity sensor) which will cause deviations on the measured axial velocity

The disturbances on the measured axial velocity can also be caused by variations in the amount of flux in the air gap of the magnetic circuit during one rotation of the spindle. This effect will occur if soft magnetic material is in the vicinity of the rotating magnetic circuit and the flux distribution around the magnetic circuit (leakage

field) is nonrotationally symmetric. Also in this case a disturbance signal with a periodicity of one spindle revolution and with an amplitude proportional to the angular velocity of the spindle, is injected in the closed-loop system.

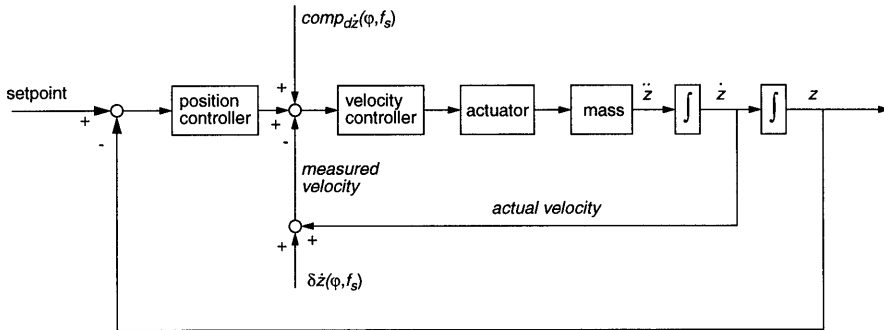


FIGURE 6.7 Simplified representation of the control system, showing the disturbances on the velocity signal and the corresponding compensation signal

The above mentioned disturbances lead to systematic axial error motions of the spindle. These error motions can be reduced by software error compensation. Therefore a compensation signal $comp_{dz}$ has to be generated which has also periodicity of one spindle revolution and an amplitude proportional to the angular velocity of the spindle (see figure 6.7). Since the spindle angle is measured, a signal with a periodicity of one revolution can be realised by creating a look-up table which describes the compensation signal as a function of the spindle angle. The proportionality of this signal to the angular velocity of the spindle can be implemented in the control program. Therefore the values of the look-up table must be multiplied by the actual angular velocity and divided by the reference velocity (angular velocity at which the correction is determined). The actual angular velocity of the spindle must be measured by an additional sensor or it can be calculated from the measured spindle angle as a function of time. However, these operations will enlarge the cycle time of the control program. Because the compensation signal is periodic, proportionality between the amplitude of the compensation signal and the angular velocity can be

realised also by applying an analog differentiating network. This will be explained next.

Since the compensation signal will be periodic it can be described by a Fourier series. For the compensation signal as described in the look-up table ($d\dot{z}(\varphi)$) this means:

$$d\dot{z}(\varphi) = \sum_{n=-N}^N d\dot{z}_n e^{jn\varphi} \quad (6.2)$$

Where the Fourier coefficients $d\dot{z}_n$ and $d\dot{z}_{-n}$ are complex conjugated. As a function of time, this signal can be presented as:

$$d\dot{z}(t) = \sum_{n=-N}^N d\dot{z}_n e^{2\pi j n f_s t} \quad (6.3)$$

Here f_s is the actual rotation frequency of the spindle. Calculating the time derivative of this signal yields:

$$\frac{d(d\dot{z}(t))}{dt} = 2\pi j f_s \sum_{n=-N}^N n d\dot{z}_n e^{jn\omega_s t} = \text{comp}_{d\dot{z}} \quad (6.4)$$

From this equation it can be seen that the differentiated signal is proportional to the rotational velocity of the spindle. Additional effects of differentiating the signal are a phase shift of 90 degrees of each of the harmonics of the Fourier series and an amplification proportional to the frequency of the harmonics of the Fourier series. However these additional effects of the differentiating network will cause no problems, since they can be taken into account when calculating the compensation table signal $d\dot{z}(\varphi)$. The differentiated signal $d(d\dot{z})/dt$ will be injected in the analog velocity loop.

Besides the described disturbances of the velocity signal, the system can also be subjected to periodic disturbances of the position signal. These disturbances will be caused by alignment errors or manufacturing errors of the grating structure. The errors of the grating structure are independent of the angular velocity of the spindle, so the compensation has not to be differentiated. The compensation signal has to be

added to the (angular dependent) setpoint signal. To minimise the cycle time of the computer this addition can be carried out off-line.

Besides these activities which have to be completed within every cycle, the program also has the possibility to carry out other activities. These are carried out in the remaining time and are distributed over a number of cycles. The most important of these activities are:

- Data acquisition
- Calculation of the compensation signals
- Executing CNC programs

Next these activities will be discussed separately

Data acquisition

To be able to evaluate the performance of the system, the computer system can also carry out some data acquisition activities. Several signals such as the analog and digital axial position, the rotation angle, the axial velocity and a number of additional test signals can be recorded over a certain time and stored into the memory of the computer. Subsequently these measurement data can be displayed graphically on the screen as function of time or as function of the spindle angle. The measurement data can also be written to a file. Furthermore Fourier calculations can be made on the recorded data, these calculations will be used to determine the compensation signals.

Calculation of the compensation signals

In general the systematic axial error motions, caused by the disturbances on the velocity signal, show a smooth shape as function of the spindle angle. For as long as the system shows a linear behaviour, the parameters which describe the compensation signal (coefficients of the Fourier series) can be determined in a relatively easy way, using Fourier calculations. Therefore a procedure has been implemented in the control software, which will be described below.

To determine the compensation signal for the disturbances on the velocity signal, the axial position control of the spindle operates in the analog mode. This means the axial position information is obtained from the focus error sensor (which will be

considered as a reference). The resulting axial error motion Eo will be caused mainly by disturbances on the measured velocity signal. These error motions are measured as a function of the spindle angle. From these measurement data the coefficients (Eo_n) of the Fourier series, which describes the axial error motion as a function of the spindle angle φ , are calculated.

$$Eo(\varphi) = \sum_{n=-N}^N Eo_n e^{jn\varphi} \quad (6.5)$$

Where the Fourier coefficients Eo_n and Eo_{-n} are complex conjugated. From experiments it appeared that the axial error motions caused by disturbances on the velocity signal show a smooth shape as function of the spindle angle. Therefore they can be described accurately by a small number of Fourier coefficients ($N < 6$).

Secondly a 'random' compensation test signal R is generated. This signal is obtained from a Fourier series of N random coefficients and their complex conjugates:

$$R(\varphi) = \sum_{n=-N}^N R_n e^{jn\varphi} \quad (6.6)$$

This signal is injected in the closed-loop system and the resulting axial error motions of the spindle are measured as a function of the spindle angle ($Er(\varphi)$). From these measurement data the Fourier coefficients Er_n are calculated.

Now the transfer of the system for a compensation signal described by a Fourier series of N coefficients can be calculated:

$$T_n = \frac{Er_n - Eo_n}{R_n} \quad (6.7)$$

The Fourier coefficients of the signal to compensate for the original error motions $Eo(\varphi)$ can now be calculated by:

$$d\dot{z}_n = \frac{-Eo_n}{T_n} \quad (6.8)$$

From these coefficients the compensation signal can be calculated as function of the spindle angle (using equation 6.2) and can be put into a look-up table.

The mentioned additional effects of the differentiating network (phase shift and amplification of the higher harmonics) will cause no problems, since the compensation test signal (which is used to determine the transfer of the system) will also be differentiated. In this way the additional effects of the differentiating network are automatically taken into account when calculating the compensation signal.

On a similar way a compensation signal for angular depending deviations (straightness errors, see chapter 4) of the grating structure can be calculated. Therefore the analog position sensor will be considered as reference again. The axial error motions of the spindle will now be measured by the analog position sensor, while the position control of the spindle is realised by the incremental position measuring system. From these measurement data the compensation signal can be calculated.

Executing CNC programs

The control program offers the possibility to carry out a limited number of CNC commands. These commands can be entered by keyboard or can be stored in a file. Using these commands, the spindle can be moved with a specified velocity to a specified axial position. Other commands which can be executed are related to: resetting the position value, making position steps, changing of the program settings such as gain of the controller, maximum acceleration, length of the cycle time, etc.

6.2.3 The counter-mass controller

The counter-mass has to follow the 'quasi static' motions of the spindle. Therefore an additional control system (position sensor, controller and actuator) have been implemented.

Position sensor

The optical position sensor which is attached to the counter-mass measures the axial position of the counter-mass with respect to the axial position of the spindle. Since in this way the differential axial position of the spindle and the counter-mass is measured directly, the analog output signal of the sensor can be used for position feedback.

Controller

Since the requirements of the position control of the counter-mass are poor (low bandwidth and relative large position error (up to a few tenths of a millimetre) are allowed), a simple commercially available analog servo controller can be used. The gain of this system will be tuned to obtain a bandwidth of about 5 Hz. Stability of this system is obtained by adding a differentiating action to the controller (PD). The output signal of the controller is used as drive signal of the counter-mass actuator (voice coil).

6.3 Practical limitations on the system performance

The performance of the axial controlled spindle is limited by several practical aspects: the maximum axial stroke of the spindle, the maximum velocity, the maximum actuator current and discretisation effects caused by the digital controller. The influence of these effects on the performance of the spindle will be considered for sinusoidal axial motions of the spindle with a frequency f_i and an amplitude \hat{z} :

$$z(t) = \hat{z} \sin(2\pi f_i t) \quad (6.9)$$

Maximum stroke of the spindle

The maximum stroke of the spindle is limited by the mechanics. In the prototype the stroke is limited to 20 mm. This limitation on the amplitude of the sinusoidal motions is independent of the frequency f_i :

$$\hat{z}_{stroke}(f_i) = \text{constant} \quad (6.10)$$

Maximum velocity

The maximum velocity of the system is limited by the electronics which are applied for interpolation and counting of the output signals of the reading head of the position measuring system. The highest velocity can be reached when using a pc-interface board delivered by *Heidenhain (IK 121 PC Counter Card)*. When using this board the maximum velocity of 0.2 m/s can be reached at a resolution of 0.002 μm . The influence of the maximum velocity v_{max} on the maximum amplitude of the sinusoidal motions can be expressed as:

$$\hat{z}_{velocity}(f_i) = \frac{1}{2\pi f_i} v_{max} \quad (6.11)$$

Maximum actuator current

The maximum current in the coils of the spindle actuators is limited by the maximum output current of the power amplifier. The electronics are designed to generate a maximum actuator current of 4 A. The maximum current of the actuator limits the maximum propulsion force of the actuator and thus the maximum acceleration of the spindle. The influence of the maximum current I_{max} on the maximum amplitude of the sinusoidal motions can be expressed as:

$$\hat{z}_{current}(f_i) = \frac{1}{(2\pi f_i)^2} \frac{K_f}{M} I_{max} \quad (6.12)$$

where K_f represents the force factor of the spindle actuator (6.8 N/A) and M represents the total moving mass (approximately 2 kg).

The influences of the above mentioned limitations on the performance of the designed system, with respect to the maximum amplitude of sinusoidal axial motions, are graphically presented in figure 6.8.

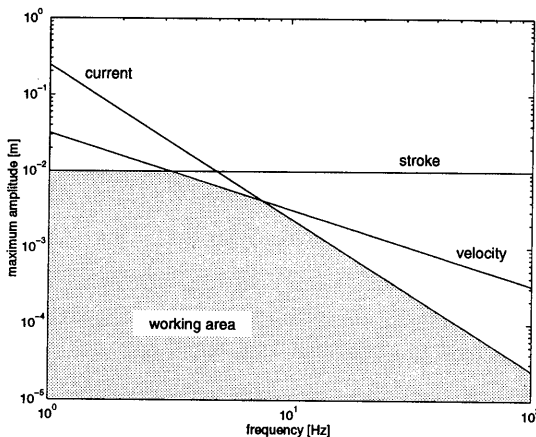


FIGURE 6.8 Influence of the limited stroke, velocity and current on the maximum amplitude of sinusoidal motions of the spindle as a function of the frequency of these motions

Discretisation effects:

Because of the fact that a digital controller is applied, the output signal of the controller will be subjected to discretisation effects. These discretisation effects can lead to high-frequency position disturbances of the spindle, which will have an adverse effect on the surface roughness of a turned surface. The magnitude of the discretisation effects is mainly determined by the cycle frequency of the controller, the resolution of the position measurement system and by the resolution of the rotation measurement system. The position disturbances which arise as a result of these effects will be calculated from the discontinuities in the setpoint signal (generated by the digital controller). To compare the influence of the individual effects with respect to the resulting discontinuities in the setpoint signal, the frequency of the harmonic motions of the spindle f_i is expressed as the product of rotational frequency f_r of the spindle and the number of harmonic motions within one revolution n :

$$f_i = n f_r \quad (6.13)$$

The largest discontinuities in the setpoint signal will arise at the moment, that the axial velocity is maximal. At this moment the amplitude of the discontinuities will be calculated.

The maximum discontinuity caused by the cycle frequency f_c is equal to:

$$\Delta z_{f_c} = \hat{z} \sin\left(n 2\pi \frac{f_r}{f_c}\right) \quad (6.14)$$

In general $f_c \gg n f_r$, which means we can write:

$$\Delta z_{f_c} \approx \hat{z} n 2\pi \frac{f_r}{f_c} \quad (6.15)$$

The maximum discontinuity caused by the limited resolution of the rotation measurement system R_r (counts per revolution) is equal to:

$$\Delta z_{R_r} = \hat{z} \sin\left(\frac{n 2\pi}{R_r}\right) \quad (6.16)$$

In general $R_r \gg n 2\pi$, so we can write:

$$\Delta z_{R_r} \approx \hat{z} n 2\pi \frac{1}{R_r} \quad (6.17)$$

The discontinuity caused by the limited resolution R_p of the position measurement system is constant and equal to:

$$\Delta z_{R_p} = R_p \quad (6.18)$$

To determine the amplitude of the discontinuities caused by the three mentioned effects in a practical situation, the following (realistic) case will be considered:

$\hat{z} = 100 \mu\text{m}$, $f_c = 3300 \text{ Hz}$, $f_r = 16.6 \text{ Hz}$ (1000 rpm), $n = 2$, $R_a = 1800$ counts per revolution and $R_p = 0.005 \mu\text{m}$.

This leads to: $\Delta z_{f_c} = 6.3 \mu\text{m}$, $\Delta z_{R_a} = 0.7 \mu\text{m}$ and $\Delta z_{R_p} = 0.005 \mu\text{m}$.

This means, the discontinuities in the setpoint signal are mainly caused by the limited cycle frequency of the controller. Therefore, the influence of the cycle frequency on the position disturbances of the spindle will be discussed further.

During a cycle period T_c of the control program the setpoint value will be kept constant, after this period a step in this signal will occur (as illustrated in figure 6.9).

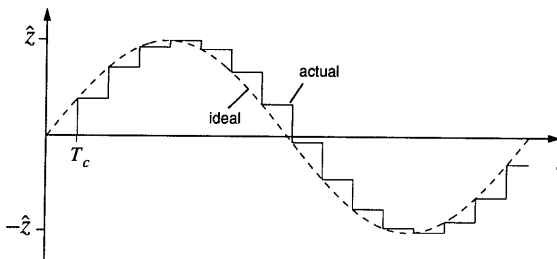


FIGURE 6.9 Ideal sinusoidal setpoint signal and actual discontinuous signal which is generated by the digital computer with cycle time T_c .

The effect as shown in figure 6.9 can be represented by a so-called 'sampler and zero-order hold' system. Figure 6.10 gives a schematic representation of such a system.

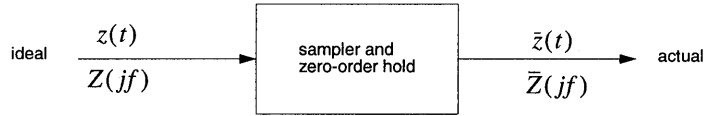


FIGURE 6.10 Sampler and zero-order hold system

The influence of the sampler and zero-order hold system on a sinusoidal signal can be well understood if the system is described in the frequency domain. The calculations which are made to describe the (non-linear) sampler and zero-order hold system in the frequency domain are presented in appendix A. As a result of these calculations, the spectra of the ideal ($z(t)$) and the actual signal ($\bar{z}(t)$) are presented in figure 6.11. The spectrum of an ideal sinusoidal setpoint signal ($Z(jf)$) contains only one frequency component f_i , whereas the actual setpoint signal ($\bar{Z}(jf)$) comprises also higher frequency components, which are paired around multiples of the cycle frequency f_c .

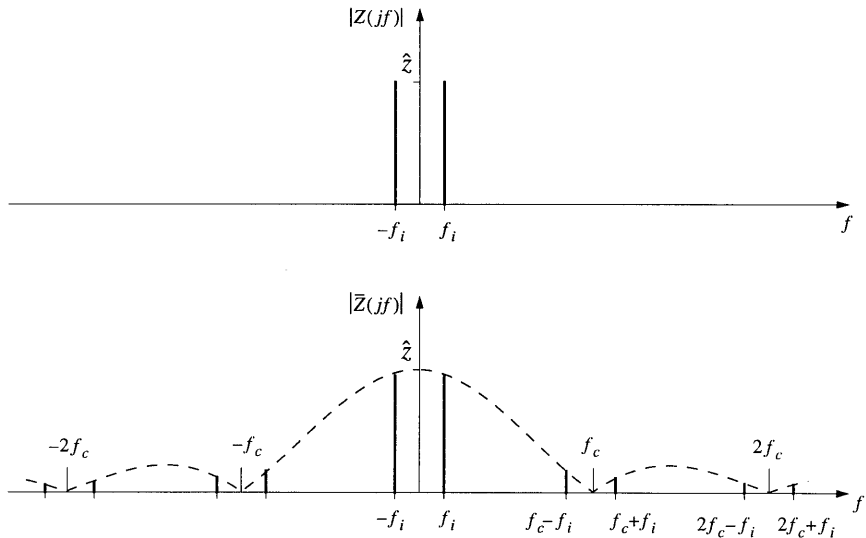


FIGURE 6.11 Amplitude spectra of an ideal sinusoidal setpoint signal (upper) and the resulting actual setpoint signal (lower)

These higher frequency components of the actual setpoint signal will introduce disturbances on the position of the spindle. The amplitude of these position disturbances can be determined by multiplying the spectrum of the actual setpoint signal $\bar{Z}(jf)$ by transfer function of the closed-loop system. An estimation of this transfer function can be obtained by representing the system by a second order system with an eigenfrequency equal to the bandwidth of the closed-loop system. Figure 6.12 shows the gain of the transfer function of such a system with an eigenfrequency of 700 Hz (equal to the bandwidth of the prototype, which will be presented in chapter 8) and a relative damping of 0.5.

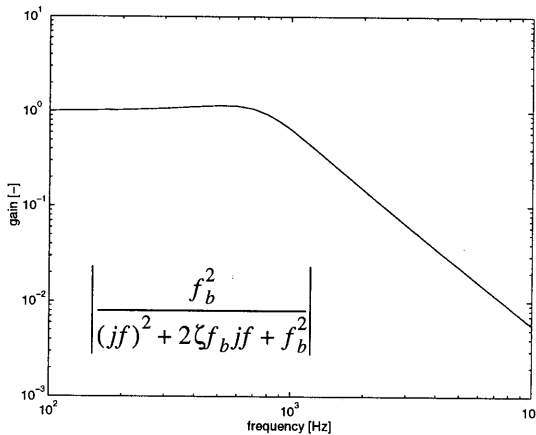


FIGURE 6.12 Gain of the transfer function of a second order system with an eigenfrequency f_b of 700 Hz and a relative damping ζ of 0.5.

The cycle frequency will always be higher than the bandwidth of the system. In the frequency range above the bandwidth, the closed-loop transfer function decreases with 40 dB per decade. This means the most relevant position disturbances will be caused by the two frequency components around the cycle frequency. (Because the suppression by the closed-loop transfer functions for the frequency components around the double cycle frequency ($2f_c$) will be about 30 times higher than for the frequency components around f_c).

Since the cycle frequency f_c will be considerably higher than the frequency of the setpoint signal f_i , the frequency components $f_c - f_i$ and $f_c + f_i$ will lead to position dis-

turbances with a frequency f_c with a beat frequency of $2f_i$ superimposed on it, as shown in figure 6.13. Due to the relative high frequency of these disturbances they will mainly lead to an increase of the roughness of the turned surfaces.

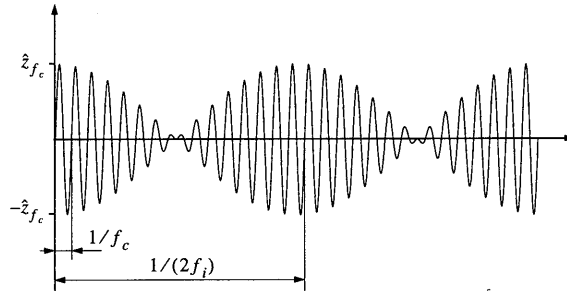


FIGURE 6.13 Position disturbances caused by the frequency components f_c-f_i and f_c+f_i .

The calculated relative amplitude of the position disturbances (\hat{z}_{f_c}/\hat{z}) is plotted in figure 6.14 as function of the cycle frequency f_c for several values of the setpoint frequency f_i .

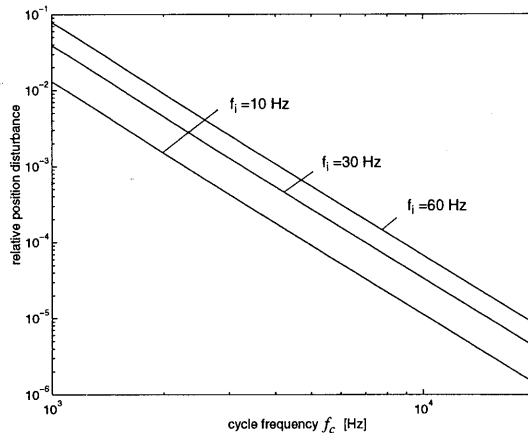


FIGURE 6.14 Relative amplitude of the position disturbances \hat{z}_{f_c}/\hat{z} caused by the frequency components f_c-f_i and f_c+f_i , as a function of the cycle frequency f_c for several values of the setpoint frequency ($f_i = 10, 30$ and 60 Hz)

For the test setup (cycle frequency 3.3 kHz) this means that the specified sinusoidal motions with a frequency of 30 Hz and an amplitude of 250 μm (500 μm peak-valley) will show position disturbances of 0.24 μm . This value will be too large to realise an optical surface quality (specified roughness value: $R_a = 10$ nm). To reduce the amplitude of the position disturbances of the specified sinusoidal motion to a level of 0.01 μm , the cycle frequency should at least be 9.4 kHz. However, to realise non-rotationally products with an optical surface quality on the test setup, the frequency or the amplitude of the setpoint signal must be reduced (see also chapter 7).

If a more dedicated control architecture will be applied in future (e.g. based on a DSP-controller), a cycle frequency of 10 kHz and even higher can be reached without any problems.

7. Experimental evaluation

A prototype based on the concept of the spindle unit presented in the previous chapters has been realised. In this chapter this prototype will be presented. Thereafter the performance of the prototype will be experimentally evaluated with respect to the axial error motions, the dynamic behaviour and the performance of the interference grating system. To evaluate the diamond turning performance, the spindle unit has been mounted on a test-lathe. The turning experiments will be described and finally the test-results will be discussed.

7.1 The prototype

Figure 7.1 shows a photograph of the realised prototype. With respect to the mechanical aspects this prototype is fully consistent with the design as presented in chapter 5. Considering the control system, the prototype will show some shortcomings with respect to the specified dynamic motions, due to the applied electronics in the test setup. As a result of a maximum input frequency of 300 kHz of the applied encoder interface, the maximum axial velocity of the spindle will be limited to 0.006 m/s. This value is considerably smaller than the specified maximum velocity of 0.1 m/s. Besides this limitation of the maximum velocity, the maximum actuator current is limited temporarily to 1 A. This restriction was made to avoid damage of the prototype during the experiments. However, the electronics are designed to generate the specified maximum of 4 A. Figure 7.2 shows the resulting working area of the prototype for dynamic motions.

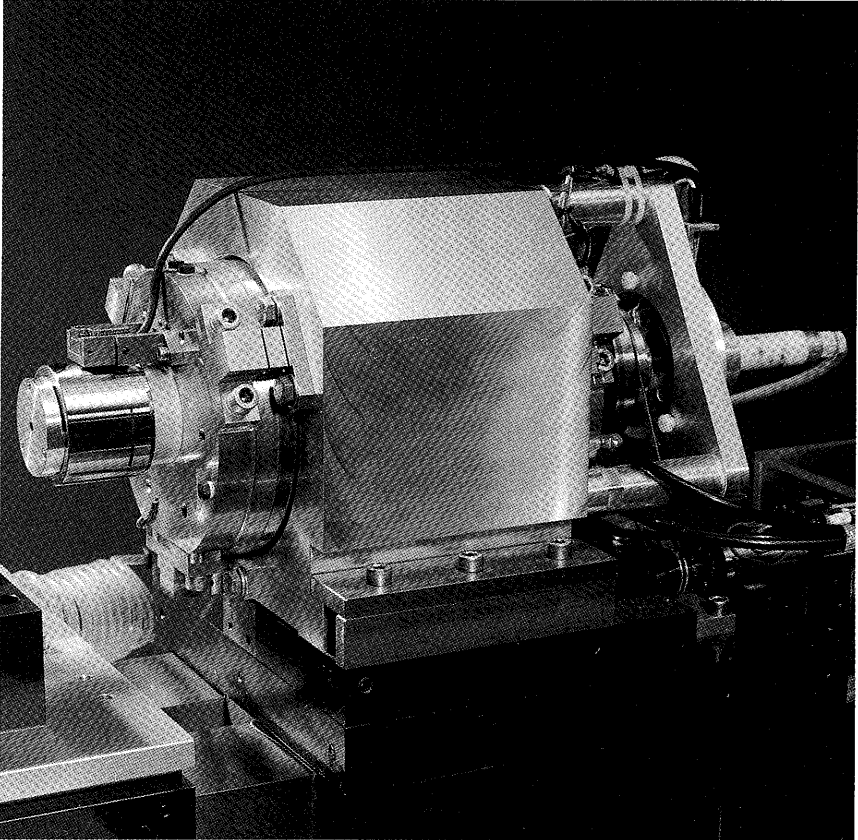


FIGURE 7.1 Picture of the prototype of the spindle unit

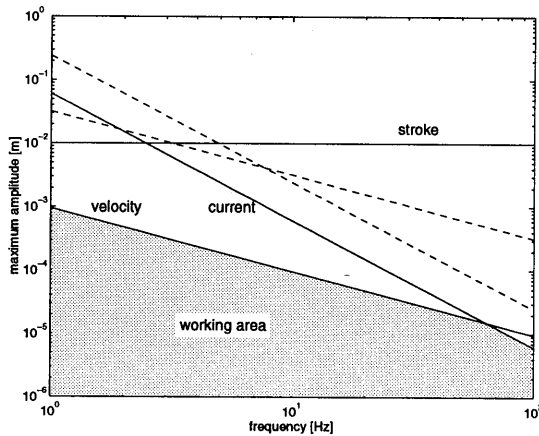


FIGURE 7.2 Reduced working area as a result of the velocity and current limitation of the prototype (dashed lines represent the working area of figure 6.8)

With respect to the working area based on the design specifications (as presented in figure 6.8), the working area of the prototype is considerably reduced. As a consequence, nonrotationally symmetric products with large amplitudes have to be turned at a lower angular spindle speed. This will cause a rise of the cutting time. Considering the intended (preliminary) application of the spindle in a research environment this restriction will not be very dramatic. In this environment the spindle will be used for the production of single products or small series. This means, the actual cutting time will only be a small part of the lead time of the products. The main part of the lead time of the product will be occupied by work preparation (planning, programming, tool setting, alignment etc.) and inspection.

However, in a production environment a minimal cutting time will be essential. So, if the spindle will be applied in such an environment in future, a raise of the current and velocity limitation to the specified values will be necessary. The current limitation can be raised by a simple modification of the analog electronics. The velocity limitation can be raised by applying another encoder interface board: e.g. the *Heidenhain IK 121 PC Counter Card* allows a maximum velocity of 0.2 m/s at a resolution of 2 nm (interpolation factor: 1024).

7.2 Axial error motions

The focus error which is placed at the back side of the spindle, concentric with the axis of rotation, is used to determine the axial error motions. This sensor measures the axial displacement of a mirror which is attached to the magnetic circuit of the velocity sensor. The sensor is also used for position control, when the spindle operates in the analog mode (e.g. during the cutting of the grating pattern, see also chapter 6). The maximum accuracy of measuring the axial error motion of the spindle by this sensor is mainly limited by:

- The eccentricity of the optical axis of the focus error sensor with respect to the axis of rotation of the spindle, combined with a non-parallelism between the rotation axis and the normal of the mirror plane. The resulting error can be calculated by equation 2.1. The eccentricity of the sensor relative to the rotation axis is smaller than 0.02 mm. The misalignment of the mirror plane with respect to the rotation axis of the spindle is smaller than 10^{-4} rad. Using equation 2.1 this yields a maximum measurement error of 4 nm.
- The surface roughness of the mirror. Due to the small spotsize of the sensor (about 1 μm) the measurement will be disturbed by the surface roughness of the mirror. These disturbances will show a repetitive pattern with a period of one spindle revolution. The surface roughness of the applied mirror has been measured, which yielded an Ra-value of 0.8 nm and an Rt-value (peak-to-valley roughness value) of 7.5 nm
- The electronic noise of the system. The peak-to-valley noise level of the position signal of the controlled (non-rotating) spindle is equal to 15 nm. Since the axial error motion is determined from the mean of 4 measurements at each angular position, the effect of the noise on this measurement is reduced to 7.5 nm.

During the measurements, the effects of (thermal) drift can be neglected since the axial error motions are measured over about 5 revolutions of the spindle at a rotational speed of 1000 rpm (in most cases) which will take less than one second. Since the above mentioned error sources are independent to each other, the resulting measurement inaccuracy can be calculated by the RMS value of the separate error sources. This yields a measurement uncertainty of 11 nm (peak-to-valley).

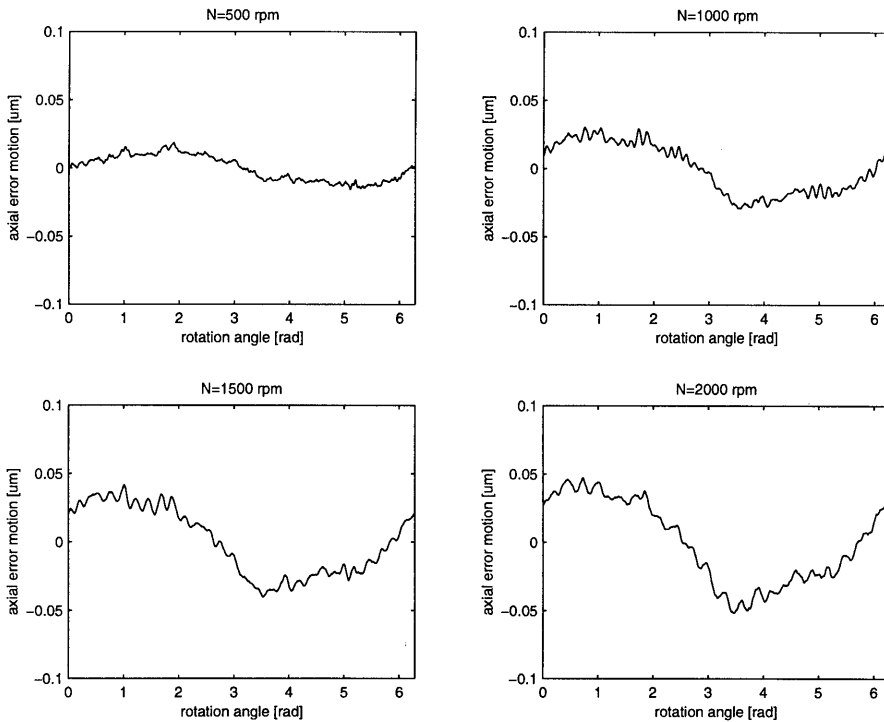


FIGURE 7.3 Axial error motions in analog mode without software error compensation measured at different angular speeds

Figure 7.3 shows the axial error motions in the analog control mode (position signal of the focus error sensor is used for axial position control) measured at different angular speeds. In this mode the error motions are mainly caused by disturbances on the velocity signal (as explained in chapter 6). This is validated by the fact that the amplitude of the error motions is linear to the angular speed of the spindle. At an angular speed of 2000 rpm the axial error motions are around ± 50 nm. Since this value is considerably larger than the specified value of ± 10 nm, software error compensation will be applied to reduce the axial error motions.

The software error compensation for these axial error motions was realised by the method presented in paragraph 6.2.2. This means, the error motions in the analog mode were supposed to be caused by disturbances on the velocity signal only. The

estimation of the correction parameters was based on the axial error motions at an angular speed of 1000 rpm.

Figure 7.4 shows the error motions in the analog mode when applying software error compensation. As expected, the highest accuracy will be achieved at the same spindle speed as the correction parameters were calculated at: at a speed 1000 rpm the axial error motions are reduced to ± 9 nm. At other angular speeds the remaining axial error motions have a maximum amplitude of ± 11 nm. This means, by applying software error compensation the axial error motions are reduced by about a factor 5. (The assumption that the axial error motions in the analog mode are mainly caused by disturbances on the velocity signal, is justified by these results.)

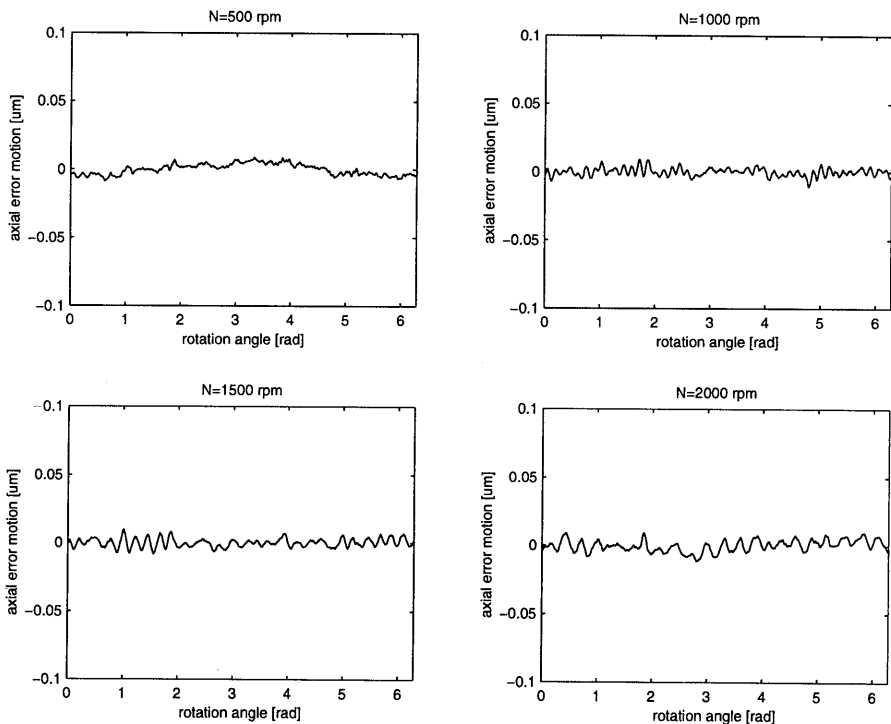


FIGURE 7.4 Axial error motions in analog mode with software error compensation measured at different angular speeds. Estimation of the correction parameters was based on the axial error motions measured at 1000 rpm.

To evaluate the accuracy of the interference grating system with respect to the axial error motions, the spindle is controlled in the digital mode (using the position signal of the interference grating system) while the axial position of the spindle is measured by the focus error sensor at the back side of the spindle. Figure 7.5 shows the results of this measurement. In the left part of the figure only the correction for the disturbances on the velocity was active. The axial error motions in this situation were mainly caused by disturbance on the position signal of the interference grating system. For these disturbances a compensation signal is generated also. From the right part of figure 7.5 it can be concluded that by using software error compensation for disturbances on the velocity as well as the position signal the axial error motions of the spindle can be reduced to ± 11 nm.

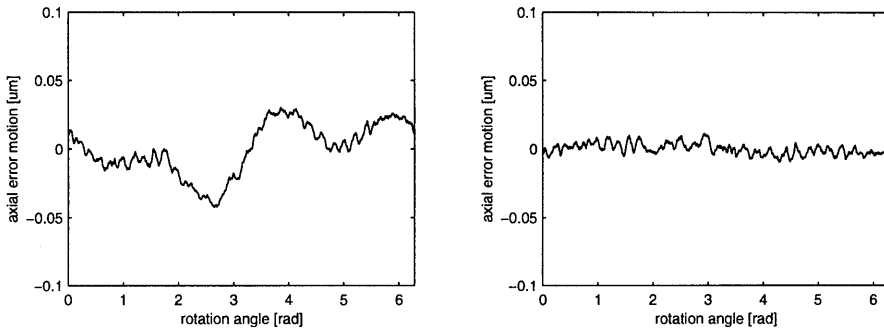


FIGURE 7.5 Axial error motion in the digital control mode (using the position signal of the interference grating system). Left figure: software error compensation for disturbances on the velocity signal. Right figure: software error compensation for disturbances on velocity as well as position signal.

However, it has to be realised that these results are close to the noise level of the applied test-setup. This means the actual axial error motions can even be smaller than ± 11 nm. The amplitude of the fundamental axial error motion (sinusoidal motion with a frequency equal to the rotation frequency of the spindle), which appeared to be more than 100 nm for the conventional precision spindles, is reduced to a level of 3 nm. This value is obtained from the Fourier series of the signal which is presented in figure 7.5 (right).

7.3 Dynamic behaviour

As mentioned in the previous chapter, the tuning of the controller is focused on a maximum bandwidth. Figure 7.6 shows the closed-loop transfer function of the system. The bandwidth of the system is determined by the 0 dB crossing of the open loop and is about 700 Hz. An increase of the bandwidth of this system is limited by mechanical resonances in the system. The mechanical resonance with the lowest frequency is found at about 4 kHz. At a frequency of 50 Hz a peak can be observed in the amplitude as well as the phase plot. These are caused by disturbances on the measurement signals caused by cross talk from the power supply. Since random noise is used as input signal to determine the frequency response, the energy level of the 50 Hz component in the measurement signals is relative small to the 50 Hz disturbances. This causes a relatively large measurement error at this frequency.

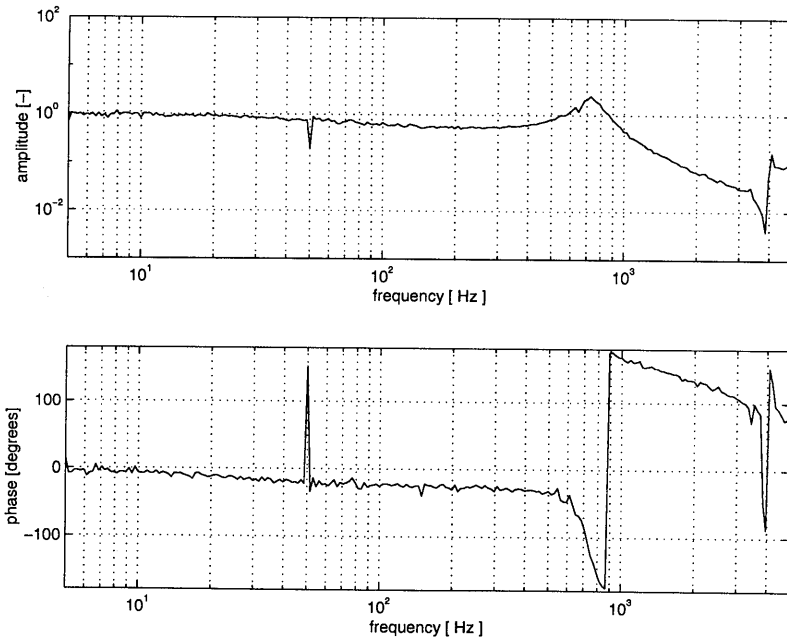


FIGURE 7.6 Frequency response of the closed-loop system

To determine the linearity of the system, the closed-loop frequency response is also measured at different levels of the input signal. The results of these measurements

are shown in figure 7.7. In contrast to the closed-loop frequency response of a friction wheel drive as presented in figure 1.6, the frequency response of this system is nearly independent on the amplitude level of the setpoint signal. This implies a high level of linearity of the system. These results are in accordance with the expectations, because from a mechanical point of view we have to deal with an almost ideal system: a rigid body (within the frequency range which was considered) which is driven by a force actuator and is not subjected to any friction. This means, with respect to linearity this drive system is highly superior to friction wheel drives.

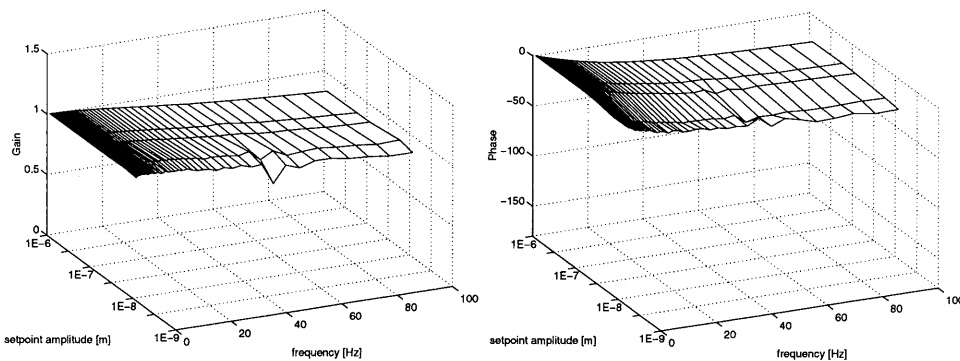


FIGURE 7.7 Closed-loop frequency response of the system, measured at various amplitude levels

The absence of hysteresis in the system can be demonstrated in the time domain. Figure 7.8 shows the motion profile of the spindle corresponding to a setpoint signal of 5 positive and 5 negative steps with an amplitude of 5 nm. During this experiment the spindle was controlled by the position information of the interference grating system, whereas the shown measurement results were obtained from the signal of the focus error sensor. To reduce the influence of electronic noise, the output signal of the focus error sensor was filtered by a low pass filter with a cut-off frequency of 10 Hz. From the figure it can be seen that the spindle returns to the starting position with an accuracy of about 1 nm. This implies that the maximum hysteresis of the system during this experiment was also equal to about 1 nm.

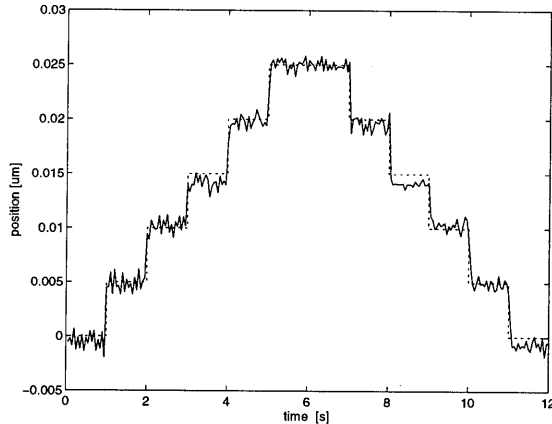


FIGURE 7.8 Response of the controlled system to a stepwise setpoint signal (dashed)

The static stiffness of the controlled system was measured by applying a static disturbance force of 5 N to the front of the spindle, while the system was under digital control with a setpoint signal equal to zero. The maximum resulting position error was equal to the noise level of the controlled system (1 position increment = 5 nm). This implies a static stiffness of at least 1000 N/ μm . It must be realised that the static stiffness will reduce to zero at the moment that the current in the coil reaches the maximum value.

In order to suppress the dynamic reaction forces on the machine frame (to avoid vibrations of the frame), the counter-mass control was tuned to a low bandwidth of 6 Hz. Figure 7.9 shows the closed-loop frequency response of the position-controlled counter-mass (position of the counter-mass measured with respect to the spindle position). As expected, in the frequency range above the bandwidth the frequency response shows a slope of -2 (-40 dB/decade).

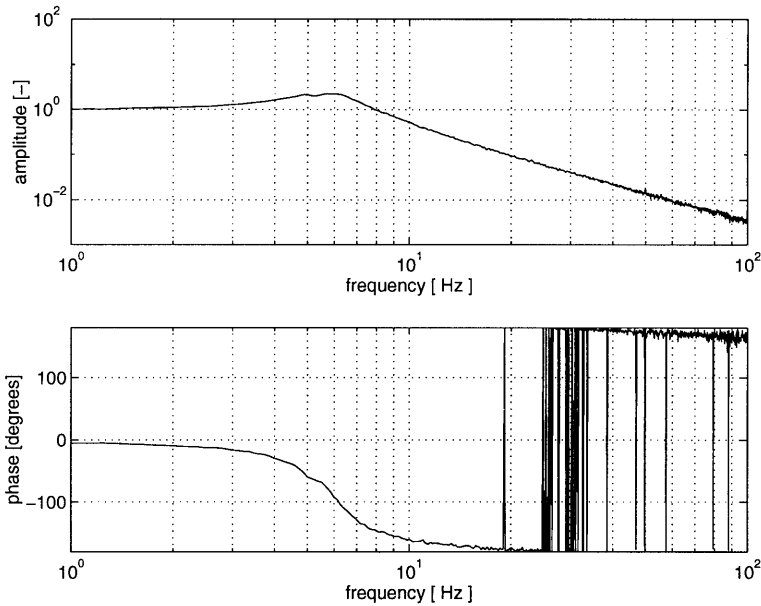


FIGURE 7.9 Closed-loop frequency response of the counter-mass

It has to be realised that only the driving force of the counter-mass actuator will introduce reaction forces on the machine frame. The driving forces of the spindle actuator will only introduce reaction forces on the counter-mass and not on the machine frame. This means, in the frequency range above the bandwidth the resulting reaction forces on the machine frame will also be reduced by -40 dB/decade with respect to the driving forces of the spindle (as explained in paragraph 3.4.5). Figure 7.10 shows the ratio of forces in the spindle actuator and the counter-mass actuator as a function of the frequency. The forces are determined by measuring the currents in both actuators and multiplying the measured values by the force factors of the actuators. From 10 to 100 Hz the ratio of the forces generated by the counter-mass actuator and the forces generated by the spindle actuator are reduced by about a factor 85 (38.5 dB). This is almost equal to the theoretical value of the reaction force reduction of 40 dB/decade.

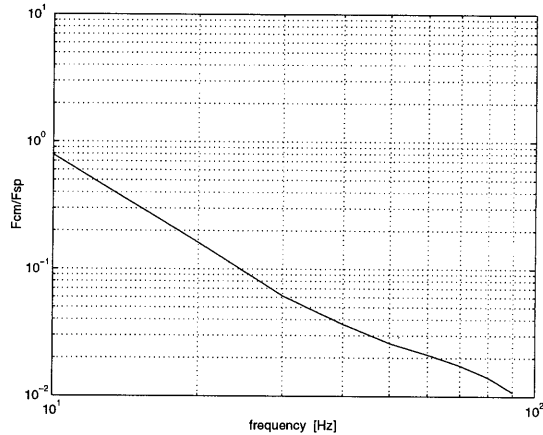


FIGURE 7.10 Ratio of the measured forces of the counter-mass actuator and the spindle actuator as a function of the driving frequency of the spindle.

7.4 The interference grating system

Figure 7.11 shows a picture of the interference grating system on the spindle. For this application Heidenhain has manufactured a special reading head which has a small modification with respect to commercially available ones. An additional optical filter was implemented to minimise the influence of the higher diffraction orders. This was done since the phase quadrature signals would be negatively influenced by higher diffraction orders caused by shape deviations of the groove pattern (e.g. if the width of the grooves is not equal to half a grating period [31]). At the current system this can occur as a result of the wear of the diamond tool during the cutting of the grating pattern.

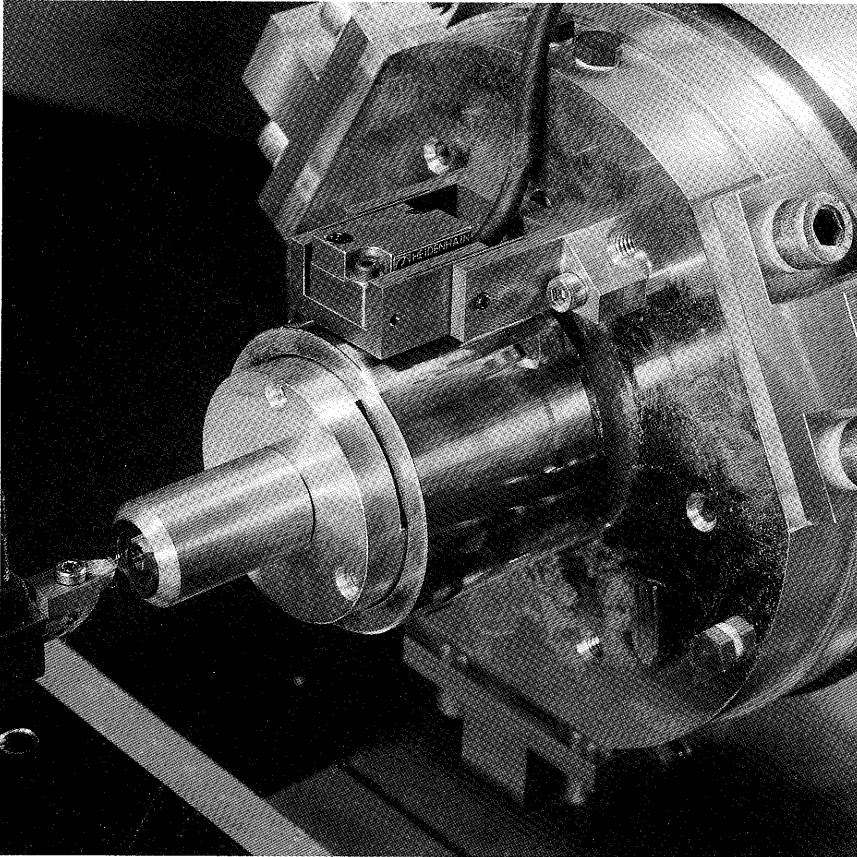


FIGURE 7.11 Picture of the interference grating system on the spindle

After careful alignment of the reading head with respect to the cylindrical grating pattern the reading head produces measuring signals with an amplitude and signal to noise ratio, equal to those of usual systems with a linear scale. The most critical alignment directions of the reading head are the rotation around the vertical axis (which is already known from the usual systems) and the translation in the x-direction (this direction is not critical when using linear scales).

The linearity errors of the measurement system on the spindle were estimated by comparing it to the linear interference grating system that measures the translation

of the slide where the prototype was mounted on. Therefore the axial position of the spindle was not controlled but mechanically fixed to the frame of the experimental lathe (see paragraph 7.5). In this way the spindle was translated with respect to the reading head by moving the slide where the bearing support was mounted on. Figure 7.12 shows the difference between the translation measured by the grating system on the spindle and the grating system on the slide. The deviations of the cylindrical grating with respect to the linear grating on the slide are probably caused by thermal effects during the manufacturing of the grating, because this was done in a non-conditioned environment. The duration of the manufacturing process was about 6 hours, whereas the temperature variations of the environment were equal to 1.5 degree Celsius.

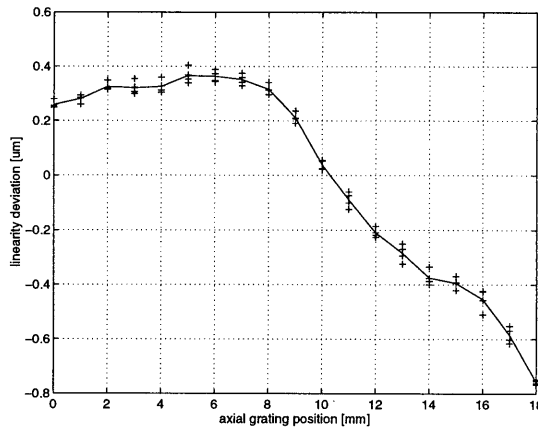


FIGURE 7.12 Linearity deviations of the cylindrical grating pattern relative to the linear grating on the z-slide of the experimental lathe

An actual calibration of the linearity errors of the cylindrical grating pattern has not been carried out yet. This must preferably be done by use of a laser interferometer. The measurement must be carried out in a conditioned environment with high thermal stability. The calibration results can be used for software error compensation. Considering the smooth profile of the deviations in figure 7.12 and a reproducibility of $\pm 0.05 \mu\text{m}$ under poor thermal conditions, a reduction of the linearity errors to

$\pm 0.05 \mu\text{m}$ in a conditioned environment and by applying software error compensation must be achievable.

Another error source which has to be considered is made up by the interpolation errors. As explained in chapter 4, these errors are a result of distortions on the phase quadrature signals (the harmonic output signals of the reading head with a period equal to half a grating period). To explain how the interpolation errors of the system can be determined, the simplified model of the system as presented in figure 7.13 will be used.

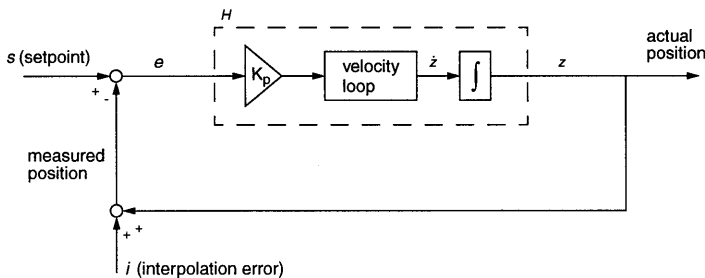


FIGURE 7.13 Simplified model of the controlled system

The system of figure 7.13 will be considered in the frequency domain. Here H describes the frequency transfer from the position error e to the actual position of the spindle z (frequency response of the open loop). If the interpolation errors i are supposed to be zero, a setpoint signal which prescribes a constant velocity v will cause a constant position error e , which is proportional to the velocity v . (Because the position error signal e is proportional to the input signal of the velocity controlled system.) However in the actual system interpolation errors will occur which are fundamentals or higher harmonics of the phase quadrature signals. Emanating from a constant velocity v [m/s], the frequency of the phase quadrature signals will be equal to $v/(2 \cdot 10^{-6})$ [Hz]. Since a setpoint signal of constant velocity will only lead to a DC-offset of the position error signal, the dynamic part of the position error signal will only be caused by the interpolation errors. This means that if the frequency

transfer between the interpolation errors and the position error is known, the frequency spectrum of the interpolation errors can be calculated from the measured spectrum of the position error signal.

The frequency transfer from the interpolation errors i to the position errors e described by:

$$\frac{e(f)}{i(f)} = \frac{-1}{1 + H(f)} \quad (7.1)$$

thus:

$$i(f) = -e(f) (1 + H(f)) \quad (7.2)$$

The transfer function $H(f)$ can be calculated from the closed-loop transfer function $H_c(f)$. Because:

$$H_c(f) = \frac{z(f)}{s(f)} = \frac{H(f)}{1 + H(f)} \quad (7.3)$$

thus:

$$H(f) = \frac{H_c(f)}{1 - H_c(f)} \quad (7.4)$$

Substituting equation 7.4 into equation 7.2 yields:

$$i(f) = \frac{-1}{1 - H_c(f)} e(f) \quad (7.5)$$

Now the frequency spectrum of the interpolation errors can be calculated from the measured frequency spectrum of the position errors at a constant velocity and the measured closed-loop transfer function.

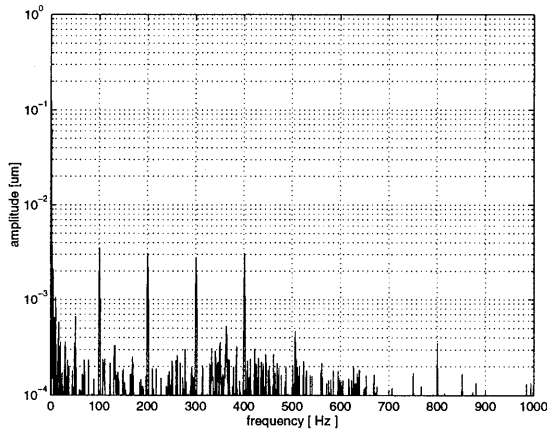


FIGURE 7.14 Frequency spectrum of the interpolation errors at a velocity of 0.2 mm/s (position $z=0$)

Figure 7.14 shows the frequency spectrum of the interpolation errors, calculated from the measured frequency spectrum of the position error signal. The setpoint velocity v was equal to 0.2 mm/s, which corresponds to a frequency of the phase quadrature signals of 100 Hz. As expected the interpolation errors arise as the fundamental and multiples of this frequency. By optimal adjustment of the electronics (setting the dc-level, phase-shift and amplification ratio of the phase quadrature signals) all frequency components can be reduced to a value below 1 increment (5 nm).

However, despite the modification on the reading head, the distortions on the phase quadrature signals are still varying as a function of the axial position on the grating. Figure 7.15 show the frequency spectra of the interpolation errors at different axial positions ($z = -5$ and -10 mm), while the electronic settings were kept the same as in figure 7.14 ($z = 0$ mm). Specially the frequency component of 100 Hz (fundamental of the signal frequency) shows a strong increase (up to 74 nm at $z = -10$ mm).

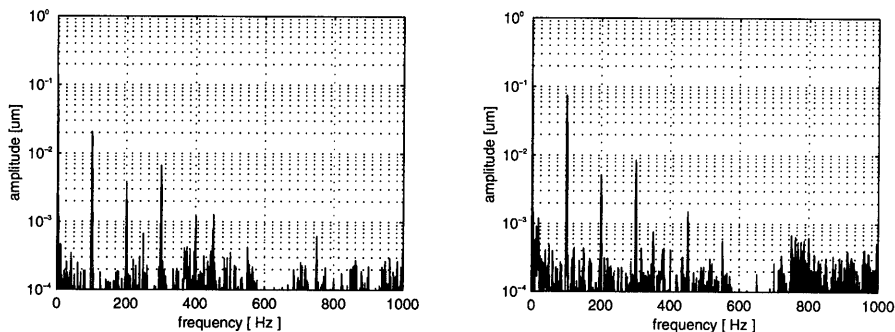


FIGURE 7.15 Frequency spectra of the interpolation errors at the positions $z = -5$ mm (left) and $z = -10$ mm (right) at a velocity of 0.2 mm/s.

In paragraph 4.2.2 it has been shown that interpolation errors with a frequency equal to the frequency of the phase quadrature signals can be caused by a dc-shift of one of the phase quadrature signals. The dc-levels of both phase quadrature signals were measured as a function of the axial position. The measurement results are shown in figure 7.16. One of the dc-levels shows a relative large shift over the measuring range. At the position $z = -10$ mm the shift of both levels are equal to -0.03 V and -0.15 V. Since the ac-amplitude of the both signals is known (1.5 V), the resulting relative interpolation error can be calculated using equation 4.5. This yields a relative interpolation error of 3.4%, corresponding to an absolute interpolation error of 68 nm. This value is very close to the measured 100 Hz component of the frequency spectrum (74 nm) at this position.

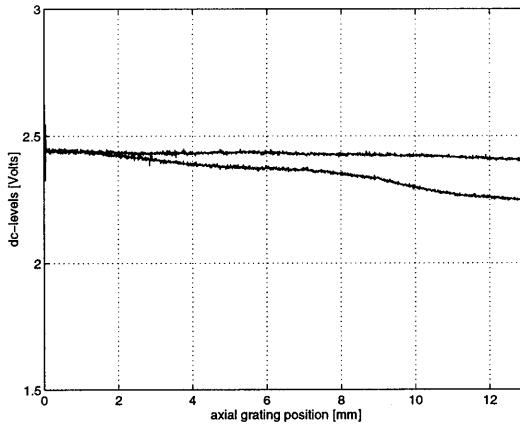


FIGURE 7.16 *dc-levels of the phase quadrature signals as a function of the axial position on the grating*

From these results it can be concluded that the increase of the interpolation errors over the measuring range is mainly caused by a gradual shift of the dc-level of one of the phase quadrature signals over the complete measuring range. The actual cause of this shift of the dc-level is still unknown. Probably this effect is related to changes in the shape of the grooves of the grating pattern over the length of the cylinder, caused by wear of the diamond tool during the cutting process. At the moment it is not possible to correct for these errors. However at the Heidenhain company new electronics are under development which offer the opportunity to update the settings of the electronics (dc-level, phase shift and amplitude ratio of the phase quadrature signals) as a function of the position on the scale. Using these electronics the shift of the dc-level could be compensated by position-dependent setting of the electronics.

7.5 The experimental lathe



FIGURE 7.17 Picture of the experimental lathe

Figure 7.17 shows a picture of the experimental lathe, which is used to manufacture the cylindrical grating system and to evaluate the performance of the prototype of the new spindle under cutting conditions. The base of the lathe is formed by a granite stone which is supported by four (passive) vibration isolators. On the granite base the x- and the z-slide are mounted. These slides are guided by hydrostatic bearings and are driven by friction wheel drives. The displacements of the slides are measured by interferential scales with a resolution of 5 nm. On the z-slide the bearing support of the spindle has been mounted, whereas the tools will be mounted on the x-slide. The motions of both slides are controlled by a NUM 760 CNC, which can be seen at the right side of the picture. The axial motions of the spindle are control-

led by the personal computer and the electronics which can be seen at the left side of the picture.

As mentioned in chapter 6, due to the chosen hardware configuration (an encoder interface with two input channels) the axial motion of the spindle can not be synchronised to the motions of the slides. This means in the test configuration the axial motion control of the spindle will only be used to generate the nonrotationally symmetric part of the shape. The rotationally symmetric part of the shape will be generated by the slides controlled by the CNC. This puts limitations to the kind of nonrotationally symmetric shapes which can be manufactured, because a large group of products asks for a varying axial motion profile of the spindle as a function of the radial position of the tool ($\Delta z = f(x, \varphi)$). For instance, to produce the beam-shaper which was presented in chapter 1, the motion profile during one revolution must be varied as a function of the radial position of the tool (see figure 1.5). This type of products can not be manufactured in the current configuration.

7.6 Diamond turning tests

To evaluate the performance of the prototype under cutting conditions, a number of diamond turning tests have been carried out.

To check if an optical surface quality could be achieved, a number of face turning tests have been carried out. During these tests the setpoint signal of the spindle controller was equal to zero. These tests were carried out under the following conditions:

- diamond tool radius: 250 μm
- cutting depth: 10 μm
- feed: 4 $\mu\text{m}/\text{revolution}$
- spindle speed: 300 - 2000 rpm
- material: copper / brass

The measured Ra-values of the test-products were all in a range from 5 to 10 nm. This means that the roughness specification ($Ra \leq 0.01 \mu\text{m}$ of a copper test-product) was achieved.

However, when the cut surfaces were inspected by an optical microscope, disturbances with high spatial frequencies could be observed, as presented in figure 7.18. To compare this result to the conventional spindles (aerostatic bearings in radial as well as axial direction), another test-product was cut on the 'Colath' (one of the precision lathes of the Philips Research Laboratories) under identical conditions. Figure 7.19 shows a photograph of this surface (Note the magnification of this photograph with respect to figure 7.18). The typical disturbances of figure 7.18 can not be observed at this surfaces. This implies that these disturbances are caused by the axial position control of the prototype. Axial motions of the spindle with high frequencies could possibly be induced by resonances of the spindle or by electronic noise. It has to be realised that the amplitude of these motions must be small (maximum a few tens of nanometres) otherwise the surface roughness would be considerably higher.

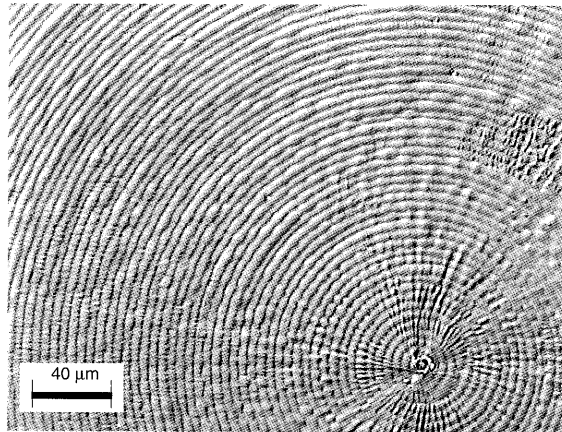


FIGURE 7.18 Optical microscope image of a surface cut on the prototype. Material: copper, spindle speed: 1000 rpm, Ra-value: 10 nm

To suppress high-frequency motions of the spindle a first order low-pass filter is applied at the output of the controller. This filter has a cut-off frequency of 5 kHz (considerably higher than the system bandwidth). Figure 7.20 shows that the high-frequency disturbances are strongly reduced by applying this filter.

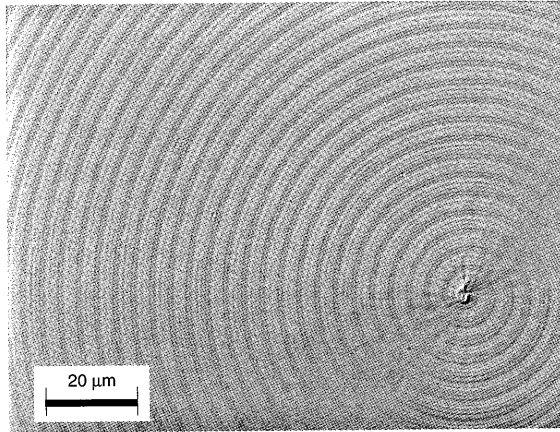


FIGURE 7.19 Optical microscope image of a surface cut on the 'Colath'. Material: copper, spindle speed: 1000 rpm, Ra-value: 6 nm

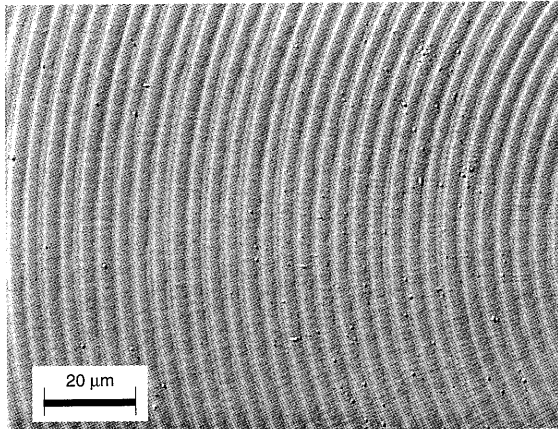


FIGURE 7.20 Optical microscope image of a surface cut on the prototype using a low pass filter (cut-off frequency: 5 kHz) at the controller output. Material: copper, spindle speed: 1000 rpm, Ra-value: 7 nm

To evaluate the performance of the system with respect to nonrotationally symmetric cutting, several (nonrotationally symmetric) test-products have been cut. Since the surface quality of the first test-products was unsatisfactory, the cycle frequency

of the digital controller was raised from 3.3 kHz to 10 kHz. This has been realised by eliminating a part of the measurement and display capabilities of the control program and by substituting the 80486 processor by a pentium processor.

Figure 7.21 shows the shape of a nonrotationally symmetric test-product. The inner and the outer ring of this test-product are flat, the middle ring is nonrotationally symmetric and can be described as: $z(\varphi) = \hat{z}\sin(4\pi\varphi)$.

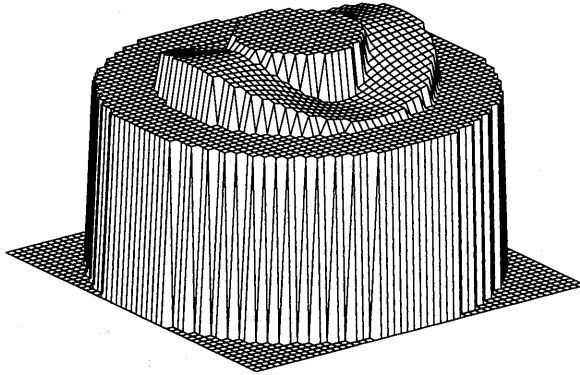


FIGURE 7.21 Shape of a nonrotationally symmetric test-product (exaggerated)

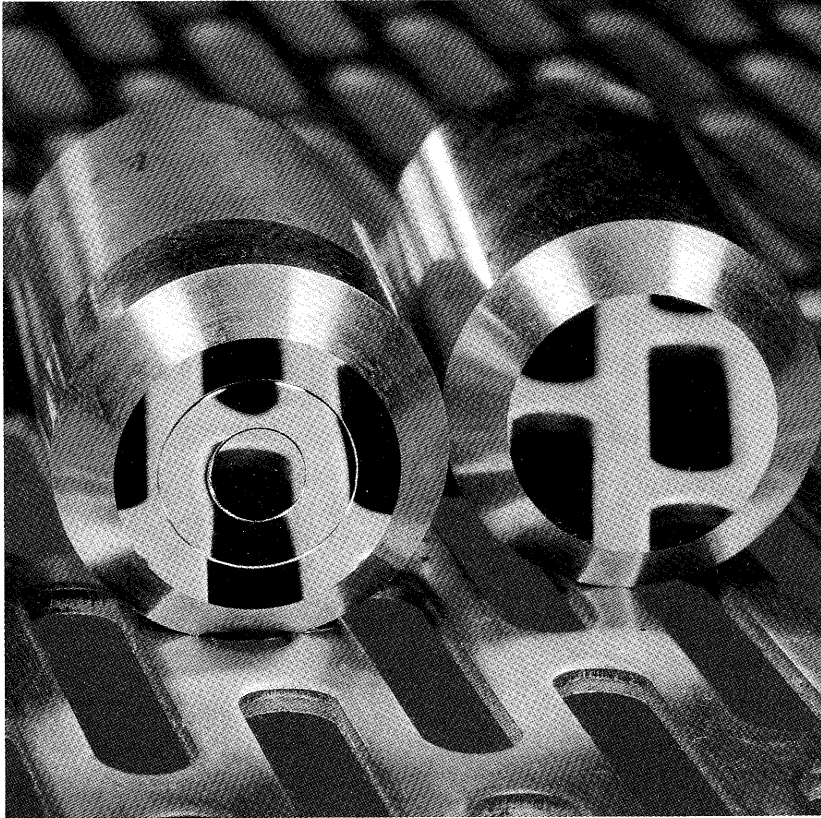


FIGURE 7.22 Photograph of a flat and a nonrotationally symmetric test-product (material: brass)

A test-product of this shape has been turned in brass, with a sine amplitude of $25\ \mu\text{m}$ ($50\ \mu\text{m}$ peak-to-valley). This product is presented in figure 7.22 together with a flat surface. The photograph illustrates the optical surface quality of the product in the flat parts of the surface as well as in the nonrotationally symmetric part. The nonrotationally symmetric shape of the middle ring appears from the deformation of the mirrored image in this area.

The peak-to-valley amplitude of the sine profile of the middle ring has been measured and appeared to be $50.1 \mu\text{m}$. The difference with respect to the programmed profile ($50.0 \mu\text{m}$) is considerably smaller than expected, because this product was manufactured under poor conditions: no calibration of the measuring system has been carried out and no temperature control of the machine and the environment was used.

The surface roughness of the test-product has been measured at three different locations: on the outer ring, on a top of the sine profile and on a flange of the sine profile. Figure 7.23 shows the measured roughness profiles. The corresponding R_a -values are: 6 nm (upper), 7 nm (middle) and 12 nm (lower).

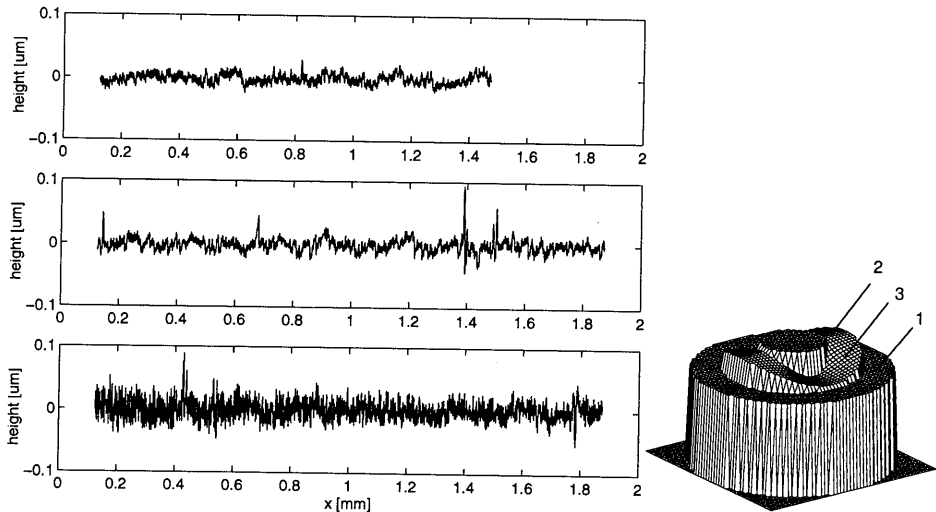


FIGURE 7.23 Roughness profiles measured on three locations of the nonrotationally symmetric test-product. Upper track: location 1, middle track: location 2, lower track: location 3. (Cut-off length: $250 \mu\text{m}$)

The relative high surface roughness on the flanges of the sine profile is caused by the large discontinuities in the output signal of the digital controller in these areas. These discontinuities are mainly caused by the limited cycle frequency of the digital controller. However, using the model as presented in paragraph 6.3, a relative maximum position error of 0.6 nm is expected at a cycle frequency of 10 kHz and a set-

point amplitude of 25 μm . This relatively large difference between the theoretical value and the measured surface roughness will probably be caused by the fact that the actual system can not be considered as a rigid body in this frequency range (resonances will appear). This was recognised already in the closed frequency response of figure 7.6. Above 3 kHz the closed-loop gain of the actual system is much higher than the closed-loop gain of the theoretical system (figure 6.12). This means the position errors caused by the high-frequency components of the setpoint signal will be much larger than theoretically expected from by the model of paragraph 6.3. At a setpoint amplitude of 100 μm the measured Ra-value of a test-product raises even to 30 nm. This means the system must be improved with respect to this aspect.

7.7 Discussion

The surface roughness will improve if the amplitude of the high-frequency components of the output signal of the digital controller are reduced. One way to realise this is by increasing the cycle frequency of the digital controller. Using the current controller configuration (based on a pentium processor) the limits seem to be reached with respect to this aspect. This problem can be overcome partly, by using a digital signal processor (DSP). A raise of the cycle frequency with at least a factor 5 seems achievable. This option has to be investigated during future research.

Nevertheless, it has to be realised that a further increase of the cycle frequency is only useful if the cycle frequency is smaller than the product of the actual rotational frequency of the spindle and the resolution of the rotation measurement system (counts per revolution). Otherwise the frequency at which a new setpoint signal is generated is not determined by the cycle frequency of the controller but by the frequency of the output signal of the rotation measurement system. In this case the amplitude of the discontinuities in the output signal of the digital controller can be reduced by an increase of the resolution of the rotation measurement system or by increasing the rotational frequency of the spindle. However, increasing the rotational frequency will not reduce the amplitudes of the high frequency components of the control signal, but will only transform them to higher frequencies. The effect on the resulting position disturbances depends upon the presence of mechanical resonances in this frequency range.

Another way to suppress the high frequency position disturbances of the spindle, is by reducing the gain of the closed-loop system at these high frequencies. One way to realise this is by lowering the cut-off frequency of the low-pass filter at the controller output. To avoid a reduction of the bandwidth a second order filter can possibly be applied. This filter causes a gain reduction of -40 dB/decade, whereas the first order filter causes a reduction of -20 dB/decade.

Another way to reduce the amplitude of the discontinuities in the output signal of the digital controller which are caused by the limited cycle frequency, is by applying a low-pass filtered velocity and/or acceleration feedforward. This will lead to a configuration as presented in figure 7.24. The use of feedforward will cause a reduction of the position error e , leading to a reduced amplitude of the output signal of the digital controller and thus to a reduction of the amplitude of the discontinuities in this signal caused by sampling. The feedforward signals will be based on the setpoint signal and a model of the low pass filter(s) and the open loop system. This means the feedforward signals can be calculated off-line. Low-pass filtering (with a cut-off frequency of a few hundred Herz) of the feedforward signals is applied to suppress the high frequency components in these signals. To implement feedforward in the control configurations, additional DA-convertors will be necessary.

Velocity and acceleration feedforward have not been implemented yet, but seem a promising alternative to improve the systems performance.

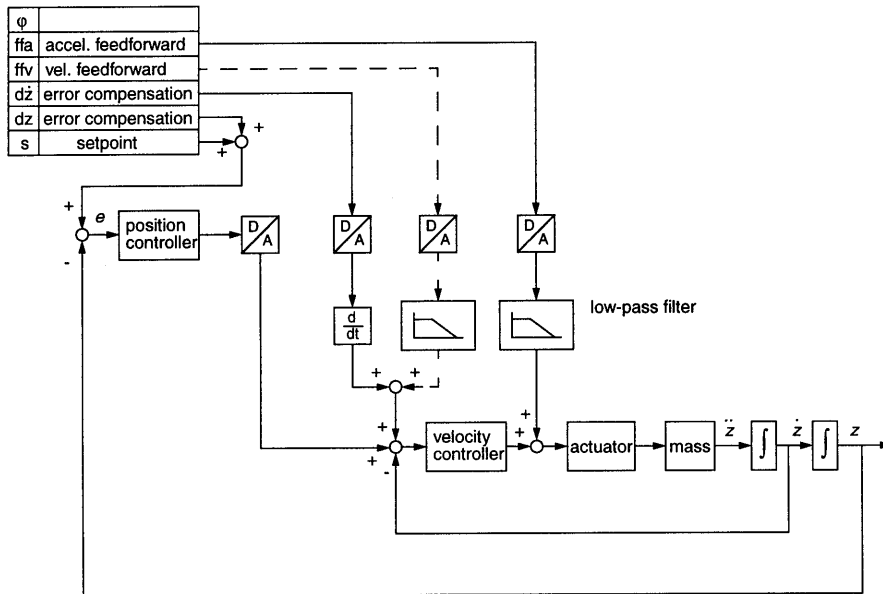


FIGURE 7.24 Control configuration (in digital mode) with velocity (hidden) and acceleration feedforward. (Counter-mass control and voltage to current convertor are not presented)

8. Conclusions and recommendations

Within the project a spindle unit for a high precision diamond turning lathe, based on a new concept, has been designed, realised and tested. This new spindle unit has a double function: rotation and axial translation of the product. In radial direction the spindle is supported by air bearings. In axial direction the spindle position is controlled by an actuator and a feedback (position and velocity) control system.

8.1 Conclusions

Since the spindle can make axial motions (within one revolution), it is possible to produce nonrotationally symmetric products in a relatively simple way. Besides, the spindle unit can take over the function of the axial slide of a lathe, which leads to a reduction of the total number of guides of the lathe. This will cause an increased stiffness of the structural loop between the product and the tool, an elimination of the alignment error between the rotation axis of the spindle and the axial motion direction and a reduction of the manufacturing costs of the precision lathe.

The voice coil actuator has proven to be a very suitable drive system for precision machining applications. A voice coil actuator combined with current control behaves as an ideal force actuator: a force between two objects can be generated which is independent of the position of both objects (no stiffness between both parts is introduced). Since there is no mechanical contact between the coil and the magnetic circuit any kind of friction can be neglected. This leads to a high level of line-

arity of the controlled system, which is demonstrated by the fact that the measured closed loop frequency transfer is as good as independent of the amplitude of the input signal. Besides, the applied drive system is maintenance-free. By coupling the voice coil actuator to the frame via a counter mass, the dynamic reaction forces on the frame can be significantly reduced. In this way the relatively large dynamic driving forces, which are needed for nonrotationally symmetric cutting, will not cause unacceptable vibrations of the machine frame. The maximum stroke of the spindle actuator is about 1 mm. To realise axial spindle motions over a range of 20 mm, the counter mass is driven by a second voice coil actuator with a stroke of 20 mm. This configuration guarantees an high energetic efficiency of the spindle actuator, without applying commutation. It can be stated that the applied drive system is in many respects superior to the commonly used friction wheel drives.

The axial translation of the rotating spindle is measured by an interference grating system. Since this system measures the axial position of the spindle very close to the product (at the nose of the spindle), the influence of thermal effects will be minimal. With respect to alternative measurement systems (e.g. laser interferometer), this system shows less sensitivity to environmental influences (pressure variations of the air, variation in the constituents of the air etc.) and is considerably cheaper (about 10 times with respect to a laser interferometer). The applied grating is a cylindrical phase grating which has been developed for this application. It is applied in combination with a commercially available reading head. The grating consists of rectangular shaped grooves on the outer surface of a cylinder which is attached to the spindle. The system has a resolution of 5 nm.

Two manufacturing methods for the cylindrical phase grating have been evaluated: diamond turning and plasma etching. Diamond turning has proven to be a suitable manufacturing method: a prototype has been realised which meets the specified requirements. To guarantee a maximum accuracy of the cylindrical grating (minimal grating and alignment errors) it has been cut using the spindle itself while the axial position control was realised by a focus error sensor. The main limitation of this manufacturing method is the wear of the tool during the cutting process. This causes a modification of the groove shape as a function of the axial position on the grating. As a result, the interpolation errors vary as a function of the axial position on the grating and rise to a level of about 0.1 μm . This problem can be solved if the settings of the interpolation electronics can be updated as a function of the axial position of

the grating. Electronics which incorporates this feature will be available in the near future.

To manufacture a cylindrical phase grating by plasma etching an etching mask must be created first. This etching mask can be made by a lithographic process. The successive steps of this process have been investigated and tested. Subsequently, groove structures have been etched in a quartz cylinder. Plasma etching in a radial direction could be realised by using a special reactor configuration which was created for this purpose. Despite the fact that no actual grating structure (meeting the specifications) has been made by this method, plasma etching appears to be a feasible manufacturing method for cylindrical grating structures. However, for the production of a single or a few prototypes this method is rather laborious and complicated. Therefore, the grating structure on the prototype of the spindle unit has been made by diamond turning. For the production of larger series, plasma etching could be a suitable manufacturing method.

Since the axial position of the spindle is controlled by a system based on a digital controller, reproducible errors in the measured position and velocity can be eliminated in a relatively simple way, by applying software error compensation (after calibration). By this technique the axial error motions of the spindle could be reduced to about $\pm 0.01 \mu\text{m}$, which is equal to the specifications as presented in chapter 1. The amplitude of the fundamental axial error motion, which appeared to be larger than $\pm 0.1 \mu\text{m}$ for the conventional precision spindles, is now reduced to a level of $\pm 3 \text{ nm}$. The noise level (non-reproducible position errors) is equal to $\pm 7.5 \text{ nm}$. This is slightly higher than the specified noise level of $\pm 5 \text{ nm}$. This means the accuracy of the system could be improved without making higher demands on the mechanics of the spindle unit (which would lead to a considerable increase of the production costs of the spindle unit).

The measured static axial stiffness of the spindle equals $1000 \text{ N}/\mu\text{m}$. This is considerably higher than the specified value ($\geq 100 \text{ N}/\mu\text{m}$). The closed loop bandwidth of the system is equal to 700 Hz . The prototype was designed to meet the specified performance with respect to dynamic motions (harmonic motions with an amplitude of $250 \mu\text{m}$ at a frequency of 30 Hz). However, in the test setup these specifications could not be realised since the maximum velocity and acceleration were limited. This was caused by the applied encoder interface board and the current limitation in

the electronics of the test-setup. No serious problems are expected to meet the specifications if another encoder interface board is implemented and the current limitation is raised.

Diamond turning experiments have been carried out to evaluate the cutting performance of the prototype; therefore the spindle unit was mounted on a precision lathe. The experiments showed that for rotationally symmetric products the specification with respect to surface roughness ($R_a \leq 10$ nm) was achieved easily. A nonrotationally symmetric test-product was cut while the spindle moved harmonically in the axial direction with an amplitude of 25 μm at a frequency of 10 Hz. The maximum measured surface roughness (R_a) of this test-product was equal to 12 nm. However, at larger amplitudes or at higher frequencies of the axial motions (both leading to higher axial velocities), an unacceptable increase of the surface roughness was observed. This was caused by an increase of the discontinuities in the output signal of the digital controller, which leads to high frequency position disturbances of the spindle. The discontinuities are mainly caused by the limited cycle frequency of the digital controller. To obtain a better (lower) surface roughness of nonrotationally symmetric products the amplitude of the discontinuities must be minimised (see also paragraph 8.2). In the current configuration this can be realised by reducing the rotational speed of the spindle during finishing. Obviously, rough-turning can still be carried out at higher rotational speeds.

The design of the spindle unit was focused on high thermal stability of the radial as well as axial position the spindle. However, within this project it was not possible to evaluate the performance of the prototype experimentally with respect to this aspect.

In conclusion it can be stated that by applying a mechatronic approach, a new concept of a spindle unit was developed with improved performance with respect to axial error motions, axial stiffness and functionality, whereas the number of precision components was kept minimal. The feasibility of the presented concept has been demonstrated on the basis of the prototype which has been built and tested. A patent application of this design and the corresponding method of making nonrotationally symmetric products has been made [34].

8.2 Recommendations

Despite the fact that the realised prototype meets the major part of the specifications, the performance of the prototype must still be evaluated with respect to a few aspects. Besides, a further development will be necessary to obtain a spindle unit capable to operate in a production environment. The main activities which must be carried out with respect to both aspects will be discussed next.

The thermal stability of the spindle has to be determined experimentally. In order to obtain representative test results the spindle has to be mounted on a temperature controlled precision lathe in a conditioned environment. Specially the radial and axial position stability of the spindle under turning conditions have to be considered. The temperature variations of the cylindrical phase grating must be determined also. From these results it must be decided whether the actual grating material (copper) can be maintained or must be replaced by a material with a significantly lower thermal expansion coefficient (e.g. invar). To achieve maximum dimensional accuracy of the turned products, the linearity of the grating system must be calibrated by a laser interferometer.

To operate as a production tool, an universal product fixture must be integrated into the spindle. In order to avoid pollution of the cylindrical phase grating an universal shielding must be developed. To maintain good dynamic performance, the mass of the product fixture and the dust protection unit must be minimal. In order to minimise axial disturbance forces generated by the rope (of the rotation drive), due to the fact that the motor is fixed to the frame while the spindle moves in axial direction, the rotation drive configuration must be developed further. A simple solution could be the mounting of a cylindrical drum on the motor of the rotation drive (instead of a pulley), which allows a free translation of the rope in axial direction.

In order to improve the surface quality during nonrotationally symmetric cutting with large amplitudes and high frequencies (high axial velocity), the discontinuities in the output signal of the digital controller must be minimised. To realise this two possible solutions can be investigated. First, the cycle frequency of the digital controller can be increased, e.g. by using a digital signal processor. While doing this, attention must be paid to the fact that the resolution of the rotation measurement system can become the limiting factor now. In that case the resolution of this system

must be increased. Secondly, (low-pass) filtered velocity and/or acceleration feedforward can be applied to reduce the amplitude of the discontinuities in the output signal of the digital controller (as discussed in paragraph 7.7). This will lead to a reduction of the position error signal and thus to a reduction of the amplitude of the discontinuities in the output signal of the digital controller caused by sampling. In general, the use of velocity and/or acceleration feedforward (along with feedback) is recommended, because it reduces the position error during dynamic motions of the spindle.

To meet the specifications with respect to the frequency and the amplitude of the harmonic motions, the limitations on the maximum velocity and the acceleration must be raised to the specified values. Some small modifications of the used electronics are necessary to rise the current (acceleration) limitation to the specified value. To be able to reach the specified velocity, an encoder interface with higher specifications must be implemented (e.g. *Heidenhain IK 121 PC Counter Card*).

The position dependency of the interpolation errors can be reduced if the settings of the interpolation electronics can be updated as a function of the measured position. Electronics which are capable to realise this, are likely to be available soon. The performance of these electronics must be tested and evaluated.

To produce the intended nonrotationally symmetric products (e.g. beamshapers, astigmatic lenses), the axial motion profile within one revolution of the spindle must be modified as a function of the radial position of the cutting tool. To realise this, a further extension of the control system is necessary. The radial position of the tool should be used as an additional input signal of the control system. Determination of the optimal control configuration for this application, must be a part of further research.

Bibliography

- [1] J. Bryan et al. 'Spindle Accuracy'. *The American Machinist*, december 4, 1967. Pages 149-164.
- [2] G.J. de Jong. 'Straightness measurements on the ESDO'. Nat.Lab. Technical Note 176/89 (internal Philips report) 1989.
- [3] M. Renkens. 'Ontwerp van een geregeld axiaal lager'. IVO Eindhoven University of Technology, 1994. ISBN 90-5282-329-4. (In Dutch)
- [4] M.T. Meuwese et al. 'Device for the axial support of a rotatable body, positioning device provided with such a device'. United States Patent, No.: 5,397,185. Mar. 14, 1995.
- [5] P.J. Falter, T.A. Dow. 'Design and performance of a small-scale diamond turning machine'. *Precision Engineering*, Vol.9 (No.4), 1987. Pages 185-190.
- [6] S.R. Patterson, E.B. Magrab. 'Design and testing of a fast toll servo for diamond turning'. *Precision Engineering*, Vol.7 (No.3), 1985. Pages 123-128.
- [7] T.A. Dow, M.H. Miller, P.J. Falter. 'Application of a fast tool servo for diamond turning of nonrotationally symmetric surfaces'. *Precision Engineering*, Vol.13 (No.4), 1991. Pages 243-250.
- [8] M.H. Miller et al. 'A controller architecture for integrating a fast tool servo into a diamond turning machine'. *Precision Engineering*, Vol.16 (No.1), 1994. Pages 42-48.
- [9] M.Q. Chen, C.H. Yang. 'Dynamic compensation technology of the spindle error motion of a precision lathe'. *Precision Engineering*, Vol.11 (No.3), 1989. Pages 135-138.
- [10] S.C. Fawcett. 'Small amplitude vibration compensation for precision diamond turning'. *Precision Engineering*, Vol.12 (No.2), 1990. Pages 91-96.
- [11] G. Bouwhuis et al. 'Principals of Optical Disc Systems'. Adam Hilger Ltd, Bristol, 1985. ISBN 0-85274-785-3.
- [12] M. Visscher. 'The measurement of film thickness and the roughness deformation of lubricated elastomers'. Ph.D. Thesis, Eindhoven University of Technology, 1992.
- [13] J.J. Kok. 'Werktuigkundige Regeltechniek 1'. Eindhoven University of Technology, 1991. (In Dutch)

- [14] G.J. Sidall, R.R. Baldwin. 'Development in laser interferometry for position sensing'. *Precision Engineering*, Vol.6 (No.3), 1984. Pages 175-180.
- [15] G.E. Sommargren. 'A new laser measurement system for precision metrology'. *Precision Engineering*, Vol.9 (No.4), 1987. Pages 179-184.
- [16] W. Hou, G. Wilkening. 'Investigation and Compensation of Non-linearity of Heterodyne Interferometers'. Proc. of the 7th IPES, Buttermann Heinemann, Boston, 1993. Pages 1-14.
- [17] A. Spies. 'Längen in der Ultrapräzisionstechnik messen'. *Feinwerktechnik & Messtechnik* 98, 10, 1990. Pages 406-410.
- [18] A.M. Rankers, J. van Eijk. 'The influence of reaction forces on the behaviour of high performance motion systems'. Internal Philips Publication, Presented at the CFT Exhibition 1995.
- [19] H. Kunzmann et al. 'Scales vs Laser Interferometers Performance and Comparison of Two Measuring Systems'. *Annals of the CIRP*, Vol 42/2, 1993. Pages 753-767.
- [20] K.P. Birch. 'Optical fringe subdivision with nanometric accuracy'. *Precision Engineering*, Vol.12 (No.4), 1990. Pages 195-198.
- [21] P. Morantz. 'The real-time reduction of electronic interpolation errors in precision machine servos'. Proceedings of the 7th IPES, Buttermann Heinemann, Boston, 1993. Pages 224-228.
- [22] C.R. Friedrich, S.D. Kang. 'Micro heat exchangers fabricated by diamond machining'. *Precision Engineering*, Vol.16 (No.1), 1994. Pages 56-59.
- [23] Th. Schaller et al. 'Mechanische Mikrostrukturierung metallischer Oberflächen'. *F & M*, 1994 5-6. Pages 274-278.
- [24] H.A. Haus. 'Waves and fields in optoelectronics'. Prentice Hall, Inc. 1984. Page 111.
- [25] B. Chapman. 'Glow Discharge Processes'. John Wiley & Sons, 1980. Chapter 7.
- [26] D.G. Chetwynd. 'Selection of structural materials for precision devices'. *Precision Engineering*, Vol.9 (No.1), 1987. Pages 3-6.
- [27] F.B. Sperling. 'Stage Motion Noise: The Influence of Stone Porosity'. Nat.Lab. Technical Note 322/93 (internal Philips report).

-
- [28] P.L. Holster, J.A. Jacobs. 'Derivation of finite element equations for full film bearings'. Nat.Lab. Report 6317 (internal Philips report).
- [29] J. Jacobs. 'Rody: A Program for Calculations on Rotordynamics'. Nat.Lab. Technical Note 101/89 (internal Philips report)
- [30] A.H. Slocum. 'Precision Machine Design'. Prentice Hall, Inc. 1992. Chapter 3.
- [31] W. Holzapfel (Dr. Johannes Heidenhain GmbH, Germany). Personal communication.
- [32] C.L. Philips, R.D. Harbor. 'Feedback Control Systems'. Prentice Hall, Inc. 1996. ISBN 0-13-371691-0. Chapter 12.
- [33] C.L. Philips, H.T. Nagle. 'Digital Control System Analysis and Design'. 3rd ed. Prentice Hall, Inc. 1995.
- [34] A. van Tooren, M. Renkens, J van Leest, A. Verhulst. 'Machine tool for and method of providing a surface which is not rotationally symmetrical on a workpiece, and control for such machine tool'. European Patent Application No. 0722378.

Appendix A

Frequency transfer of a sample and zero-order hold system

In this appendix the frequency transfer of a sample and zero-order hold system will be calculated. An elaborate derivation of the used equations can be found in [32].

Figure A.1 shows a schematic representation of a sample and zero-order hold system. In this system $z(t)$ is sampled, which yields the output signal $\bar{z}(t)$.

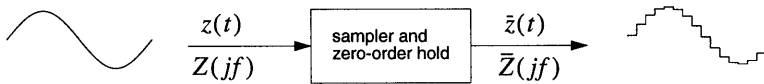


FIGURE A.1 Schematic representations of a sampler and zero-order hold system

Emanating from a constant sample period T_c the output signal $\bar{z}(t)$ can be described in the frequency domain as:

$$\bar{Z}(jf) = \frac{1 - e^{-j f T_c}}{j f} \cdot \sum_{n=-\infty}^{\infty} z(n T_c) e^{-j n f T_c} \quad (\text{A.1})$$

The second factor of this equation is seen to be a function of the input signal $z(t)$ and the sample period T_c . The first factor is seen to be independent of $z(t)$. Thus the first factor can be considered to be a transfer function. Therefore, the sample-and-hold operation can be represented as shown in figure A.2, where the function $Z^*(jf)$, called the *starred transform*, is defined as:

$$Z^*(jf) = \sum_{n=-\infty}^{\infty} z(n T_c) e^{-j n f T_c} \quad (\text{A.2})$$

The sampler (switch) in this figure represents a so-called *ideal sampler*, the operation denoted by the transfer function is called an *ideal hold*. It has to be emphasized that the switch does not represent a physical sampler and the block does not model a physical data-hold. However, the combination does accurately model the input-output characteristics of the sampler and zero-order hold system.

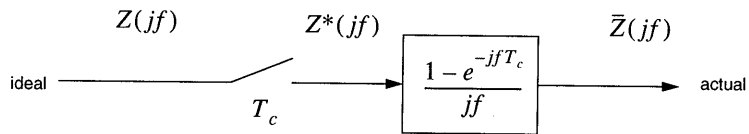


FIGURE A.2 Sampler and zero-order hold system split in an ideal sampler and ideal data-hold

This means the equation can be rewritten to:

$$\bar{Z}(jf) = G_{ho}(jf) \cdot Z^*(jf) \quad (\text{A.3})$$

From literature it is known that the starred form can also be expressed as [33]:

$$Z^*(jf) = \frac{1}{T_c} \sum_{n=-\infty}^{\infty} Z(jf + njf_c) \quad (\text{A.4})$$

This is represented in figure A.3 for a sinusoidal input signal with frequency f_i and amplitude \hat{z} . The upper graph shows the amplitude spectrum of this input signal. The second graph shows the amplitude spectrum of the starred form. The resulting higher frequency components are paired around multiples of the sample frequency f_c .

The transfer function of the ideal hold can be rewritten:

$$G_{ho} = \frac{1 - e^{-jfT_c}}{jf} = T_c \frac{\sin\left(\pi \frac{f}{f_c}\right)}{\pi \frac{f}{f_c}} \cdot e^{-\pi j \frac{f}{f_c}} \quad (\text{A.5})$$

The gain of this transfer function is depicted in the third graph of figure A.3. The fourth graph shows the sinusoidal response of the complete sample and zero-order hold system.

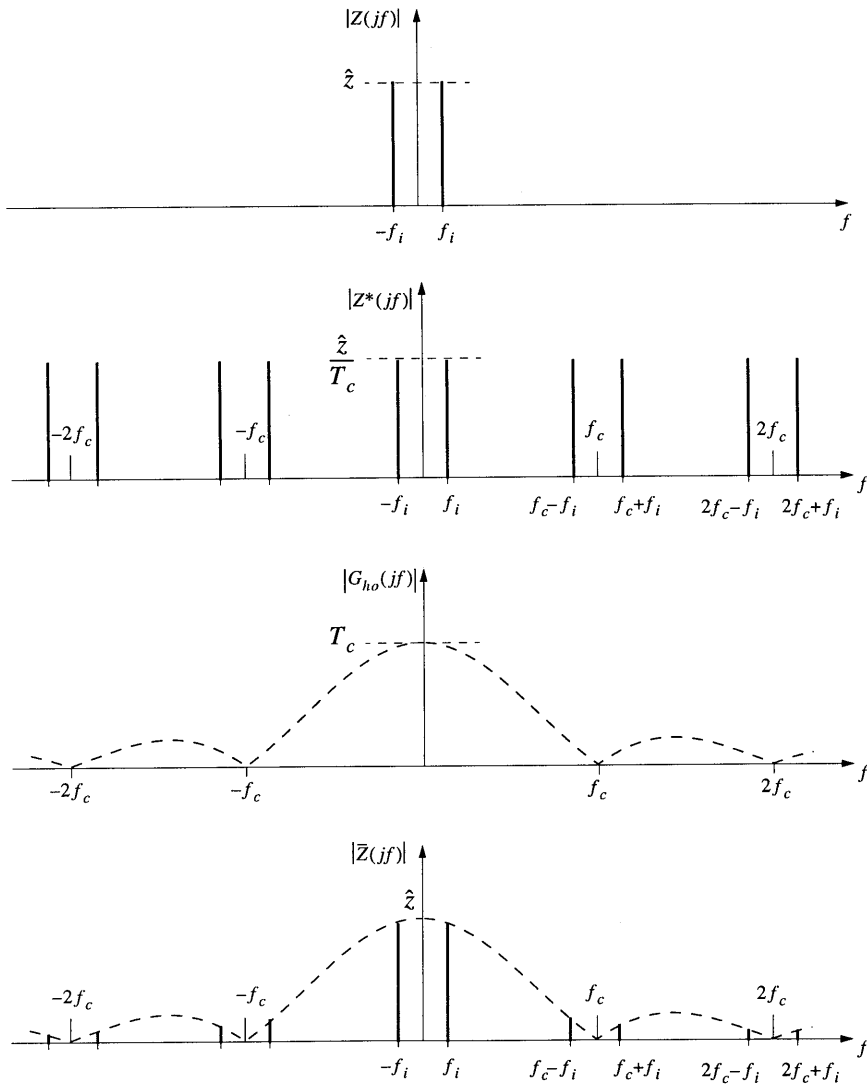


FIGURE A.3 Sinusoidal frequency response of a sample and zero-order hold system

Appendix B

Specification voice coil systems

In this appendix the specifications of the voice coil systems used for the spindle actuator, the counter-mass actuator and the velocity sensor will be presented.

Spindle actuator

Coil (specified for 1 coil):

Mean diameter:	80 mm
Total number of turns:	21
Number of turns within gap:	15
Resistance:	0.5 Ω

Permanent-magnetic circuit:

Mean radial flux density in the gap:	0.91 T
--------------------------------------	--------

Voice coil:

Force factor:	6.8 N/A
---------------	---------

Counter-mass actuator

Coil:

Mean diameter:	78 mm
Total number of turns:	211
Number of turns within gap:	35
Resistance:	18.4 Ω

Permanent-magnetic circuit:

Mean radial flux density in the gap:	0.96 T
--------------------------------------	--------

Voice coil:

Force factor:	8.2 N/A
---------------	---------

Axial velocity sensor*Coil (specifications for 1 coil):*

Mean diameter:	35 mm
Total number of turns:	287
Number of turns within gap:	48
Resistance:	0.5 Ω

Permanent-magnetic circuit:

Mean radial flux density in the gap:	1.4 T
--------------------------------------	-------

Voice coil:

Force factor:	7.4 N/A
---------------	---------

Appendix C

Technical data of the etching experiments

Laser

Type:	Argon-ion
Wavelength:	351.1 nm and 363.8 nm
Output power:	approx. 1 mW

Objective

Power \times NA:	6.3×0.18
Theoretical spot size:	10 μm

Optical components

Efficiency (intensity):	60%
-------------------------	-----

Resist:

Type:	HPR504
Diluent:	Waycoat
Resist/diluent ratio:	1/5
Sensitivity:	approx. 100 mJ/cm ²
Lifting velocity:	1 mm/s
Layer thickness:	0.8 μm

Plasma etching:

Applied gas:	CHF ₃
Radial etching velocity:	approx. 1 $\mu\text{m}/\text{hour}$

Samenvatting

In deze thesis wordt het ontwerp en de realisatie van een nieuw type spindel-unit voor een precisie-draaibank beschreven. Bij het ontwerp van deze spindel-unit is gestreefd naar het verhogen van de axiale rondloopnauwkeurigheid en de axiale stijfheid ten opzichte van de bestaande spindels. Tevens dient de spindel-unit gebruikt te kunnen worden voor het vervaardigen van niet-rotatiesymmetrische producten met optische oppervlaktekwaliteit (o.a. astigmatische lenzen, beamshapers enz.). Bij het ontwerp is gekozen voor een mechatronische aanpak. Hierdoor is het mogelijk gebleken een spindel-unit te realiseren met een verhoogde nauwkeurigheid en functionaliteit, terwijl het gebruik van precisie-componenten tot een minimum beperkt is gebleven.

De spindel-unit bestaat uit een cilindrische (holle) as, die in radiale richting wordt gelagerd door aerostatische lagers. De axiale positie wordt geregeld met behulp van een duikspoel-actuator. De radiale lagers worden hierbij tevens gebruikt als geleiding voor de axiale beweging. Door de spindel axiale bewegingen binnen een omwenteling te laten uitvoeren kunnen niet-rotatiesymmetrische vormen vervaardigd worden. Om ongewenste trillingen ten gevolge van de dynamische reactiekrachten te voorkomen is een contramassa toegepast. Aan deze contramassa zijn de spoelen van de actuator bevestigd, terwijl het permanent-magneetcircuit is bevestigd aan de spindel. De contramassa kan bewogen worden met behulp van een tweede duikspoel-actuator, die dienst doet als lange slag actuator (de totale axiale slag van de spindel bedraagt 20 mm). Door toepassing van dit concept, waarbij de spindel naast dynamische bewegingen over een kleine slag ook over een groot bereik kan transleren in axiale richting, kan de spindel-unit de taak overnemen van de axiale slede van de draaibank. Hierdoor kan deze slede vervallen, hetgeen leidt tot een verhoogde stijfheid, een verhoogde nauwkeurigheid en een vereenvoudiging van het machineconcept ten opzichte van de huidige precisiedraaibanken.

De axiale positie van de roterende spindel wordt gemeten met behulp van een interferentie-rastermeetsysteem met een resolutie van 5 nm. Hiertoe is een cilindrisch faseraster nodig, dat speciaal voor dit doel is ontwikkeld. Voor het vervaardigen van dit raster zijn twee methoden onderzocht: diamantverspanen en plasma-etsen. Beide

methoden bleken geschikt te zijn. Vanwege de eenvoud is gekozen om het faseraster van het prototype te realiseren met behulp van diamantverspanen.

De positieregeling wordt gerealiseerd met een digitale regelaar (gebaseerd op een PC). Dit biedt een hoge mate van flexibiliteit en geeft bovendien de mogelijkheid om correcties uit te voeren voor reproduceerbare afwijkingen in de gemeten snelheid en positie met behulp van softwarecompensatie. De duikspoel-actuator van de spindel wordt gebruikt in combinatie met stroomsturing, op deze wijze ontstaat een ideale krachtactuator (kracht tussen twee lichamen wordt gegenereerd zonder dat hierbij stijfheid wordt geïntroduceerd). Mede als gevolg hiervan bezit het geregelde systeem een zeer hoge mate van lineariteit.

Een prototype, gebaseerd op het beschreven concept, is gebouwd en getest. De maximale axiale rondloopafwijkingen van de spindel blijken $\pm 0,01 \mu\text{m}$ te bedragen (de maximale fundamentele rondloopfout is gelijk aan $\pm 0,003 \mu\text{m}$). De gemeten axiale statische stijfheid bedraagt ca. $1000 \text{ N}/\mu\text{m}$. Het geregeld systeem heeft een bandbreedte van 700 Hz. De met behulp van deze spindel-unit vervaardigde testproducten blijken optische oppervlaktekwaliteit te bezitten ($R_a \leq 0,01 \mu\text{m}$). Bij hoge axiale snelheden neemt de oppervlakteruwheid toe ten gevolge van discretisatie-effecten, die veroorzaakt worden door de digitale regeling.

Op het beschreven ontwerp en de bijbehorende methode voor het maken van niet-rotatiesymmetrische producten is een patent aangevraagd.

Dankwoord

Zoveel mensen hebben een bijdrage geleverd aan het tot stand komen van dit proefontwerp dat ik hen onmogelijk allen hier kan noemen en persoonlijk bedanken. Een aantal mensen ben ik echter bijzondere dank verschuldigd, hen wil ik hier dan ook speciaal noemen:

In de eerste plaats Professor Piet Schellekens, die mij enthousiast heeft gemaakt voor de mechatronica en het vakgebied van de precision engineering in het bijzonder. Arie van Tooren, de initiatiefnemer van dit project, was met zijn enorme kennis en ervaring op mechatronisch gebied altijd een grote steun voor mij. Mijn tweede promotor prof.dr.ir. A.J.A. Vandenput en de overige leden van de kerncommissie prof.dr.ir. M.W.J. Schouten en dr.ir. H.M.G.J. Trum wil ik bedanken voor de tijd die zij besteed hebben aan het doornemen en bespreken van de thesis.

Mijn kamergenoot Frank Jaartsveld ben ik speciale dank verschuldigd voor de tijd die hij besteed heeft aan het kritisch doornemen van het manuscript. Tevens voor de vele verhelderende discussies die we hebben gevoerd en voor de waardevolle suggesties die hij heeft aangedragen. Jan van Leest heeft met zijn veelzijdig technisch inzicht en bijzonder vakmanschap een belangrijke bijdrage geleverd aan de realisatie van het prototype en het uitvoeren van de experimenten. André Verhulst was altijd in staat om binnen minimale tijd geniale oplossingen te bedenken en te realiseren op het gebied van elektronica en software. De discussies met mede AiO Henk Goossens dwongen mij om kritisch te blijven ten aanzien van mijn eigen werk. Het was voor mij een bijzonder voorrecht om te kunnen samenwerken met Johan Wijn, Ad Huijbregts, Peter van Dooren, Harry Nulens, Harry van Erp en Cor Salij, die met hun grote vakmanschap een belangrijke bijdrage hebben geleverd aan het tot stand komen van het proefontwerp. Ook de overige leden van de groep complexe systemen wil ik hier noemen, zij zorgden er voor dat ik dit project in een zeer prettige sfeer heb kunnen uitvoeren.

Mijn ouders, mijn vrienden en in het bijzonder Angela wil ik bedanken voor de interesse die zij toonden en voor de aanmoedigen, die zij mij altijd weer gaven.

Curriculum Vitae

Marcel Renkens was born on September 29th, 1968 in Puth, The Netherlands. He attended the Albert Schweitzer Scholengemeenschap in Geleen, where he obtained his Atheneum diploma in 1986. During the same year, he commenced his study of Mechanical Engineering at the Eindhoven University of Technology. During the last year of his study he worked on the design of an interference refractometer based on a permanent vacuum chamber. He received his Master's degree in February 1992. In march 1992 he started the post graduate programme Mechatronic Design at The Eindhoven University of Technology. In April 1994 he graduated on the design of an axially controlled spindle unit for high precision diamond turning. This project was carried out within the group Complex Systems of the Mechanical Service of the Philips Research Laboratories, Eindhoven. Until October 1996 this work at the Laboratories was continued as a PhD project, supported by the Stan Ackermans Institute of the Eindhoven University of Technology. Since November 1996 he works within the group Mechanics of the Philips Research Laboratories, Eindhoven.

Stellingen

behorende bij het proefontwerp

Design of an Axially Controlled Spindle Unit for High Precision Diamond Turning

Marcel Renkens

Eindhoven, 1 oktober 1997

1. Door het feit dat een duikspoelactuator een kracht tussen twee lichamen kan genereren zonder stijfheid te introduceren, kan een aandrijfmotor gerealiseerd worden die voor dynamische precisie-toepassingen op nagenoeg alle aspecten superieur is ten opzichte van andere aandrijfsystemen.

Dit proefontwerp

2. Bij het draaien van niet-rotatiesymmetrische producten wordt de invloed van digitaliseringseffecten in het meet- en regelsysteem op de haalbare vorm- en oppervlaktekwaliteit van het product vaak ten onrechte verwaarloosd.

Dit proefontwerp

3. Het toepassen van een contramassa is een succesvolle methode om ongewenste machinetrillingen, ten gevolge van dynamische reactiekrachten veroorzaakt door de aandrijving, te vermijden.

Dit proefontwerp

4. In tegenstelling tot de algemeen geldende regel 'stilstand is achteruitgang' geldt bij veel applicaties binnen de Precision Engineering 'stilstand is vooruitgang'.

5. De nauwkeurigheid van precisiedraaibanken zou aanzienlijk verhoogd kunnen worden indien het mogelijk zou zijn om de relatieve positie tussen de beitel en het product direct te meten.

6. Het onderscheid dat gemaakt wordt tussen 'toevallige' en 'systematische' afwijkingen wordt meer bepaald de kennis van het systeem dan door de eigenschappen van de afwijkingen.

7. Voor het meten en bewerken met nanometer-nauwkeurigheid zal niet met een evolutionaire ontwikkeling van de huidige toegepaste technieken volstaan kunnen worden, maar zullen nieuwe technieken, gebaseerd op andere fysische principes, ontwikkeld dienen te worden.

8. *Experience does not even err, it is only your judgement that errs in promising itself results which are not caused by your experiments.*

Leonardo da Vinci (c. 1510)

9. Binnen de academische wereld dient men zich beter te realiseren dat niet de mate waarin een ontwerpmethodiek wordt toegepast de kwaliteit van een ontwerp bepaalt, maar slechts de mate waarin het ontwerp voldoet aan de gestelde specificaties.
10. Gezien het uitblijven van de verwachte economische groei als gevolg van de Duitse eenwording, dienen ook de voorspellingen aangaande de economische voordelen van de Europese eenwording met de nodige scepsis bekeken te worden.
11. Het wetenschappelijk gehalte van een technisch rapport wordt vaak ten onrechte geassocieerd met het aantal formules per pagina.